personal buildup for

Force Motors Ltd.

MTZ worldwide 8/2010, as epaper released on 17.06.2010
http://www.mtz-worldwide.com

content:

www.MTZonline.com

MTZ WORLDWIDE

07-08 July-August 2010
Volume 71

ACOUSTIC DEVELOPMENTS FOR FUTURE ENGINE CONCEPTS

COVER FIGURE Audi **FIGURE ABOVE** BMW

ACCLAIMED

Dear Reader,

On 18 May, ATZ along with its entire product family – including MTZ – was presented with the "Business Medium of the Year 2010" award by the business association Deutsche Fachpresse (German Business Media). On presenting the award, the jury of high-ranking publishing experts recognised "the successful relaunch with high target group relevance, the modern, clear design and the very good cross-media networking."

The editorial team sees this award as a confirmation of its strategy, which is ultimately to produce quality, quality, quality. The perceived quality – the design of the cover page, the haptics of the paper, the clear presentation of the graphics – is a key aspect. After all, the packaging must be right; it must arouse curiosity and an interest in reading the articles. We have taken a major step forward with our relaunch, but further ideas for improvements have already emerged from discussions with our readers.

What is even more important for us is that we fulfil the highest standards in our magazines' contents. In recent years, we were able to achieve progress above all by addressing relevant issues at an early stage and by actively acquiring the best authors. Furthermore, since the introduction of the „peer review" process two years ago, we have been able to offer many more topics from science and technology that may already determine your working environment tomorrow. This is supported by a growing number of articles on current issues written by members of our editorial team.

The quality of our media is fundamentally determined by the fact that we choose our topics independently of our advertising customers. We offer our advertisers a highly interesting target group, namely engineers who will decide on the car of tomorrow. The acclaimed position that ATZ have worked hard to establish over 112 years comes with a responsibility to adhere to strict standards on the separation of editorial journalism and advertising. This also means that in future we will entirely abstain from authors' subsidies, which we have gradually reduced in recent years.

We will do all these things in order to live up to our own claim even more successfully: to be the world's best business medium for you.

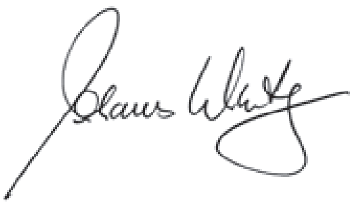

JOHANNES WINTERHAGEN, Editor-in-Chief
Wiesbaden, 1 June 2010

ACTIVE EXHAUST SILENCERS

In the past years, Eberspächer has developed active exhaust silencers for several passenger vehicles with different engines on a prototype level. In general, a substantial reduction of the exhaust noise was regularly achieved in a frequency range of 40 to 400 Hz covering the most relevant engine orders. Recent progress was made in the development of the durability and industrialization of the actuator. This component could be reduced in size and weight thus allowing the integration in different design spaces of many vehicles.

AUTHORS

DR.-ING. JAN KRÜGER
is Director Acoustics
Basic Development at
J. Eberspächer GmbH & Co KG
in Esslingen (Germany).

DIPL.-ING. MICHAEL POMMERER
is Teamleader Acoustics
Basic Development at
J. Eberspächer GmbH & Co KG
in Esslingen (Germany).

DR. RER. NAT. ROLF JEBASINSKI
is Executive Director
Basic Development at
J. Eberspächer GmbH & Co KG
in Esslingen (Germany).

ACTUATOR REPLACES REAR SILENCER COMPLETELY

There has been tremendous progress in the layout process of conventional exhaust systems by means of virtual optimization over the past years. Nevertheless, in every automotive development project the given package space as well as the targets for backpressure and acoustic levels define systematic limits which can not be overcome with the current silencer technology. These limits are also set by development time and cost and lead to an ultimate silencer volume necessary to fulfill the technical requirements of the OEM.

Under these circumstances, the main advantages of the "Active Noise Cancellation" (ANC) technology can be utilized to compensate for the extra costs which are associated with the additional components (e. g. loudspeaker and electronics). The main advantages of active silencers are as follows:

: high efficiency in reducing dominating engine orders, leading to smaller silencers
: low backpressure resulting in higher engine performance and/or to some extent lower fuel consumption
: software control of engine orders allowing an adaptive sound design and easy sound customization
: versatile silencer construction leading to more carry-over-parts
: simplified development procedures and reduced development costs and time.

Due to the above mentioned advantages intensive investigations were carried out to implement ANC in exhaust systems of internal combustion engines [1-5]. Also, Eberspächer concentrated in their first experiments on an integration of the active element (loudspeaker) in a specially designed rear silencer [6]. Although several benefits in functional performance could be shown, with this approach an introduction into automotive series products could not be reached since advantages in weight and cost could hardly be demonstrated. In a new concept the actuator was therefore rigorously redesigned and now replaces the rear silencer completely [7], ❶. The overall layout of the "ActiveSilence" system remains as in former ideas, e. g. the actuator receives its input from a microcontroller with integrated amplifier. In this electronic hardware, a complex software algorithm calculates the anti-noise signal from the input signals supplied by the ECU (Engine Control Unit) and a signal from an error microphone.

The actuator itself contains the electromagnetic loudspeaker as an active element and is driven via a digital amplifier from a micro-controller which executes the ANC algorithms implemented in dedicated software reacting on the input signals (speed, load) from the engine control unit (ECU) as well as an error sensor placed at the tailpipe. The actuator casing is of nearly spherical design and attached to the tailpipe as shown in ❷.

By this design the thermal load to the delicate loudspeaker is reduced to reasonable limits. With a volume of only about 3 l and a weight of about 3 kg this design also allows enough flexibility to adopt to different underbody package requirements to utilize the actuator in several vehicle platforms of even different OEM. The possible impact of this technology will now be explained in more detail with two case studies carried out at Eberspaecher in comparison with current serial exhaust on different vehicles. For a fair comparison with conventional rear silencers, the total volume of the active systems was estimated to about 5 l and 5 kg because it included also the y-junction (here shown in green). In each case study the hot end with its exhaust purification remained unchanged as well as the hanger positions and ground clearance of the exhaust. Thus, the vehicles could be driven normally on the road and were demonstrated to several OEM.

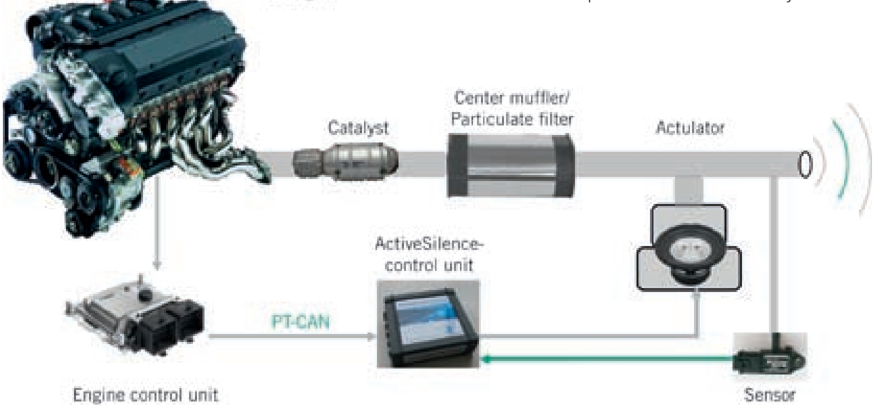

❶ General set-up of the "ActiveSilence" system

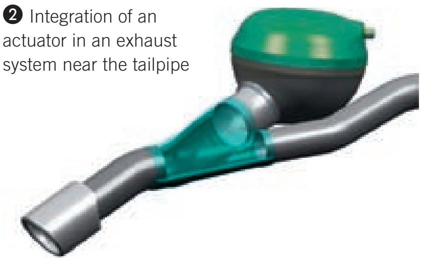

❷ Integration of an actuator in an exhaust system near the tailpipe

	PRODUCTION SYSTEM	ACTIVE SYSTEM
VOLUME OF INTER SILENCER	12.4 l	12.4 l + 3 l = 15.4 l
VOLUME OF REAR SILENCER	2 x 13.5 l = 27 l	2 x 5 l = 10 l
BACK PRESSURE	50 mbar	40 mbar
OVERALL WEIGHT	22 kg	23 kg

❸ Exhaust data of the cold-end of a 2.0 l four-cylinder gasoline turbo charged engine

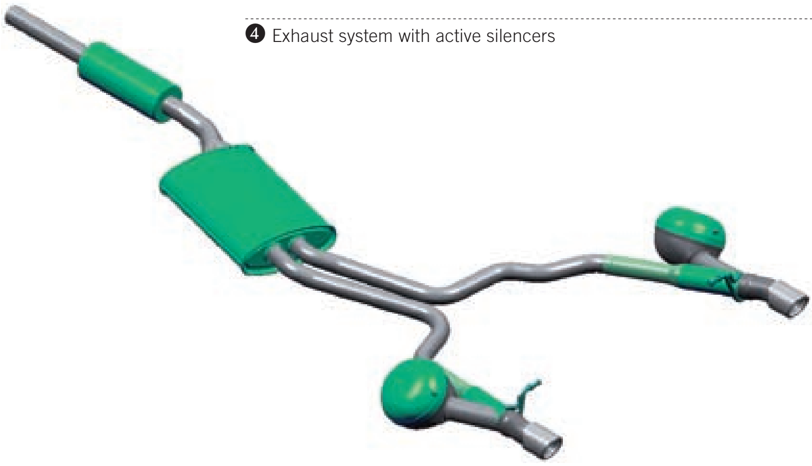

❹ Exhaust system with active silencers

CASE STUDY WITH A FOUR-CYLINDER GASOLINE ENGINE

In a first case study, an active exhaust system was developed for a premium limousine with a 2.0 l four-cylinder gasoline turbo charged engine with direct injection (147 kW; 280 Nm) with dual exhaust system. The relevant exhaust data of the cold-end are given in ❸.

In this demonstration project the main target was to increase the acoustic comfort by decreasing the firing frequency (2nd EO) without sacrificing the low backpressure of the production system and of course keeping all 3D-space limits in the underbody. This was achieved by introducing a small front silencer and replacing the two rear silencer by actuators, ❹.

Overall, a silencer volume reduction of about 14 l, equivalent to 36 %, was realized with the active exhaust silencers while backpressure and weight of the active system are similar to the production system. The acoustic results are shown in ❺ and ❻ respectively measured on a roller test bench at WOT (Wide Open Throttle = full load) and at a distance of 0.5 m and under an angle of 45° relative to the tail pipe orifice exit.

When the ANC system is switched-off, the overall level is maximum about 5 dB(A) higher than the production system. However, with the ANC turned on, a significant reduction is measured ranging from 2 to 8 dB(A), thereby achieving a small improvement over the production system in almost the entire speed range. ⑥ shows the 2nd engine order of the same measurement where the effect of the ANC-system can be seen more clearly. It starts at about 1200 rpm (40 Hz) and reaches 10 to 20 dB of active noise reduction.

CASE STUDY WITH A SIX-CYLINDER DIESEL ENGINE

In a second case study, an active exhaust system was developed for another limousine with a 3.0 l six-cylinder diesel engine with a turbo charger (170 kW; 450 Nm).

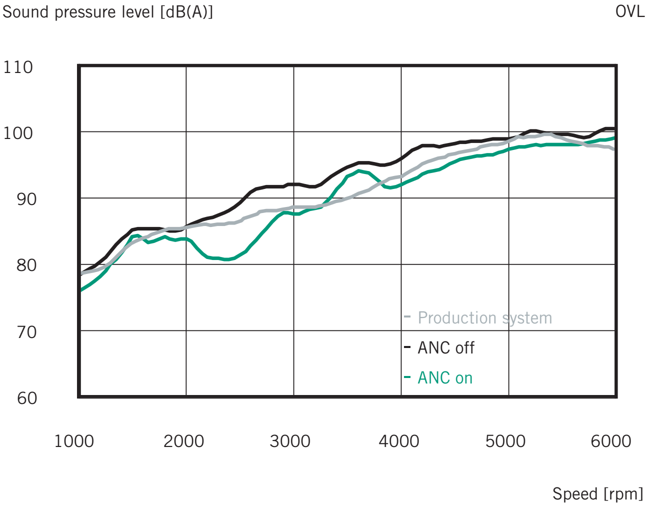

❺ Overall sound pressure level at the tailpipe of the four-cylinder gasoline engine

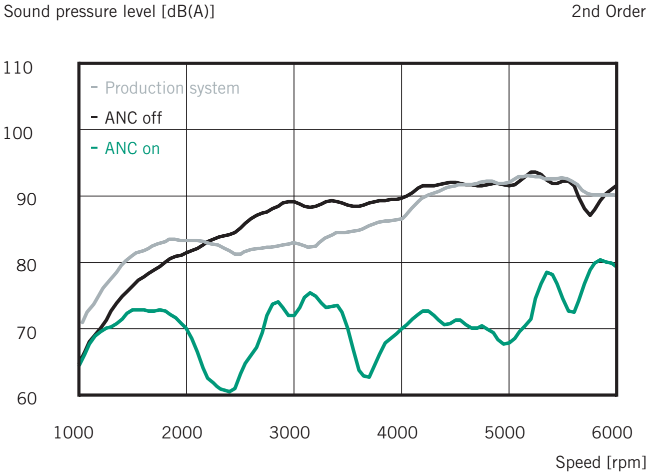

❻ 2nd engine order sound pressure level at the tailpipe of the four-cylinder gasoline engine

	PRODUCTION SYSTEM	ACTIVE SYSTEM
VOLUME OF REAR SILENCER	2 x 13.5 l = 27 l	5 l
BACK PRESSURE	205 mbar	70 mbar
OVERALL WEIGHT	19 kg	10 kg

❼ Exhaust data of the cold-end of a 3.0 l six-cylinder diesel turbo charged engine

The relevant data of the cold-end exhaust system are given in ❼.

The production exhaust system included a particulate filter but no inter silencer. In the active system, the dual flow exhaust system with two rear silencers (production) was replaced by a single flow exhaust system with just one actuator with a volume of 5 l, ❽.

Note, that the overall silencer volume reduction is now drastically about 22 l which is equivalent to about 80 %. Furthermore, the backpressure of the production exhaust could be lowered by about 135 mbar measured at the outlet cone of the particulate filter. Finally, the active system including ANC controller, cables, and amplifier weighs about 9 kg less than the production system disregarding the additional hanger and heat protection material which could be saved, too. This substantial weight reduction was only possible by sacrificing one visible tailpipe which has of course a negative impact on the visual appearance from the back of the vehicle. On the other hand, the purpose of this case study was rather to demonstrate the light weight design potential without compromising any technical function rather than the optical design.

The acoustic results are shown in ❾ and ❿ respectively and are measured the same way as in the first case study. The A-weighted overall level is dominated by flow noise rather than by engine orders which is quite typical for diesel engines. Consequently, the overall level changes by just a few dB(A) only when the ANC-system is switched on or off which is close to the production system. Nevertheless, ⑩ shows in more detail the 3rd engine order of the same measurement. The effect of the ANC-system is clearly visible in the diagram. In fact, the active noise reduction reaches about 5 to 15 dB in the entire speed range. Despite the actively controlled 3rd engine order being obviously higher than in the production system, it remains on an acceptable level which does not influence the overall tail-

❽ Design of exhaust lines for a six-cylinder diesel engine (left: production system; right: active system with two and one actuator respectively)

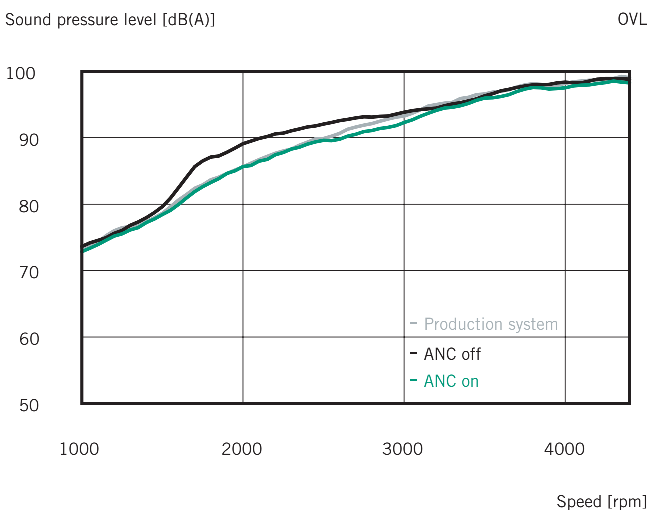

❾ Overall sound pressure level at the tailpipe of the six-cylinder diesel engine

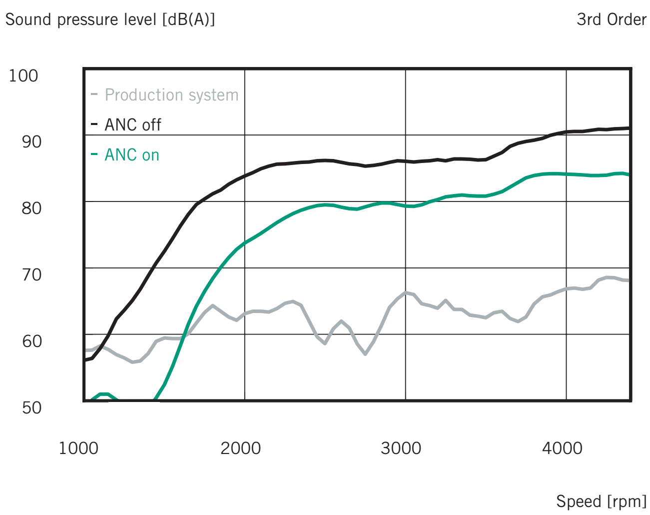

❿ 3rd engine order sound pressure level at the tailpipe of the six-cylinder diesel engine

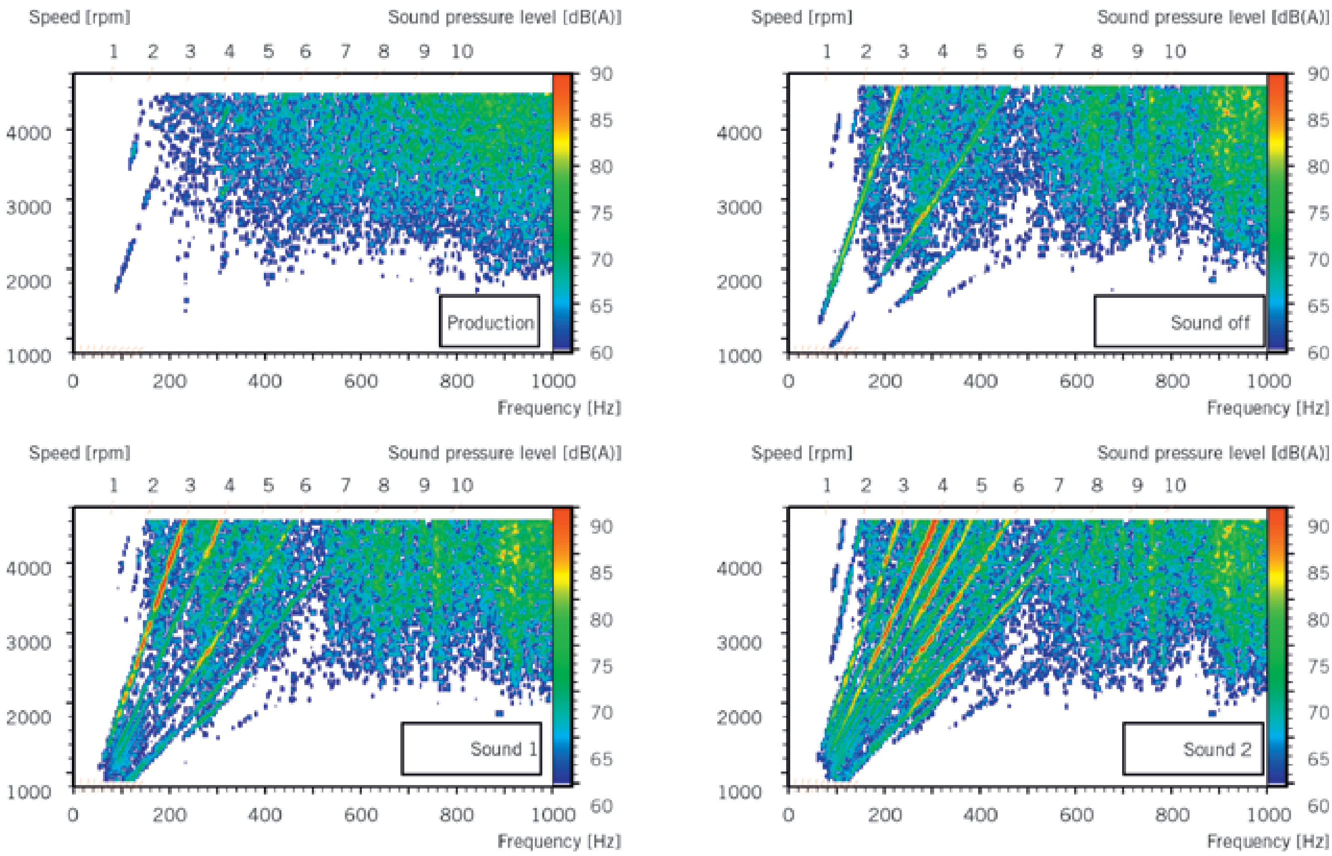

⓫ Campbell diagrams of the overall sound pressure level at the tailpipe of the six-cylinder diesel engine

pipe level or the interior noise level of this engine order.

Besides a pure noise cancellation active silencers offer the opportunity of sound enhancement of several engine orders depending on relevant engine and vehicle parameters e. g. engine speed and load as well as vehicle speed or even transmission gear. Moreover, it is possible to switch between sound designs by different data sets in the software algorithm depending on the drivers intention or even a more automatic selection between a comfort and a sport mode. To demonstrate the effect of alternative sound designs implemented purely by different data sets and applied to the same engine and a dual exhaust configuration, ⓫ shows the tailpipe noise of the above mentioned vehicle with six-cylinder diesel engine measured under full load acceleration. Clearly, one can see that the series production exhaust exhibits almost no engine order content while with the active exhaust in passive mode the engine orders are visible somewhat but not on a truly sporty level. The activated system can amplify certain engine orders thereby supporting totally different sporty sound impressions. Those impressions are not only noticed outside the vehicle but could also be recognized markedly inside the vehicle on all seats. Finally, note that through careful design of the exhaust system and in particular a substantial reduction of flow noise the A-weighted overall level remains within the limits given by European pass-by noise legislation.

DURABILITY CONSIDERATION

Naturally, the functionality of an active exhaust system has to be assured as usual for automotive components and in particular for conventional exhaust systems. Therefore, Eberspächer has carried out extensive durability investigations both on the active components itself as well as on demonstrator vehicles. Compared to the common fields of application of electromagnetic loudspeakers in the automotive industry the location at an exhaust system was a particular challenge in the development process. The durability of the loudspeaker is hereby especially affected by:

: vibration due to road load and engine excitation
: exposure to aggressive chemical substances in gaseous and liquid form (condensate)
: thermal load due to the hot exhaust gas.

The mechanical durability was developed by a careful CAD design supported by FE-simulation, special thermo-mechanical analysis, and modal analysis of loudspeaker, actuator and the whole exhaust system as it is standard in the development of exhaust systems. The chemical resistance against the exhaust gas and its condensate could only be achieved by innovative materials on all the loudspeaker components which are faced with the exhaust (e. g. membrane, surround, adhesive). The most important challenge, however, was to assure that the high exhaust gas temperature does not destroy the loudspeaker and the induced heat in the voice-coil by electrical load during driving is effectively dissipated. A closer analysis of this situation revealed that the highest thermal load exists only during longer periods of high engine loads and

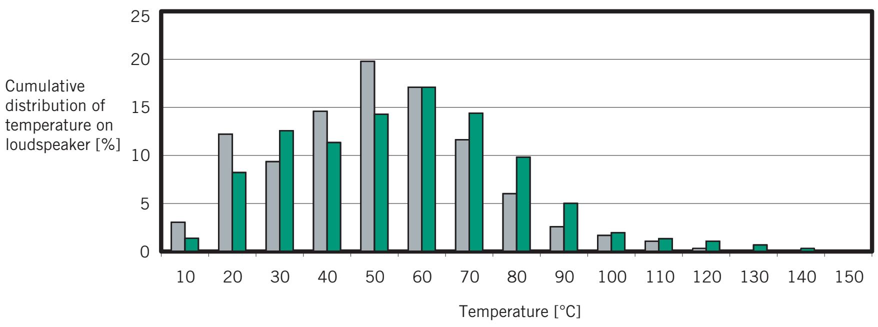

⓬ Cumulative distribution of temperature at the left (grey) and right (green) loudspeaker during a long vehicle test run

speeds typical only for high speed driving (e. g. > 200 km/h). In this case, the enormous cooling effect of underbody flow can be utilized to cool the exhaust system, the actuator and in particular the connection tube from actuator to the main exhaust pipe. Furthermore, the temperature resistance of the loudspeaker could be improved to about 150 °C which eventually allowed a robust system design which copes with even extreme situations as e. g. high speed driving for several hours. Apart from this extreme application it seems of more importance for the long time durability to cover the average driving profile of a particular vehicle equipped with a certain engine. ⓬ shows such a temperature distribution on the loudspeaker measured during a long run vehicle durability test (> 50.000 km). The measurement data are taken from a limousine with six-cylinder diesel engine and included relevant driving conditions such as idling, stop-and-go, cruising, WOT acceleration, coast down and high speed driving in middle European climate. It can be seen clearly, that most of the time the loudspeaker temperature is in a range below 100 °C. Extreme temperatures occur rarely e. g. 140 °C in less than 1 % and a critical temperature of 150 °C is hardly ever reached. In addition to special vehicle testing, several vehicles of Eberspaecher company fleet were equipped with an active exhaust system and are now continously tested in everyday use.

CONCLUSIONS

The feasibility of active silencers under the harsh conditions of automotive exhaust systems has been demonstrated. Several functional advantages were proven such as the acoustic performance, silencer volume and backpressure reduction. Besides that, the durability of the actuator in respect to vibration, chemical substances and temperature has been investigated thoroughly and improved to be able to start a series development including the industrialization of the actuator. Further emphasis in future development work will be directed towards the reduction of overall system cost. Certainly, this technology can only be introduced in automotive mass production if the additional cost for loudspeaker, controller hardware, and software can be compensated by higher functional performance or added customer value. In particular the freedom in sound design and the weight reduction potential seem to be highly attractive to the OEM especially if the market is open to a more radical functional design of the cold-end exhaust system. Current requests therefore support e. g. potential applications such as (main motivation):

- diesel engines in sporty vehicles (sound)
- downsized engines with less cylinders (sound and silence)
- cylinder deactivation of V6 and V8 engines (sound and silence)
- small internal combustion engines for range extender vehicles (volume and silence)
- rigorous integration of exhaust system in engine bay (volume and silence).

REFERENCES

[1] Jay, M. A.; Köhler, F.: Active Noise Control für Kraftfahrzeuge. In “Sound-Engineering“ von Quang-Hue Vo. Expert-Verlag ISBN 3-8169-1177-3, Renningen-Malmsheim (1994)
[2] Boonen, R.; Sas, P.: Development of an active exhaust silencer for internal combustion engines using feedback control. SAE 1999-107
[3] Heil, B.; Enderle, Ch.; Bachschmid, G.; Sartorius, C.; Ermer, H.; Unbehaun, M.; Zintel, G.: Variable Gestaltung des Abgasmündungsgeräusches am Beispiel eines V6-Motors. In: MTZ 2001, Nr. 10
[4] Garabedian, C.; Zintel, G.: Active Noise Control: Dream or Reality for Passenger Cars. SAE 2001-01-0003
[5] Rossi, F.: Active Noise Control Technique To Improve Engine Efficiency, Proceedings of “Energy and Environment“. (2002) Italy
[6] Krüger, J.; Castor, F.; Jebasinski, R.: Active Exhaust Silencers – Current Perspectives and Challenges. SAE 2007-01-2204
[7] Krüger, J.; Nicolai, M.; Jebasinski, R.: Bauraum- und Leichtbauoptimierung von Abgasanlagen mit aktiven Komponenten. 18. Aachener Kolloquium Fahrzeug- und Motorentechnik 2009

ORIFICE FLAP

FOR INTAKE SYSTEMS AT LIMITED INSTALLATION SPACE

In contemporary engines, turbocharging increases air mass flow, which, in turn, requires a larger intake pipe cross-section to reduce pressure drop. However, a larger cross-section results in higher intake noise, which must be reduced using a comparatively large volume bypass resonator. Since the necessary installation space can hardly be found in downsized engines with start-stop systems, innovative technical solutions should be thought. And exactly this is where the orifice flap design developed by Mann+Hummel can be used. This paper describes this innovative flap as a solution of the conflict between pressure drop and intake noise in vehicles.

AUTHORS

DIPL.-ING. (FH) MATTHIAS ALEX
is Chief Acoustic Engineer at Mann+Hummel GmbH in Ludwigsburg (Germany).

DIPL.-ING. (FH) THOMAS JESSBERGER
is Head of the Innovation Management Department at Mann+Hummel GmbH in Ludwigsburg (Germany).

FURTHER ENGINE DEVELOPMENT REMAINS IMPORTANT

While the development of alternative drives is continually progressing, the development of the internal combustion engine (ICE) is required in parallel, too. Yet, the ICE will remain the basic drive option for cars in the coming years, playing a crucial role in hybrid drive concepts as well (e.g. as a range extender). Considering these facts, it seems reasonable to look for new methods in the development of air intake systems to sort out conflicts between pressure drop, limited installation space and engine acoustics. The approach implemented in this particular case was the "Way of Contradiction Oriented Innovation Strategy" (WOIS). According to this strategy, the development process can be depicted as a continually rising spiral and as such it is a never-ending process. At higher stages of the development process, solutions from the past can help to break the limits of performance achieved so far. Development discrepancies provide a central thinking model in WOIS [1]. Whereas conflicts in the past were resolved by compromises, WOIS strives to obtain a more comprehensive view to break existing performance limits. At the start of the WOIS-based development, existing development directions should be considered exactly to determine key barriers which, later, should not only be optimized, but rather completely resolved. These issues will be dealt with in the section describing the initial situation for WOIS, however, let us now go back to the air intake system.

AIR INTAKE SYSTEM

A conventional air intake system consists, generally, of raw-air duct, air filter box, clean-air duct including a mass air flow meter and an intake manifold with a throttle valve. In turbocharged engines, the air intake system includes, additionally, a charge air duct between the turbocharger and cooler (hot-air side) and between the cooler and the throttle valve (cold-air side). Due to the hot side is connected with the exhaust pipe and the cold side with the intake manifold, the intake air is led once around the engine. This reduces the installation space dramatically and, consequently, new, space-saving designs must be thought.

The air intake system in cars has the following tasks: supplying air to the ICE, removing dirt, dust particles and moisture in the air to reduce engine wear and failure in engine electronics – and also noise generated by the impulse operation of the engine's pistons. Noise must be reduced primarily because of its health damage potential. Pressure drop caused by routing the air intake pipe, filter resistance, and pipe

❶ Air intake system with noise reduction components in a 2.0 l four-cylinder internal combustion engine

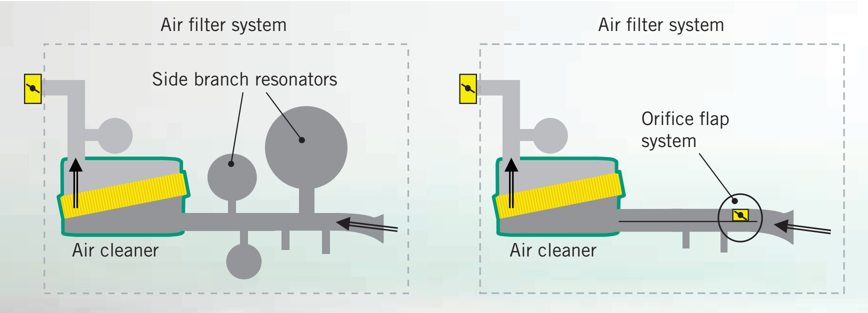

❷ Comparison of both systems, with additional components (left) and without additional components (right)

cross-section changes reduce engine efficiency. Therefore, thermodynamics experts try to minimize air flow resistance and, thus, to increase engine power output. This will be achieved by increasing the pipe cross-section, thus avoiding the installation of additional, large-volume noise reduction systems.

These additional systems (Helmholtz resonators) require different installation space, depending on frequency range. For low-frequency sound, large resonator volumes (2 to 5 l) are required to reduce the noise level to acceptable values. The air intake system of a natural aspirated four-cylinder ICE is shown in ❶. Noise reduction measures can be seen as bulges along the pipe. The biggest side branch resonator is tuned to approximately 80 Hz, requiring a volume of approximately 2.5 l. However, space for installation of this unit will hardly be provided, since it is required for other engine systems. And, at the same time, the requirements with regard to avoiding pressure losses will rise, since additional air must be supplied to the engine to increase its power output. As a result, the cross-section of the duct system must be increased. This measure reduces the dampening effect of cross-section changes in the air filter.

Smaller pipe diameters, particularly at the air intake, reduce noise; however, the pressure drop will rise dramatically due to the higher air flow rate. This conflict has been experienced in the course of developing air intake systems in the past and has been solved using more or less successful compromises.

Therefore, the air intake system of the 2.0 l four-cylinder engine, as specified above, was selected for optimization using the WOIS concept, since this series-production engine has a lot of additional noise reduction systems (side branch resonators). In order to obtain an optimized engine design, these resonators can easily be removed, thus providing additional installation space and creating a basic variant maintaining the same pressure loss values for a further optimization, ❷.

Removal of these additional measures will result – at first – in higher noise levels (up to 10 dB(A)) at overall engine speed, which is four times higher as with noise reduction components, ❸ (left). The impact of pressure drop would be negligible – as shown in ③ (right) – since the removed noise reduction components were placed exclusively in the bypass; however, the overall result was not satisfactory. Thus, both contradictory objectives of development in line with WOIS would be air intake noise and pressure drop.

INITIAL SITUATION FOR WOIS

Noise at the air intake grows continually in natural aspirated engines, proportionally to engine speed, ③ (left). Lower engine orders are dominating the overall sound pressure level in most cases, ranges from 50 to 250 Hz, at low-frequency, hence, large-volume noise reduction components are required to eliminate booming noise in the passenger compartment. This low noise can be perceived by the passengers on the rear seats at low engine speed, whereas the driver will not recognize it, since he is sitting in the node of vibration. Pressure loss, as a rule, will be optimized only for maximum mass flow, and the pipe diameter will be defined for maximum mass flow, since – in natural aspirated engines – this airflow occurs only at maximum engine speed.

Owing to the proportional correlation between volumetric flow rate and engine speed, a significantly smaller pipe diameter is sufficient for low engine speed, with the same allowed pressure drop. This fact inevitably suggests a variable pipe diameter design. At low speed, a smaller pipe diameter would provide for compliance with air intake noise specifications, whereas at higher speed, the pipe diameter, which increases along with the increasing volumetric air flow, would avoid excessive pressure drop.

The solution of this conflict in line with the WOIS, resulted in the require-

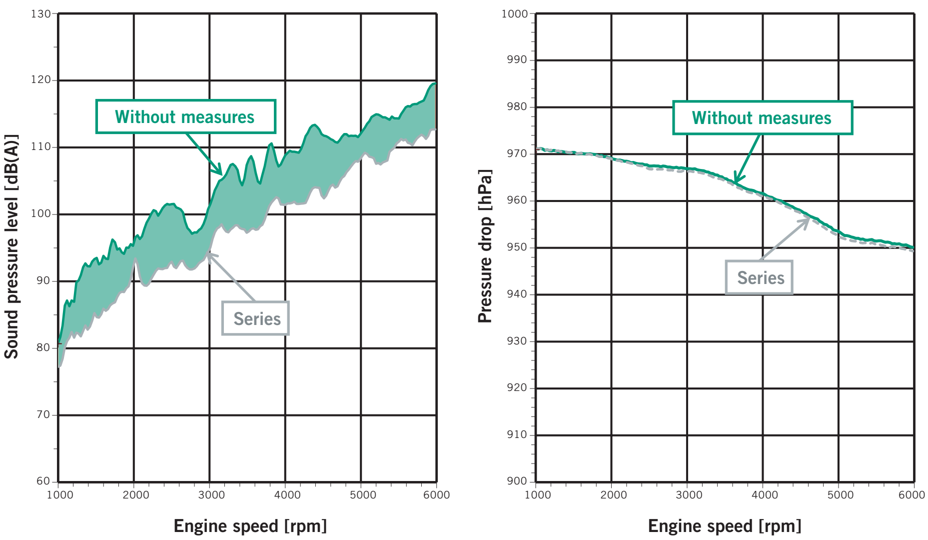

❸ Increase of orifice noise through omitting additional measures

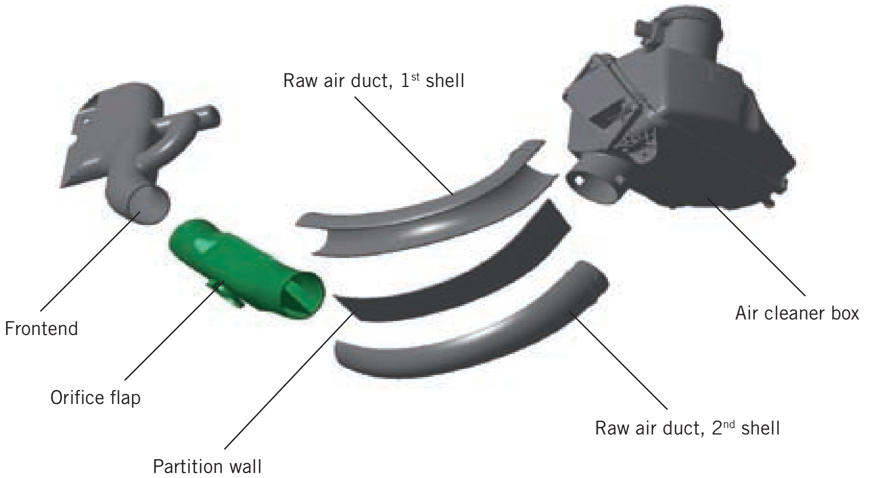

❹ Parts of a double-flow manifold with orifice flap

ment of a variable air intake pipe cross-section, continually adjustable using a flap. For this purpose, a step motor design seemed to be the first choice. However, this option would be expensive and, additionally, the risk of failure and wear should be considered, since the flap must always close the orifice completely. Therefore, the design engineers at Mann + Hummel were looking for a design without a step motor. Finally, they opted for a two-channel duct design, where one duct is permanently open and the other has a variable cross-section, controlled using a self-adjusting flap (the pressure difference on both sides of the flap is used for easier closing and opening of the flap).

SELF-ADJUSTING ORIFICE FLAP

At first, air flow was divided into two channels using a partition wall. One channel is permanently open, and the other will be closed using a flap. The end section will not be modified, since it provides a connection with the front end. The components of the air intake system are shown in ❹.

The other channel is completely closed at low engine speed, thus increasing the pressure difference on both sides of the flap as the engine speed rises. This pressure difference causes the flap to open, thus increasing the cross-section of the air duct. At maximum air flow, the flap will be fully opened, allowing the air to flow into the combustion chamber of the engine without excessive pressure drop. The acoustic air flow benefit consists of closing the other duct as long as possible (or rather not opening it too soon), thus allowing the initial flow rate.

This optimized design was tested and noise levels were measured on a Mann + Hummel vehicle roller bench. The noise curve is shown in ❺, measurement performed at a distance of 100 mm, in third gear, at full load. This innovative design allowed a reduction in the overall noise level, ⑤ (left), to the value specified for series production. Resonance peaks could even been reduced to some extent. A reduction of low-frequency noise by 6 dB was achieved in the air intake system with variable duct cross-section at an engine speed up to 2000 rpm, although the 2.5 l resonator was removed. Pressure loss did not change at maximum volumetric flow and only minor pressure reduction occurred in the medium speed range, which can be attributed to the design concept, ⑤ (right).

SUMMARY

The continuing development trend of engine downsizing and increasing specific engine power output through turbocharging means an increasingly smaller and complex installation space. Development until now has been aimed at finding technical compromises between the contradictory target requirements of noise reduction and avoiding pressure drops. For achieving these goals, large components were necessary. An adjustable flap in the intake air duct provides a solution with reduced installation space. An optimized air intake system, with removed bypass resonators, shows how to save more than 2.5 l in the engine compartment using an orifice flap in air intake, without negative consequences such as increasing noise and pressure drop at maximum air flow.

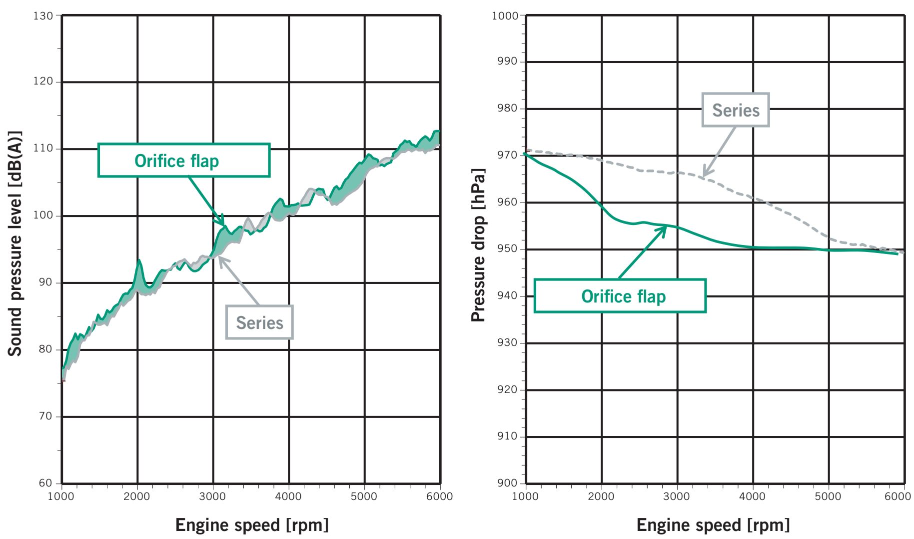

❺ Comperative measurement for an optimized air intake system with variable orifice flap

REFERENCE

[1] Linde, H.; Hill, B.: Erfolgreich erfinden, Widerspruchsorientierte Innovationsstrategie für Entwickler und Konstrukteure. Hoppenstedt Technik Tabellen Verlag, Darmstadt 1993

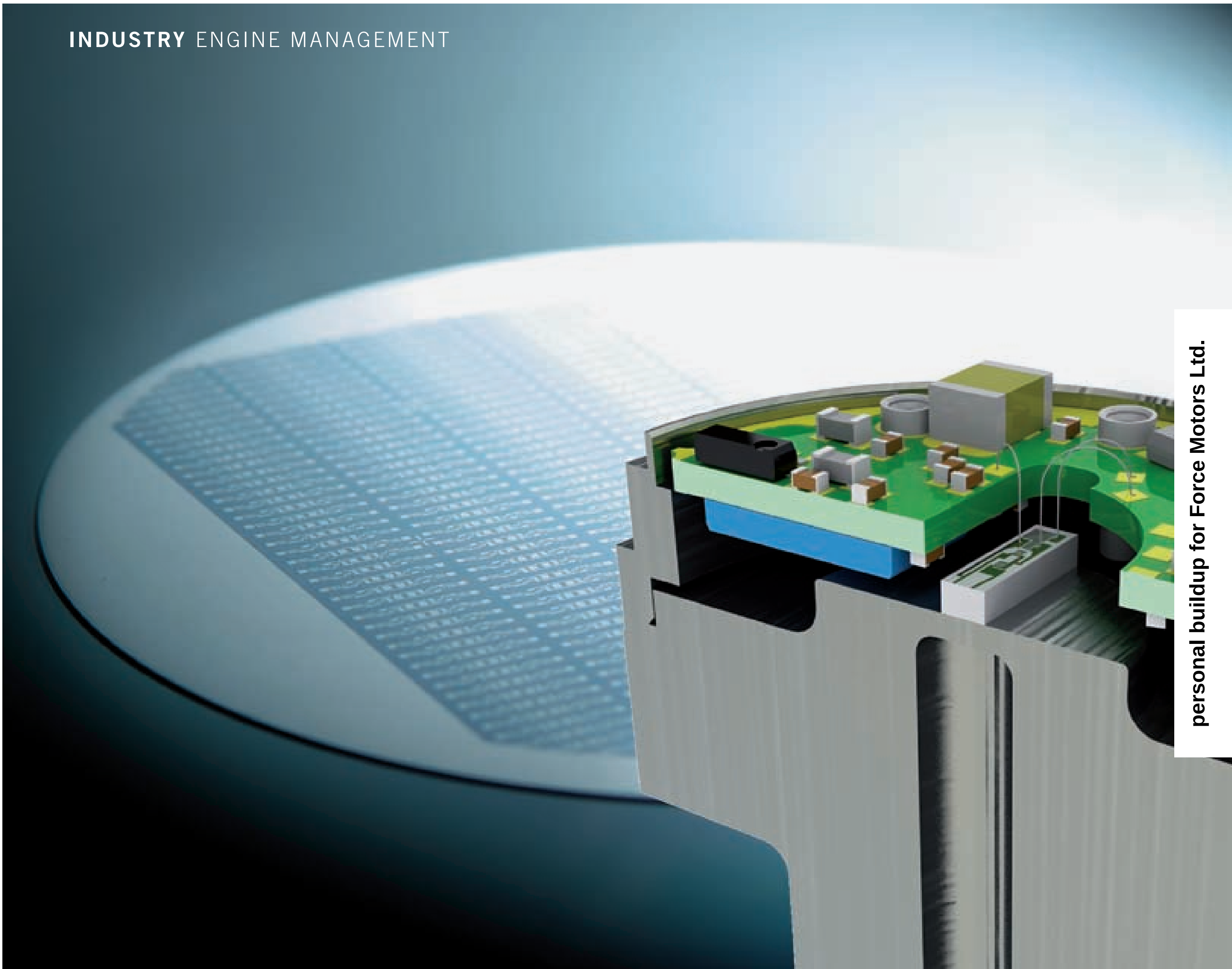

PRECISE AND WELDFREE HIGH-PRESSURE SENSOR FOR LARGE ENGINES

High pressure sensors used with large diesel motors must offer a very high level of robustness and precision. At the same time the cost of the sensor must be such that its series use in large engines is practicable. The new Trafag high-pressure sensor fulfils all three of these critical requirements, as described in the following report.

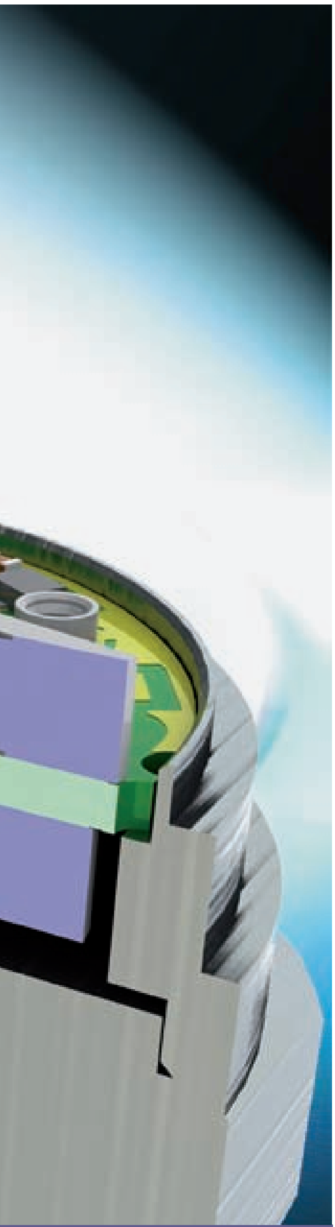

AUTHORS

DIPL.-ING. (FH) ULRICH STAIGER
is Project Manager Engine Pressure Sensors at the Trafag AG in Männedorf (Switzerland).

DR. DIETER ZEISEL
is Head of the Research and Development Department at the Trafag AG in Männedorf (Switzerland).

MOTIVATION

The elevated media temperatures – up to 150 °C – of the heavy fuel oil (HFO) and the relative variations in injection pressure in excess of 1500 bar call for sophisticated and innovative sensor design. The operational lifetime requirement of 10^{10} full load cycles and ever increasing system pressures of up to 3000 bar encountered in common rail systems must be taken into account, as must the high levels of vibration encountered.

The development and optimization of combustion control processes for large engines, such as fuel injection modulating in common rail systems, demand ever more precise and robust sensory components which are also economically priced. Trafag AG has been manufacturing common rail pressure sensors for measuring peak pressures of up to 3000 bar for ten years. These sensors are also used for monitoring peak pressures in a range of unit pump systems. On large diesel engines an operational lifetime of up to 10^{10} load cycles from 0 to 2000 bar is required, calling for an extremely robust design with outstanding long-term stability.

In essence, there are three main requirements which a high pressure sensor must meet. Firstly, it should be economically priced. Secondly, it must be extremely robust and stable in order to withstand the harsh conditions met in large engine environments. Finally, the sensor must be equipped with high performance electronics capable of processing the measured data quickly and demonstrating a high level of accuracy over a wide range of temperatures.

SENSOR DESIGN

Of the numerous sensor technologies available on the market today, that most frequently used in the high pressure sector is resistive measurement, which boasts the advantage that the pressure signal is referenced to ambient. In addition to the MSG (metal strain gauge) technology reported in MTZ some years ago [1], thin film methods are also available. This process essentially makes use of two coating techniques. Firstly, in order to electrically insulate the active sensor components from the body of the device, a SiO_2 glass layer is laid down using a CVD process (Chemical Vapour Deposition). This provides insulation from the device housing which is capable of withstanding in excess of 500 VAC. The resistors which form the Wheatstone bridge measurement circuit are made of nickel and nickel-chrome alloy, and are sputtered directly onto the SiO_2 surface. In subsequent process steps conventional lithographic techniques are used to create the meander-shaped conductor paths typical of the strain gauge.

In contrast to the widely used silicon-based pressure sensor systems [2], sensors using thin film technologies show much lower temperature errors and an increased long-term stability due to the fact that all the materials used in their construction have similar coefficients of thermal expansion.

The relative zero offset of a Wheatstone bridge circuit can be used as a parameter to measure sensor stability. In order to evaluate long term stability over the sensor lifetime under conditions met in the large engine environment, a number of different sensors were subjected to a temperature of 120 °C over a period of seven years during which time the zero offsets were recorded. ❶ shows the drift values measured, all of which lie well below 0.5 % FS (FS = Full scale measurement range). The zero offset drift of other pressure sensors based on another resistive technology, thick-film on ceramic (previously known as hybrid-technology), which were also investigated, is almost an order of magnitude higher. The NiCr alloy used to fabricate thin-film devices has the additional advantages of having a very high manufacturing reproducibility as well as temperature stability to 200 °C.

NON-WELDED CONSTRUCTION OFFERS HIGH SECURITY

The latest generation of the high-pressure sensor utilizes a non-welded design based on a monolithic body of precipitation-hardened 17-4PH CrNi stainless steel. The sensor diaphragm, which must be of an exactly defined thickness, forms the bottom of a highly accurate deep bore machined into the centre of the device body. The membrane is designed to operate at very high pressures, in excess of 3000 bar. The thin-film structure is not directly located on the diaphragm but is deposited onto a tiny cantilever beam attached to it at the thinnest point. This avoids the need to create the sensor structures on diaphragms individually, which would be laborious and inefficient. In such highly loaded sensors it is essential to maintain low stress levels in relation to the elastic limit in order to maximize the operational lifetime. While 17-4PH steel (material number 1.4542) has a maximal tensile strength of 1300 MPa, more recent studies show that its load cycle endurance in the giga-cycle range can be reduced under some circumstances [3]. In contrast to welded constructions, a monolithic sensor body offers enhanced security under fatigue stress conditions due to the seamless design and a lower internal residual stress level.

FEM CALCULATION INCORPORATING INSTALLATION CONDITIONS

During the finite element analysis of the sensor body two different load situations were investigated. The first case indicates the deformation and stress when the sensor is fitted and tightened with a specified torque. A difference in cone angle of 0.5 to 1° between the sensor body and the mounting seat results initially in a line contact between the two which usually forms a seal on the high-pressure side. The seating force generated by the tightening torque is in the > 10 kN range and this causes the contact areas of the two parts to deform until the stress in the cone surface shell falls below the elastic limit, ❷. At this point the sensor and the seat have mutually adjusted their shapes, allowing continuous sealing to occur. Important in this context is the well-defined lubrication of the sensor screw-thread.

The second loading case modelled is based on the installation conditions as described above, with the addition of operating pressure to evaluate the deformation and stresses in the sensor body and diaphragm when the device is in use. The deformation of the cantilever beam when the nominal pressure of 2500 bar is applied is just a few microns, ❸.

The electrical connection of the strain gauge on the cantilever beam to a printed circuit board (pcb) is made with the help of wire bonds in order to mechanically decouple the sensor element and electronics. In the latest generation of sensors only one pcb is required which, because of the stringent electromagnetic compatibility (EMC) and vibration requirements, is mounted directly onto the metallic sensor housing. The customer specific interface normally includes a connector integrated into the housing or an appropriate cable module.

SIGNAL PROCESSING WITH PRODUCT SPECIFIC ASIC

The output signal from the Wheatstone bridge which is generated by the very slight stretching of the diaphragm under pressure is, as already demonstrated, ①, extremely stable. On the other hand, the signal level is rather low – with a k-factor of two for NiCr strain gauges, outputs of

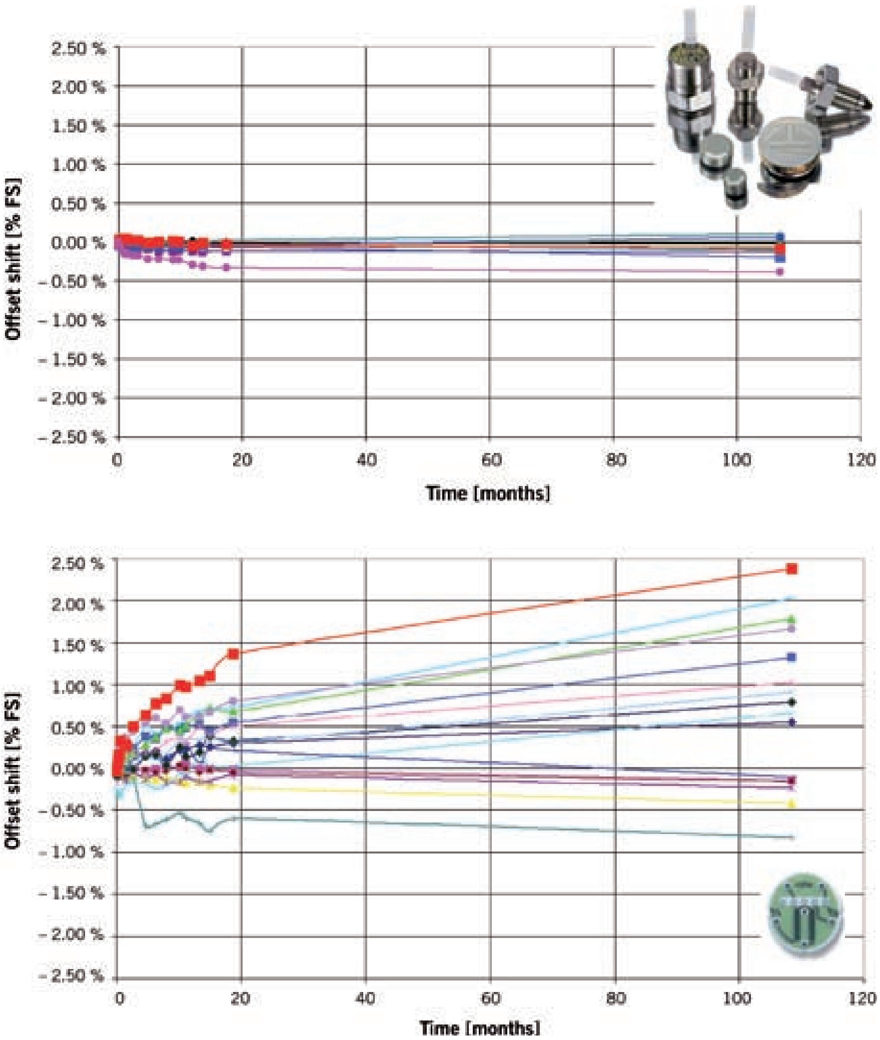

❶ Comparison of the long-term stability of two different resistive sensor technologies top: strain gauges sputtered onto steel; bottom: strain gauges printed on Al_2O_3 ceramic, then fired

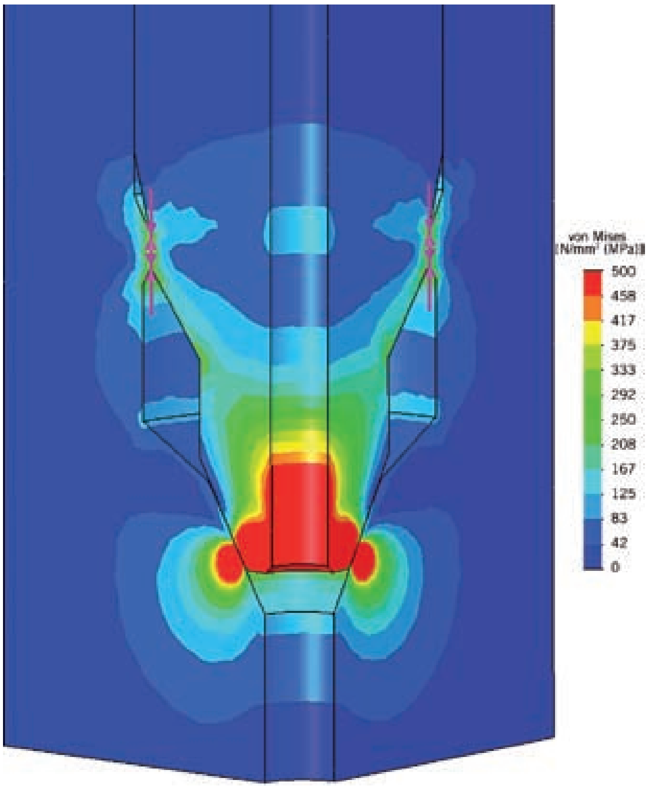

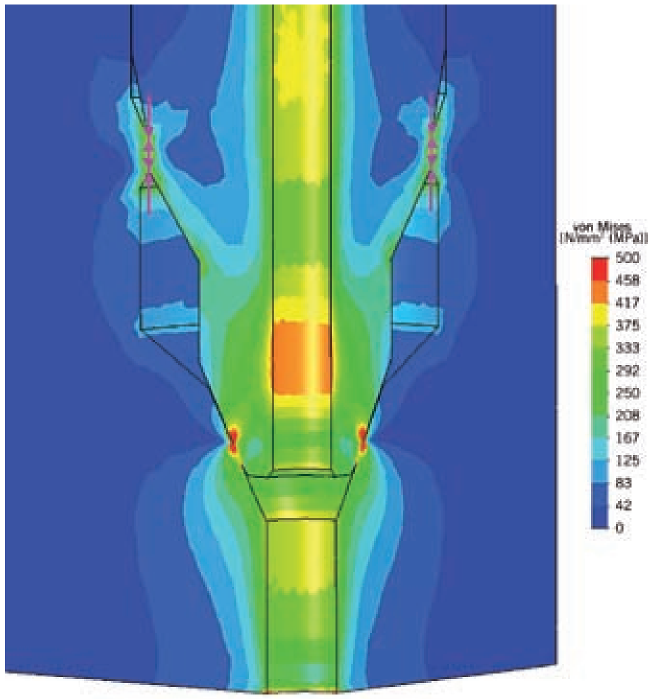

❷ Stress in sensor seat during tightening (left) and stress after sensor is tightened and under pressure (right)

2 mV/V are measured. This disadvantage can be made good with the help of the latest Application Specific Integrated Circuit (ASIC) technology. The IC used in the sensor features an offset-free amplifier which operates in a closed control loop, thereby compensating for any offset drift. This allows even small output signals below 2 mV to be amplified with a high signal-to-noise ratio and compensated, at 5 V supply voltage. In order to meet specific customer requirements zoomed (i.e. partial) measurement ranges may be selected, offering increased security against excess pressure (typically a factor of four to six times measuring range). Noise levels of ~ 40 nV/√Hz, equivalent to 0.6 μV_{eff} at 300 Hz bandwidth are achieved. ❹ shows a block diagram of the ASIC circuitry. Analogue to digital conversion is performed by a sigma-delta converter. Error compensation is effected by means of a three-dimensional lookup table – the error is evaluated and fed back via a fast pulse-width modulated (PWM) signal. Temperature is measured either by the ASIC's on-chip sensor or directly by a nickel resistor on the strain gauge itself, the latter giving a very good indication of the temperature of the pressure medium.

The signal is measured with a bandwidth of 10 kHz, so that very fast transient effects in the fuel injection process can be recorded. The sensor electronics meet all EMC requirements as per IEC 61000 (level 4) as well as current marine and railway standards. According to DIN 16086 the total error shown by a pressure sensor is the

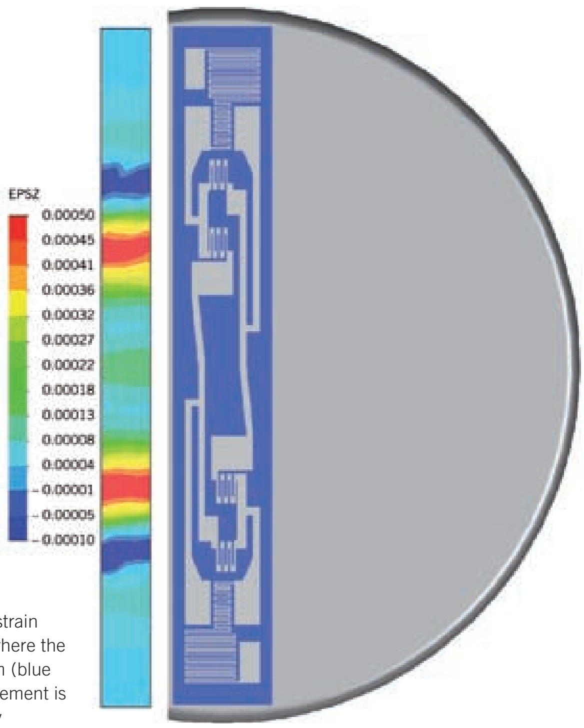

❸ Finite element simulation shows strain zones in the x direction in the area where the cantilever is welded to the diaphragm (blue compression, red strain); the displacement is enlarged by a factor of 100 for clarity

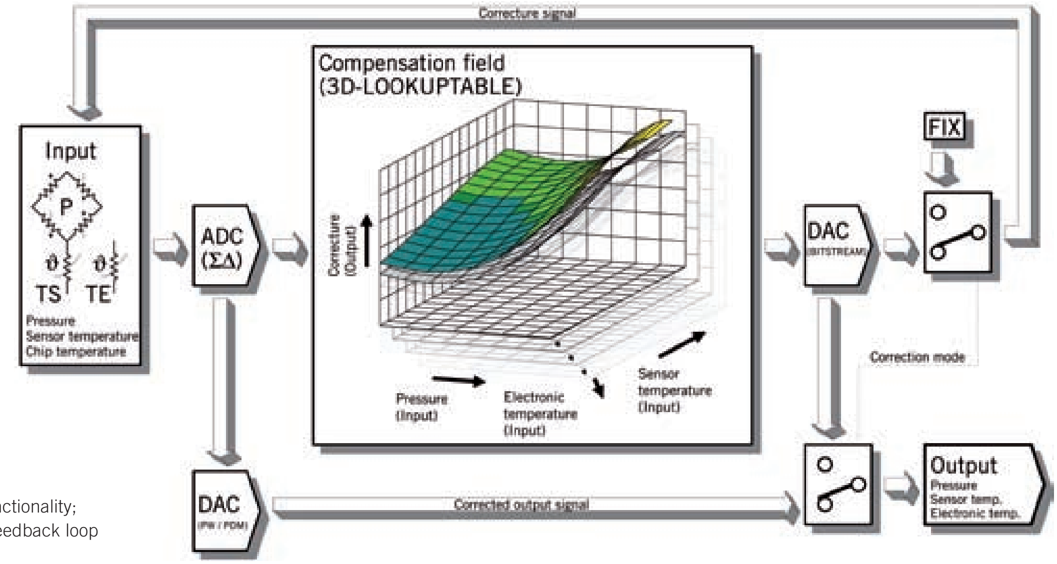

❹ Schematic diagram of ASIC functionality; compensation is performed by a feedback loop at up to 10 kHz

combination of the non-linearity and hysteresis (NLH), the temperature error and the sensor drift. The total error of the Trafag high pressure sensor in the temperature range between -20 and 135 °C has been kept very low, so that generally sensors show a total error of just 0.3 to 0.5 % FS. This is equivalent to about 10 bar error in the 2500 bar measuring range.

SENSOR QUALIFICATION THROUGH EXTENDED TESTS

Both elaborate simulated lifetime tests and intentionally destructive tests were undertaken in order to test the robustness of the design, identify weak points and enable these to be corrected. The initial tests involved exposing sensors to high operating temperatures for extended periods, as already mentioned, ①. In addition, the combination of constant, high nominal pressure and exposure to maximum operating temperature quickly provides data on the stability of a particular sensor technology. In this regard, a typical test run involved exposing the sensors for 2000 hrs to 120 to 140 °C, during which time, the offset drift values should be less than 0.5 % of the nominal pressure range.

Increasing the frequency of temperature cycles provides temperature shock data (duration of temperature change less than 10 s, hold time typically 30 to 60 mins) which often gives precise information on sensor drift, possible short circuits, soldering failures or bond wire breakage. Extended vibration testing (400 hrs) with simultaneous temperature variation from to 40 to 135 °C represents another important part of sensor qualification. This test tends to uncover weaknesses in assembly and connection techniques such as poor electrical interconnects, loose parts etc. An excellent insight into this subject is given by Wulpi et al. [4].

Finally, highly accelerated lifetime testing (HALT) was also employed to definitively evaluate the design. ❺ shows an example of one such test which quite intentionally exceeded the sensor specifica-

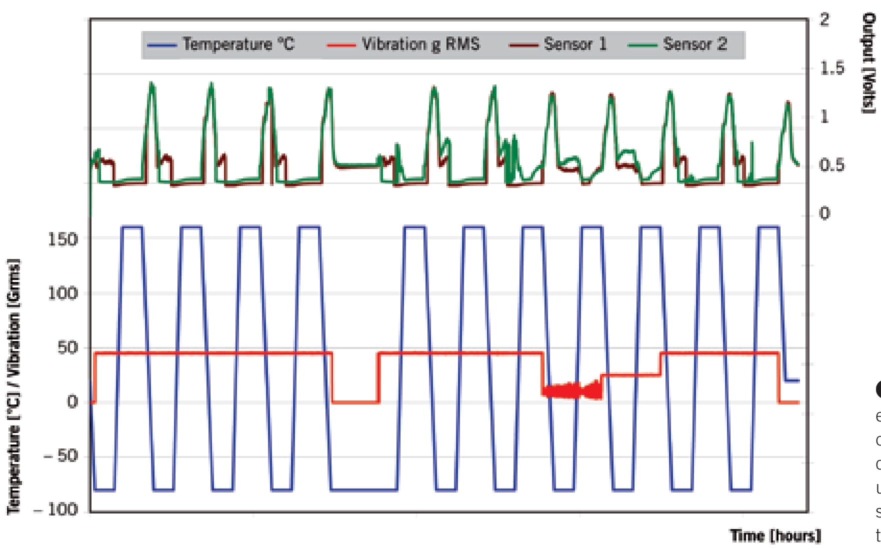

❺ Combined environmental HALT tests deliberately exceeding sensor specifications (-80 °C / 160 °C at constant vibration level of 50 g RMS, lower traces); output signals (upper traces) of the pressure sensors show uncompensated response to temperature shocks but also signal stability i.e. return to specified output at the end of the tests

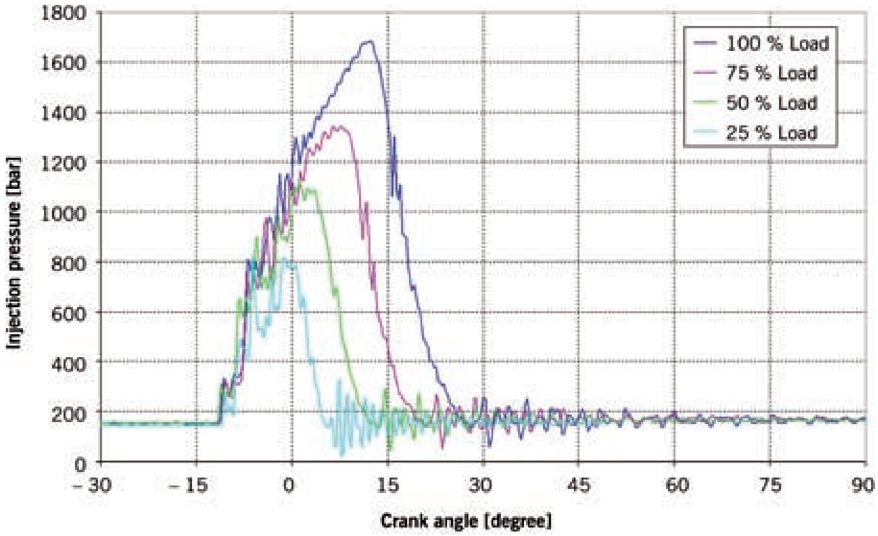

❻ Injection pressure curves recorded with an 8 kHz pressure sensor

tions. Here, sensors with a specified vibration tolerance of 25 Grms within a temperature range of -40 to 125 °C are subject to a 50 Grms vibration test. At the same time the temperature in the test chamber is raised within a few seconds from -80 °C to 160 °C. The output signals of the sensors are recorded in real time to identify the beginning of a potential wear pattern. In the example shown the cable connectors represented the limiting factors. A particular response curve of the sensors can be recognized in reaction to the external thermal effects, since the short term transient errors which appear during the test are not compensated away. Elsewhere an increase in the signal-to-noise ratios, originating from wear in an external connector, can be seen. Essential for the evaluation of the test result is that at the conclusion of the selected test series, or for as long as possible during the tests, the sensors continue to function within specification. In the case of the Trafag high-pressure sensors, valid output signals were still measured at the end of the tests (0.5 V at ambient pressure).

SENSOR VALIDATION BY OPERATION ON LARGE ENGINES

Thin film technology with its inherent media-compatible design (no O-rings) allows sensors to operate on large engines using heavy fuel oil (HFO) where the viscous oil is preheated to up to 150 °C before injection (IFO 700 containing 2 % sulphur). After 3000 hrs operation on a large, nine-cylinder engine with common rail fuel injection only a very slight offset drift (< 0.5 % FS) was observed.

❻ shows the output of a high pressure sensor located near to the injectors of a large motor. Several such tests on various customer engines show that the injection pressure curve is measured exactly at different engine loads. The rapid, high amplitude changes in pressure as well as the easily recognised oscillations in the injector pressure tubing are reproduced without error or delay. In contrast to piezoelectric measurement techniques, the static pressure is measured relative to the ambient value. The peak pressures of up to 1600 bar generated by a unit pump system were faithfully measured and monitored.

CONCLUSION AND FUTURE PROSPECTS

The non-welded high-pressure sensor design described above allows reliable operation for the direct measurement of pulsating injection pressures in large internal combustion engines. The fast signal processing electronics with 10 kHz bandwidth permits optimization of the fuel injection modulation process by the motor control system. By using in addition new, economically priced sensors to monitor injector needle lift and cylinder pressure, the combustion process in each cylinder can be individually optimized, thereby allowing operators to reduce emissions, increase fuel efficiency and monitor engine health more closely.

REFERENCES

[1] Bogers M.; Haussner M.; Houben H.; Marto A.; Pechhold F.: Drucksensorglühkerze für Dieselmotoren. In: MTZ 65 (2004), No. 11, p. 888-894
[2] Gerlach G.; Werthschützky R.: 50 Jahre Entdeckung des piezoresistiven Effekts – Geschichte und Entwicklungsstand piezoresistiver Sensoren. In: Technisches Messen 72 (2005), No. 1, p. 53-76
[3] Marines I.; Bin X.; Bathias C.: An understanding of very high cycle fatigue of metals. In: International Journal of Fatigue 25 (2003) p. 1101–1107
[4] Wulpi D. J.: Understanding How Components Fail. ASM International edited by The Materials Information Society (1999)

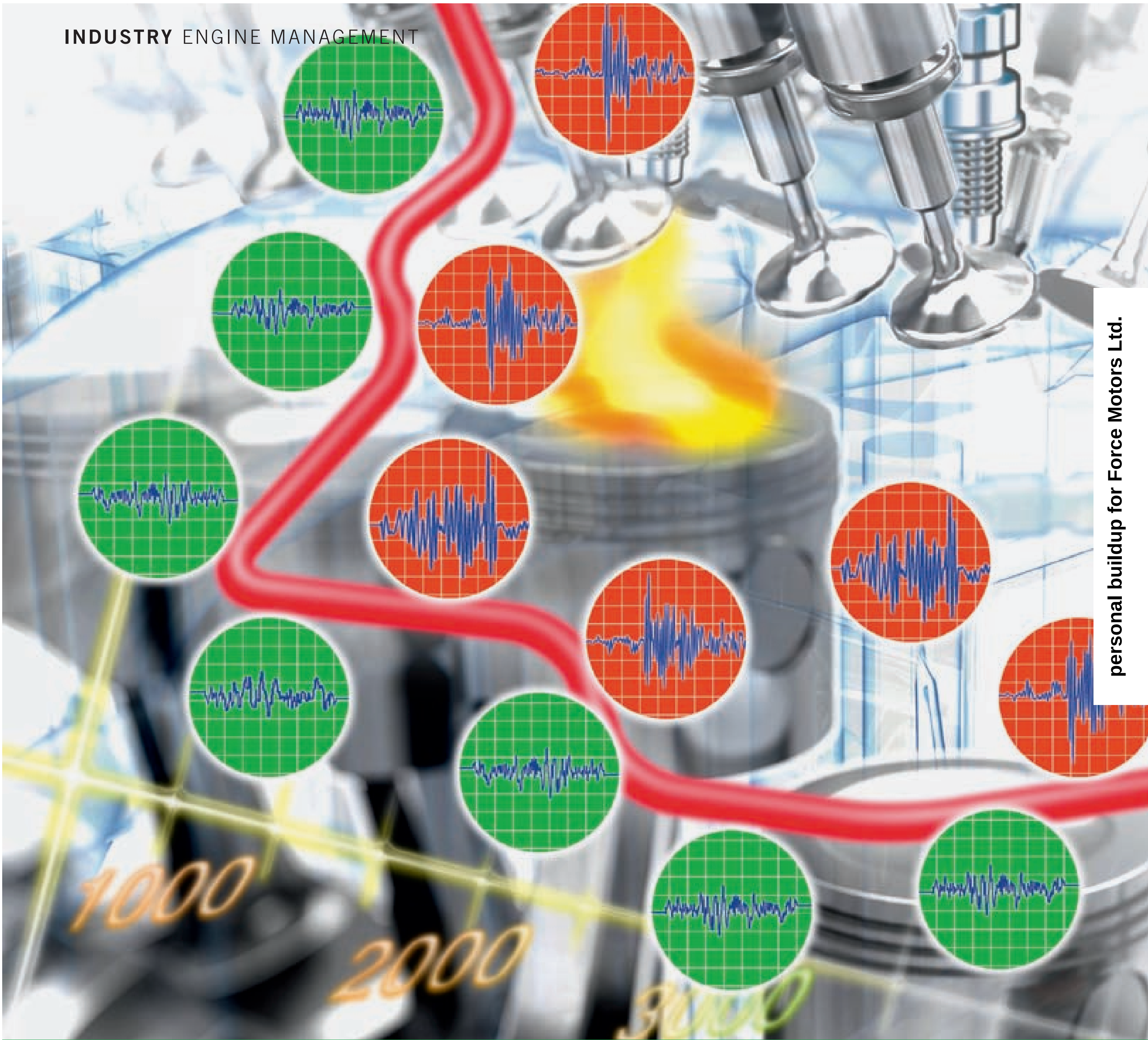

ROBUSTNESS INVESTIGATION OF A SVM-BASED KNOCK DETECTION METHOD

Knock detection on the basis of structure-borne noise signals that are processed through a sequence of filtering, rectifying, and integrating has been performed in series for many years. It is implemented in Bosch engine management systems that are used by automotive manufactures all over the world. The trend towards higher power density, lower fuel consumption and legal limitation of emissions calls for increasingly complex engines, thereby diversifying the requirements for reliable knock detection.

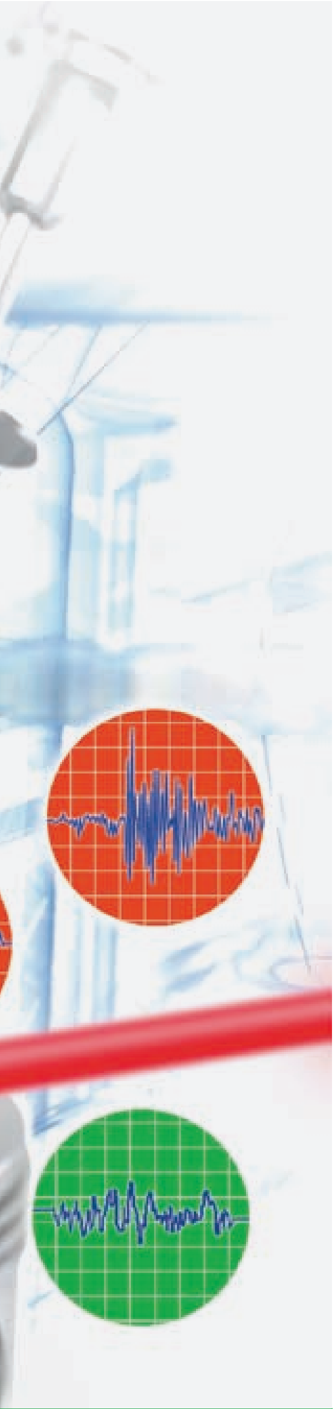

AUTHORS

M. SC. KUNCUP ISWANDY
is a Research Assistant at the Institute of Integrated Sensor Systems in the EIT Department of TU Kaiserslautern (Germany).

DIPL.-ING. STEFAN KEMPF
is Calibration Expert for Knock Control in the Calibration Developement Department for Knock- and Boostpressure – Control in the Diesel Gasoline Systems Business Unit at the Robert Bosch GmbH in Schwieberdingen (Germany).

PROF. DR.-ING. ANDREAS KÖNIG
is Head of the Institute of Integrated Sensor Systems in the EIT Department of TU Kaiserslautern (Germany).

DIPL.-ING. ROBERT SLOBODA
is Technical Lead in the Calibration Developement Department for Knock- and Boostpressure – Control in the Diesel Gasoline Systems Business Unit at the Robert Bosch GmbH in Schwieberdingen (Germany).

MOTIVATION

Background noises exhibiting high signal energy in the frequency ranges of knocking combustions that cannot be separated timewise from the knock occurrence necessitate research of new knock detection (KD) approaches that are based on non-linear, supervised methods such as the Support Vector Machine (SVM). One of the focal points of the research study was the statistically meaningful investigation of robustness and generalization features of the methods. The SVM method was proven to provide convincing background noise suppression.

Various proceedings are known in the field of pattern recognition that are based on linear and non-linear as well as supervised and unsupervised approaches. The non-linear, supervised methods are characterized by a problem-adapted, potentially high differentiation ability. For this reason, these methods are referred to in automotive technical literature in conjunction with KD, or misfire detection. So far, practical application has been prevented by several factors, such as high computing time in the electronic control unit, minor predictive capability, and possibly surprising generalization features. In particular, the effective method of SVM [1] is of interest to KD but to date has only been investigated principally with statistically limited data [2]. The Institute of Integrated Sensor Systems (ISE) at the University of Kaiserslautern in cooperation with the Robert Bosch GmbH have accepted the challenge to research new KD methods and have conducted statistically extensive studies of Support Vector Machines (SVM) and variations of it. The employed data set included extensive data from real engine measurements of two different engine concepts at considerably different points in their life cycles (engine aging) over a wide speed/load range. Furthermore, measurements were included in the study that were taken at a high background noise level (e. g. due to piston slap). The KD has problems in mastering these conditions with a single-filter concept.

NON-LINEAR SUPERVISED LEARNING FOR KNOCK DETECTION

Linear classification methods can efficiently be applied to linear, separable problems, to which the KD normally does not belong. Therefore, non-linear classifiers such as k-Nearest-Neighbour

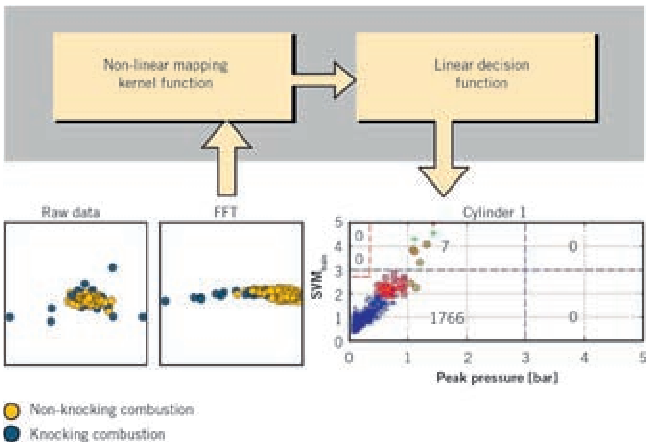

❶ Distance-preserving 2D visualization of combustion data

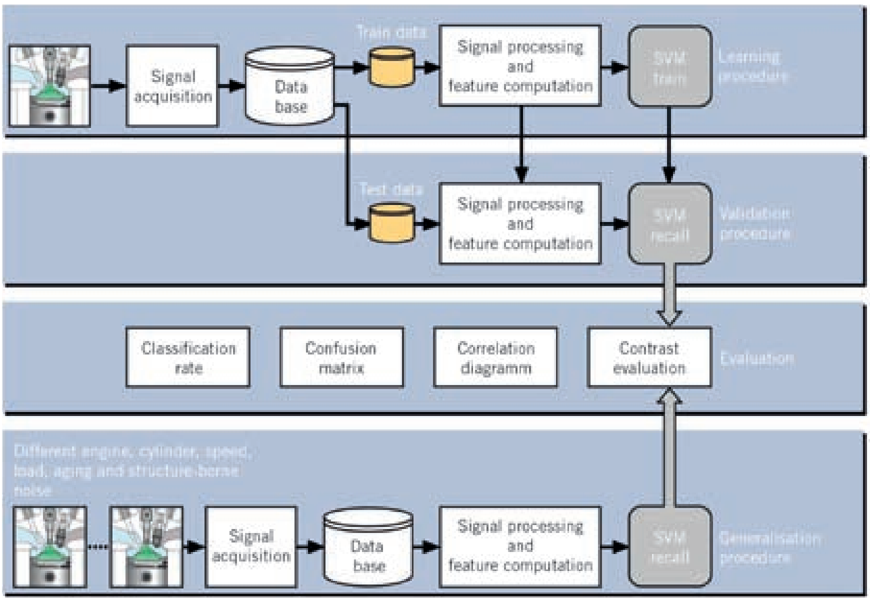

❷ Examination process of the SVM in the KD

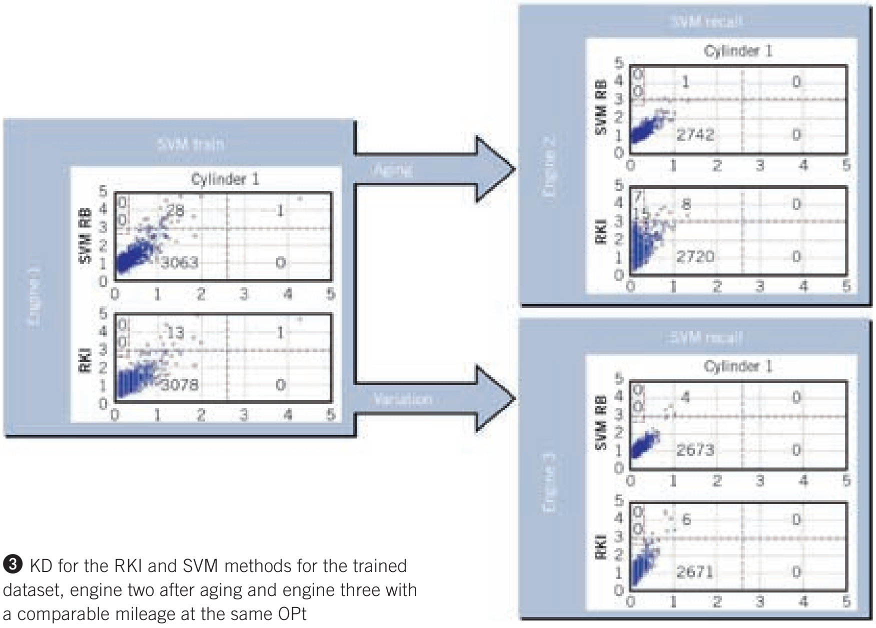

❸ KD for the RKI and SVM methods for the trained dataset, engine two after aging and engine three with a comparable mileage at the same OPt

(k-NN), Probabilistic-Neural-Networks (PNN), Restricted-Coulomb-Energy (RCE), SVM, and so on are often considered. The SVM is characterized by a special generalization capability and in the latest research with a moderate and continually decreasing computation and memory demand – thus making it attractive for a resource-efficient ECU implementation.

To begin with, the high-dimensional KD data cannot be analysed and interpreted. For the task of visualizing the data, ISE is developing methods and tools that, among others, make use of distance-preserving projections [3] for data visualization. ❶, shows this kind of representation of knock sensor raw data and the power-density spectrum of the respective Fourier transform (FT).

As can be seen in, ①, the raw signal cannot easily be separated into knocking and not knocking combustions. For the FT data, however, a much better separability is evident – a fact that is confirmed in a later experiment.

The basic idea of the SVM [1] is to optimally fit a separating hyperplane into the possibly high-dimensional feature space, such that the smallest distance (the so called margin) between the separating hyperplane and the points on the class boundaries is maximized. The vectors that are selected by the training are also referred to as support vectors (SV) and determine the position of the separating hyperplane. Additionally, misclassification of some data vectors between the classes can be allowed in the training in favour of an extended margin. Basically, the SVM is a two-class classifier that calls for a multiple-class expansion. For the KD only two classes exist, though.

For non-linear separable problems, the SVM can be expanded non-linearly by kernel functions [1], e. g. polynomial or radial basis functions (RBF). Here, the response of the SVM depends on two parameters that are selected by the user: σ (width of RBF kernel) and C (margin width). If required, suitable parameters can also be determined by means of grid search or by evolutionary computing.

For a compact and invariant representation, it is advisable to condition the raw sensor data by means of an adequate signal processing for recognition tasks and to extract suitable features. Here, the FT and spectral filtering were used and confirmed to be sufficient. The short time FT and the wavelet transformation, the moving-scaled-harmonics, or the Wigner-Ville distribution constitute alternatives. For the KD, a cylinder pressure threshold value can be defined from the filtered cylinder peak pressure that is proportional to the engine speed, by means of which knocking and not knocking occurrences can be distinguished.

Correlation diagrams and correlation coefficients were used for the comparative assessment between the SVM and the tried and tested Relative Knock Integral (RKI) method, ❷. To analyze the KD, the cylinder peak pressure is divided linearly into 5 regions depending on the engine speed for each combustion event.

: definitely not knocking
: weak knocking
: normal knocking
: strong knocking
: strong knocking and reliably detectable.

The output of the SVM has been normalized for the correlation diagrams to be able to graphically compare the results of the established RKI method with the SVM method [4]. Two different normalization approaches with very similar results were examined. Below, only the method called SVM RB will be considered, which corresponds to the known RKI normalization on the basis of the reference level computation from the current KD algorithm implemented by the Robert Bosch GmbH.

APPLICATION OF SVM TO REAL DATA IN KNOCK DETECTION

To examine the applicability of the SVM to the KD, steady-state operating points (OPt) of different engines of the same type – with distinct differences in aging – were recorded and analysed, which formed the bases for the learning and test datasets for the SVM. Extensive studies of the SVM generalization features were conducted. The detection results were evaluated with the recognition rate, the confusion matrix, the correlation diagram, and the contrast, ②, and directly compared with the RKI method.

Measurements were taken on three- and eight-cylinder-engines with the Knock-Intensity-Detector KID2 and examined offline with the SVM method. An aged counterpart of the three-cylinder-engine was available and also included in the study. The measurement files were divided into 50 % training data and 50 % test data. At the same OPt., for example, the new engine was used for training, while the old engine was used for testing. The result of the SVM (SVM RB) was compared with the corresponding correlation diagram of the conventional KD (RKI). The SVM method yielded a comparably good KD quality for all engines, ❸. The aged engine provided consistent KD with the SVM trained on the new engine.

Moreover, the generalization capability and the robustness of the SVM for different cylinders, engine speed and load ranges were studied with regard to training and testing. This was done to be able to cover all ranges with the least possible effort, possibly even with only one SVM. This was realized by training the SVM at only one single OPt (3000 rpm, 77 % load) and then applying it to the entire engine operating range. The results were surprisingly good but did show that the KD quality decreased for the not specifically learned Opts. So as to achieve a consistently good KD quality across the entire engine operating range, a speed-dependent heuristic engine speed normalization model was developed for pre-processing that allows for a compact SVM that is applicable to all ranges, ❹.

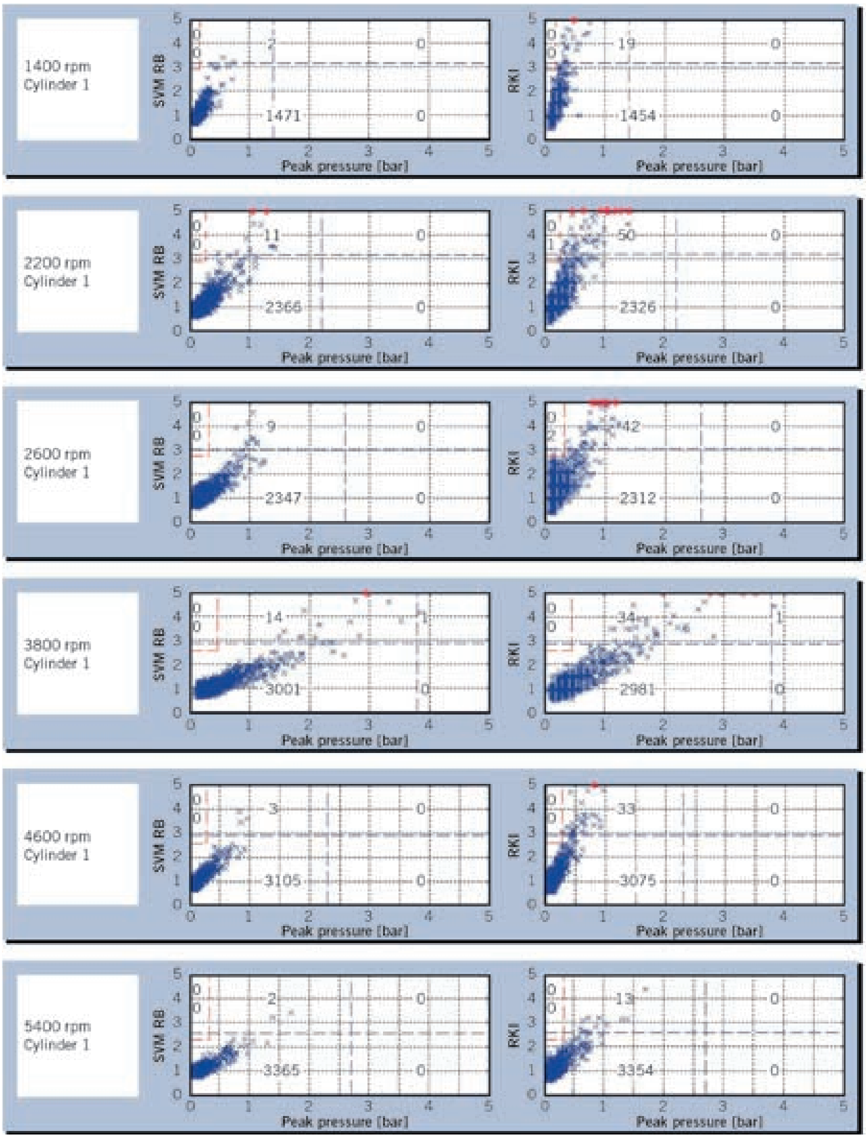

❹ RKI and SVM KD using model normalization for 1400 to 5400 rpm and 50 % load (SVM trained at 3000 rpm and 77 % load)

The SVM proved to be of particular advantage for an engine that featured distinct background noise due to piston slap in a small engine speed range around 2600 rpm. The RKI method was not capable of avoiding misdetections due to these background noises that occurred across a wide frequency range. Several datasets, one with knocking combustions and another with retarded ignition angles to assure an absence of knock occurrences, were examined with the SVM. Misdetection-free KD could be achieved with the SVM for the datasets with background noise, making it distinctly superior to the RKI method, ❺.

SUMMARY AND OUTLOOK

In the research cooperation between ISE and Bosch, an SVM in conjunction with a parametrizable normalization model in

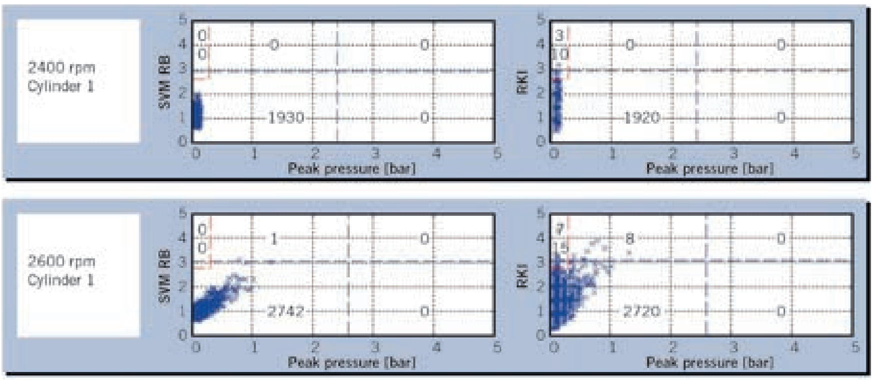

❺ KD quality when influenced by background noise during knocking and not knocking operation

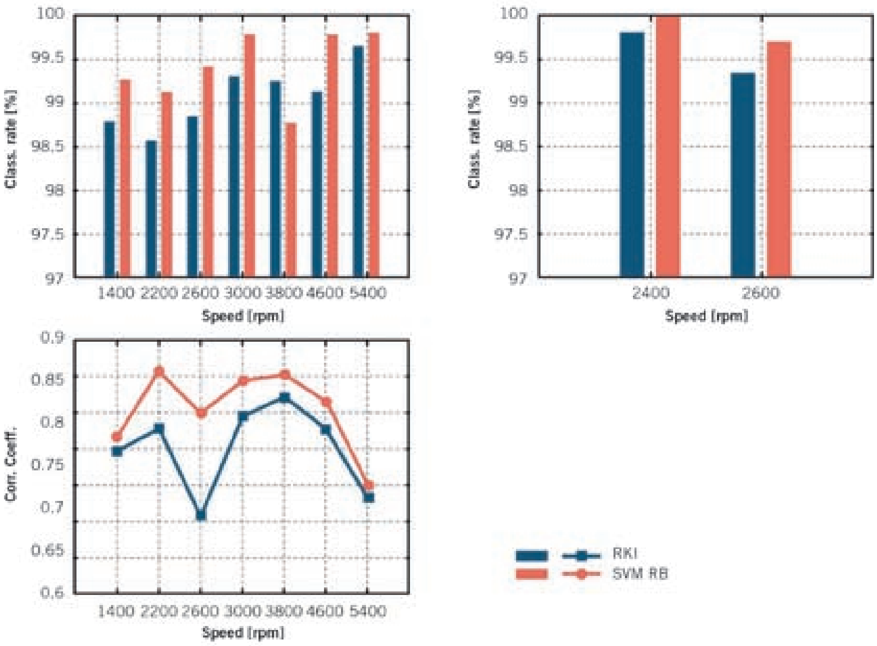

❻ KD rate for 1400-5400 rpm or 2400/2600 rpm by comparing the RKI and the SVM KD according to ④ or ⑤

the entire speed/load range was investigated as one of several approaches for KD using a statistically meaningful extent of real measurement data, including several engines with varying numbers of cylinders under the influence of aging and background noise. Summarizing, the SVM and the RKI method performed equivalently well in most instances, but in the case of background noise, the SVM was clearly superior, ❻. The approach must be developed further with regard to data reduction, frequency range limitation, and physical lucidness. Particular attention must be given to the problem of transferring this approach to real-time-computing hardware, so as to enable practical operation in a closed-loop control circuit for different engines, as well as computation during dynamic engine operation.

The results of the study constitute a first step into the direction of future engine management systems.

REFERENCES

[1] Burges, C. J. C.: A Tutorial on Support Vector Machines for Pattern Recognition. Data Mining and Knowledge Discovery, 2, 1998, p. 121-167

[2] Rychetsky, M.; Ortmann, S.; Glesner, M.: Support Vector Approaches for Engine KD. In: Int. Joint Conf. on NN (IJCNN'99), vol. 2, 1999, p. 969-974

[3] Sammon, J. W.: A Nonlinear Mapping for Data Structure Analysis, vol. C-18, No. 5, 1969, p. 401-409

[4] Sloboda, R.; Häming, W.; Fischer, W.: Toolkette zur effektiven Applikation von Klopfregelungssystemen. In: MTZ 65 (2004), No.1, p. 2-9

RING PACKS FOR FRICTION OPTIMISED ENGINES

Global environmental concerns are driving internal combustion engine designs. The worldwide legislations are setting up milestones to achieve the agreed vehicle emission goals. Development of innovative exhaust gas after-treatment systems is one approach to meet emission targets, new combustion strategies and improvement of engine mechanical efficiency is another. When it comes to reducing engine friction power losses (Friction Mean Effective Pressure), the power cell unit – and especially the piston ring pack – present great potential. Mahle calculates that the improvements could lead to a reduction of engine fuel consumption of up to 5 %.

AUTHORS

DR. DANIEL LÓPEZ MARTÍNEZ
is European Piston Ring Expert for Heavy Duty Engines at Mahle Motorenkomponenten GmbH in Stuttgart (Germany).

ENG. MARCOS VALVERDE
is Ring Dynamics Simulation Specialist within the Virtual Engine Development Department in Jundiaí (Brazil).

RÉMI RABUTÉ
is Product Expert Passenger Car Piston Ring Europe at Mahle France SAS in Rueil-Malmaison (France).

MSC. ANDRÉ FERRARESE
is Global Piston Ring Product Expert at Mahle Metal Leve SA in Jundiaí (Brazil).

CHALLENGES OUT OF ENGINE TECHNOLOGY EVOLUTIONS

The challenge to develop future power cell units (PCU) consists of reducing friction power losses and weight while maintaining „traditional“ functionality such as gas sealing, oil control and durability. This might require compromises in component design and only a system approach and a full understanding of the interactions in the engine allows for the best decisions.

Major technological evolutions on current and future engines have significant effects on the power cell unit and have to be considered as additional constraints in the continuous efforts to reduce the friction power losses generated by the ring pack. Although not exhaustive, the new engine characteristics that have a direct impact on the power cell unit environment could be classified in two main categories: those related to engine downsizing and increased power density and those related to lubrication.

Engine downsizing and increased power density – through greater thermal and mechanical loads – demand higher ring material and coating durability to support increasing cylinder pressure. Induced cylinder bore deformations, especially on lightweight engine block designs with limited cooling capacities (in regards to the targeted power density), require increased ring conformability. Higher thermal and mechanical loading applied on lightweight piston designs generates higher temperatures and deformations on piston grooves and lands. Thus specific ring features are needed to guarantee optimum management of gas and oil in the piston ring belt area to maintain acceptable blow-by and carbon deposit levels.

The piston ring pack lubrication necessary to maintain its efficiency over the engine lifetime is also greatly affected by several new engine evolutions. The lubricant protective properties, already stressed by higher operating temperatures, are also reduced due to fuel interaction. This frequently results in higher fuel dilution levels (Gasoline Direct Injection-GDI, Flex-fuel, post-injection strategy for Diesel particulate filter regeneration). The latest combustion strategies and the extensive use of exhaust gas recirculation to reduce NO_x emissions also pollutes the oil by increasing the level of soot and mixed combustion products.

Successful low friction ring pack implementation demands an interdisciplinary approach involving tribology, material science, numerical simulation, design, testing and manufacturing.

Emissions legislation milestones, reduced engine development lead time, and continuously evolving PCU operating conditions require efficient investigation techniques to simulate and validate the numerous ring pack design options and product technologies necessary to reduce ring pack friction power losses while maintaining or improving engine blow-by, oil consumption and durability.

LOW FRICTION RING PACK INVESTIGATION TECHNIQUES

Power cell FMEP reduction is one of the focal points of the Mahle R&D plan. For this purpose, several experimental and analytical investigation techniques have been implemented. On the experimental side, traditional tribological test rigs are used by material sciences – in the course of coating development – to assess the dry friction coefficient of rubbing parts. The next step is the floating liner single-cylinder technique to measure the trace of instantaneous friction force from the PCU [1]. The final step is the friction test cell to define the engine FMEP by subtraction of the measured Brake Mean Effective Pressure (BMEP) from the Indicated Mean

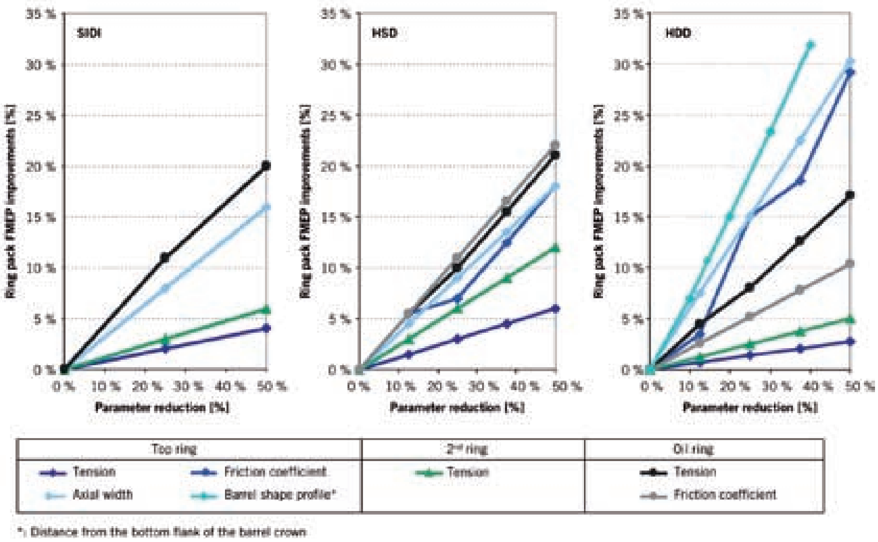

❶ Friction reduction sensitivity given isolated ring pack parameters (not to be added)

Effective Pressure (IMEP) [2]. These tools are complementary and used at different steps of a low friction ring pack development process.

On the analytical side, Mahle has been involved for several years with major engine manufacturers in a consortium at the Massachusetts Institute of Technology to perform fundamental research on the PCU-System. Among others, models were developed to study ring dynamics, ring/piston groove interaction, gas flows and ring/liner lubrication and their influences on blow-by, friction and oil transport.

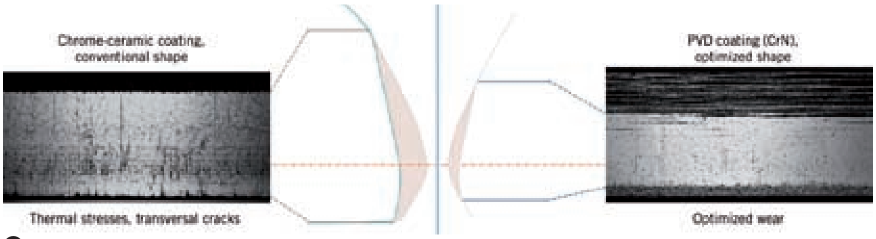

❷ Durability of CrN coatings

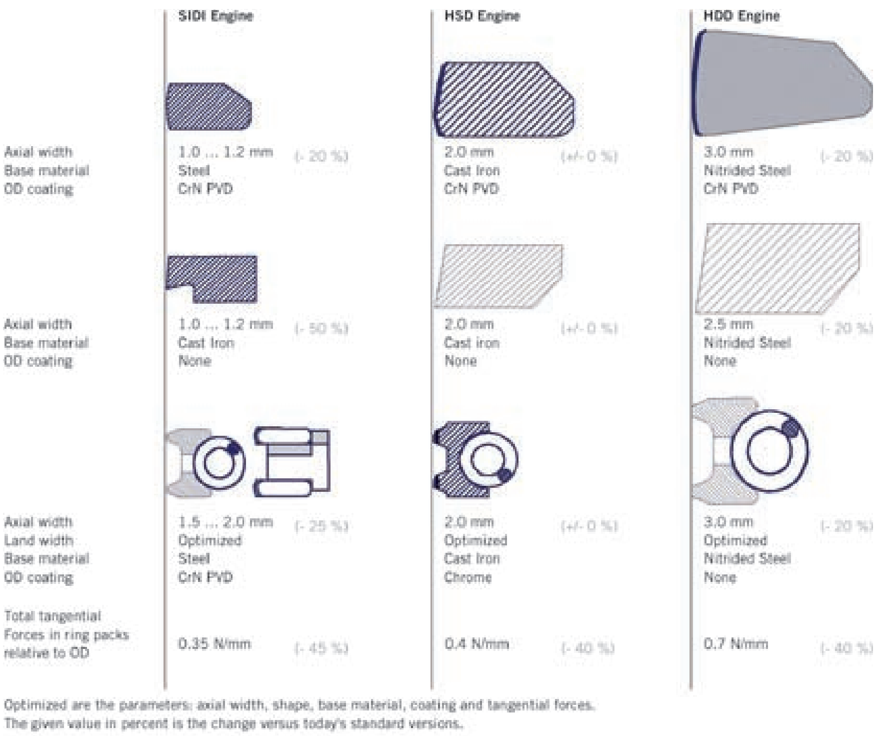

❸ Examples for friction optimised piston ring packs for the examined engine types

PARAMETRIC STUDY: RING PACK DESIGN FEATURES POTENTIAL TO REDUCE FMEP

In order to identify general piston ring design trends and rank their potential in reducing FMEP, a parametric study on different engine platforms (Turbocharged Spark Ignited Direct Injection (SIDI) engines, High Speed Diesel (HSD) and Heavy Duty Diesel (HDD) engines) was carried out. Although the main ring characteristics known to reduce ring pack friction are reduced tension, reduced axial width, and the use of coatings/treatments with low friction coefficients, it is of interest to quantify their potential in different operating conditions. ❶ presents the calculated ring pack FMEP reduction given the changes on the analysed parameter. The results in this figure were all simulated at rated power condition to facilitate engine platform comparison. One can observe that for Heavy Duty Diesel (HDD) applications a significant ring pack FMEP reduction can be achieved by optimising top ring design. This is due to the high peak cylinder pressure and the fairly significant top ring axial width present in these applications. A more pronounced barrel shape profile to counterbalance gas back pressure around Top Dead Center (TDC) compression/expansion to reduce boundary friction along with a low friction coefficient coating to limit its influence on FMEP is definitively a good direction to go as long as ring/piston groove flank wear can be kept to a reasonable level.

Top ring design features offer less potential on High Speed Diesel (HSD) and turbocharged Spark Ignited Direct Injection (SIDI) engines than on trucks because of lower axial width and peak cylinder pressure, ①. For these two passenger car applications, oil ring tension shows the biggest potential to reduce ring pack FMEP. High conformability oil rings with narrow and highly wear resistant outer diameter contact surfaces are then needed to conform to distorted bores and apply reasonable unit pressure with a low tension. On the HSD engine, the investigated oil ring along with a specific cylinder bore surface finish and a higher wall temperature enhances boundary friction and hence the potential of oil ring coating low coefficient of friction. For the three studied platforms, the 2nd ring is showing the lowest potential.

For turbocharged Spark Ignited Direct Injection (SIDI) engines, one can notice that a 20 % improvement in top ring coating dry coefficient shows a simulated above 5 % reduction ring pack FMEP. Applying a measured dry coefficient difference between gas nitrided steel and CrN coating (applied by physical vapor deposition – PVD) of around 20 %, a 5 % ring pack FMEP reduction was measured on a floating liner single-cylinder device [1].

Obviously, this parametric study is generic and as explained earlier these features potential to reduce FMEP could be ranked differently depending on specific engine designs and operating conditions. However, the continuously improved simulation tools used at Mahle offer the possibility to identify in detail the specific piston ring features, where a special attention should be given to efficiently reduce FMEP. This approach combined with an extensive product portfolio allows Mahle to apply the needed ring technologies for each specific engine. It also allows for identifying the improvements needed on other PCU components.

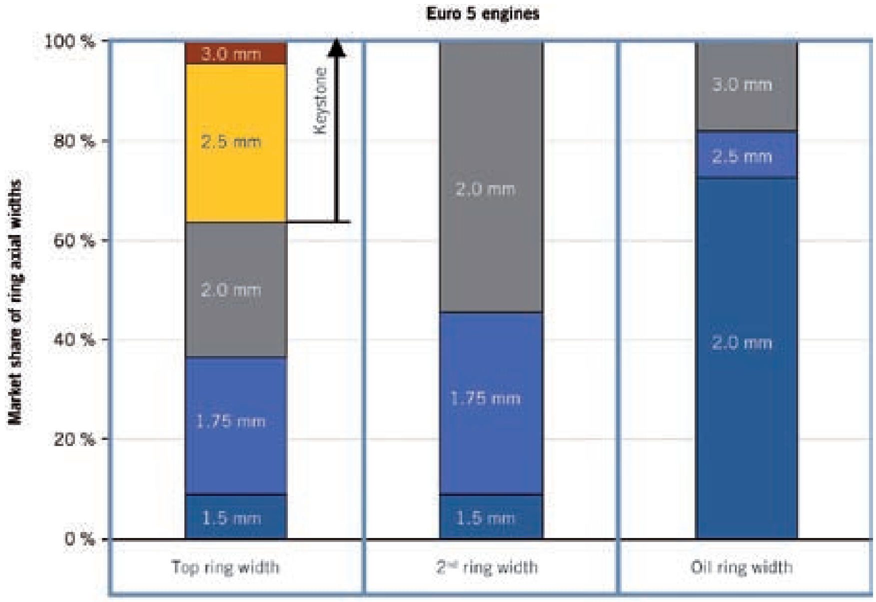

❹ Overview of market shares of ring axial width for Euro 5 engines applied for the separate rings of the pack

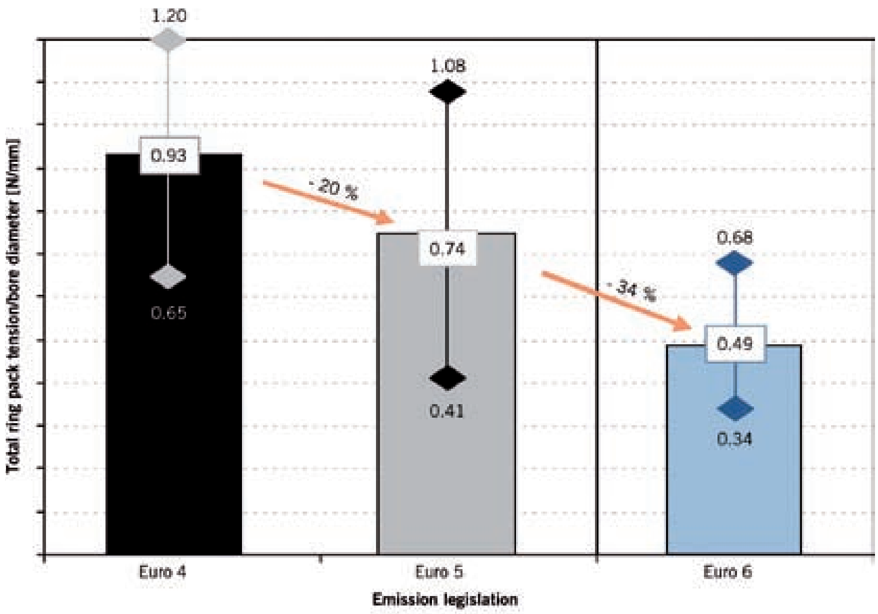

❺ Ratio between total ring pack tension and bore diameter for passenger car diesel engines depending on legislation levels

LOW FRICTION RING PACK APPLICATION APPROACH

Successfully implementing a low friction ring pack requires not only component optimisation, but also a system approach with a good understanding of the engine governing factors.

Increased engine blow-by and oil consumption or decreased durability are not allowed to satisfy the required FMEP reduction. To solve these issues and offer a robust system (ideally after the engine combustion strategy is fixed), an optimisation of the engine block architecture and cooling is needed to offer a good PCU environment. An optimised lightweight piston design is the next structural task to execute correctly before starting the tribological work. Traditional structural and wear limits have to be continuously increased to expect significant improvement of the already fairly optimised PCU. For that purpose a large choice of component materials and coatings are available in the system portfolio along with a good understanding of their interactions so that the best compromises and synergies can be achieved. As an example for the High Speed Diesel engine piston ring portfolio, ❷ illustrates the improved durability performance offered by CrN PVD top ring coatings compared to industry standard chrome ceramic coatings. This improved wear resistance, by upgrading the piston ring durability limits, allows more aggressive design toward low friction ring packs.

Ring pack FMEP reduction efforts can be observed in recent years for all engine types. Low friction ring pack examples for the three different engine types are presented in ❸.

Friction reduction is more intensive for passenger car applications due to the high focus on CO_2 emissions. ❹ illustrates the situation for High Speed Diesel engines in regard to market share for ring axial width. One can observe in this benchmarking overview that low axial width rings are being already applied for many Euro 5 applications even as peak cylinder pressure increases. This progress can be achieved through the use of state of the art materials and coatings only.

OUTLOOK

The ratio of the total ring tension of all rings in the pack relative to the nominal bore diameter is a good measure to see how far a ring pack is optimised in terms of tangential forces.

❺ shows that this ratio will be roughly divided by 2 for the ring packs used for Euro 4 to those in new Euro 6 engines. These improvements allow significantly reduced ring pack FMEP. For passenger cars, ring pack FMEP investigations are usually performed at part load engine running conditions (e.g. 2000 rpm – BMEP = 2 bars). The potential of ring packs for engine fuel consumption was measured to be up to 5 % reduction.

REFERENCES

[1] Tomanik, E; Ferrarese, A.: Low Friction Ring Pack for Gasoline Engines, ASME, ICEF1566, Sacramento, USA, 2006

[2] Ehnis, H.; Deuß, T.; Freier, R.: Friction Mapping – Reibleistungsmessungen am befeuerten Vollmotor. In: Tagungshandbuch 11. Symposium Dieselmotorentechnik, Technische Akademie Esslingen, 2008

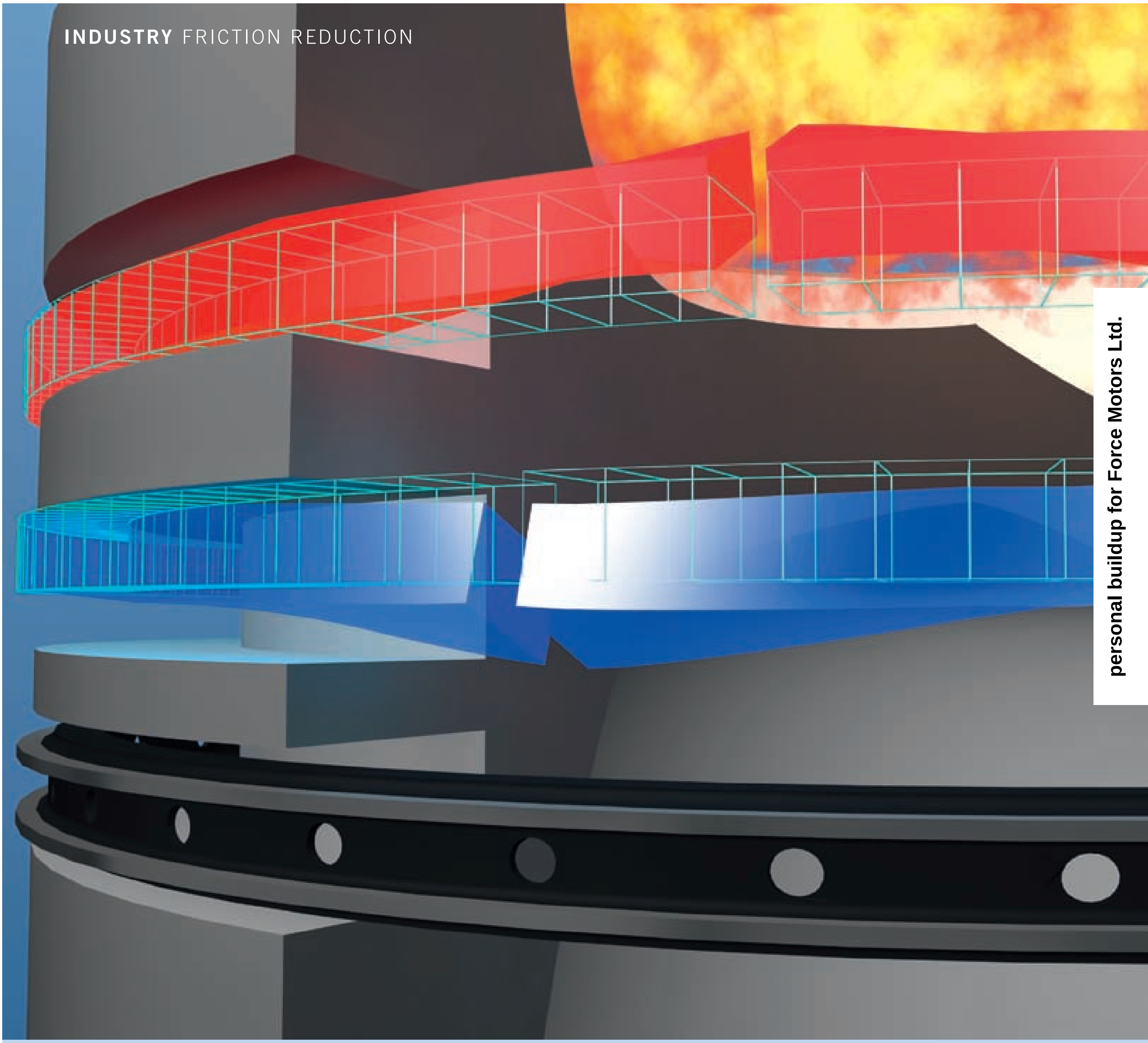

DETAILED 3D RING PACK ANALYSIS

Demanding emission targets for combustion engines must be fulfilled in increasingly shorter development cycles. Federal-Mogul utilizes the 3D Ring Pack Analysis to quickly and precisely simulate piston rings during a position change. An application example with a reduction of 15 % blow-by gas shows the potential of possible optimization measures.

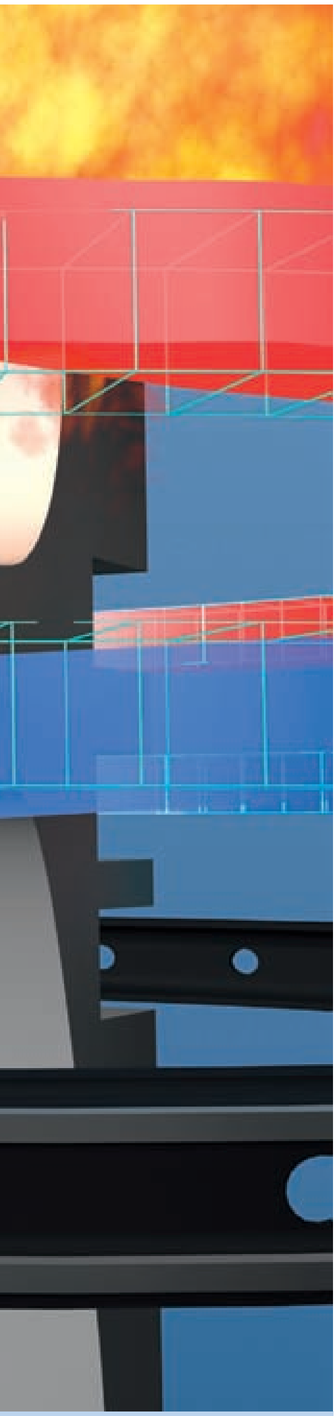

AUTHOR

DIPL.-ING. RICHARD MITTLER
is Manager of the Analysis and Product Development Department in the Area of Piston Rings and Liners at Federal-Mogul Burscheid GmbH in Burscheid (Germany).

INITIAL SITUATION

Increasing demands must be fulfilled regarding the sealing system comprising pistons, piston rings and cylinder liners. In addition to long running times and service intervals, strict emission limits must be complied with and given first priority. The sealing system can contribute to this by reducing oil loss, optimizing friction and reducing blow-by (a loss of gas in the crankcase). Two aspects make this challenging. On the one hand, the optimization of these parameters has, as a rule, already achieved a rather high standard. On the other hand, owing to diverse interactions, the dynamic sealing system reacts sensitively to small changes. The movement of the piston rings during a position change is particularly critical.

2D software tools model the behavior of ring dynamics during a power stroke. However, 2D tools are not able to clearly describe the progression of ring dynamics. Without an explicit gas dynamic solution, the ring movement can only be simulated as a rapid change from one position on the bottom groove flank to the position on the top groove flank. This change of position is triggered purely by inertial forces. The reality, however, is much more complicated. At the Aachener Kolloquium 2009, Federal-Mogul presented a new tool to the trade called Moris, which shows the importance of changes in piston ring position, not only in piston rings with non-rectangular cross sections but also in simple rectangular rings.

OPTIMIZATION MEASURE IN THE ENGINE

One of the now numerous engine projects exemplifies the validity of the tool. The aim of the optimization was a reduction of the blow-by volume. The unit is a four cylinder Otto engine with a cubic capacity of 2 liters. This engine has an engine power of 75 kW at 5600 rpm, 130 Nm torque at 4600 rpm as well as a peak pressure of 86 bar at 4000 rpm. At the selected operating point of 4600 rpm, the engine shows a blow-by ranging from 42 to 45 l/min on the

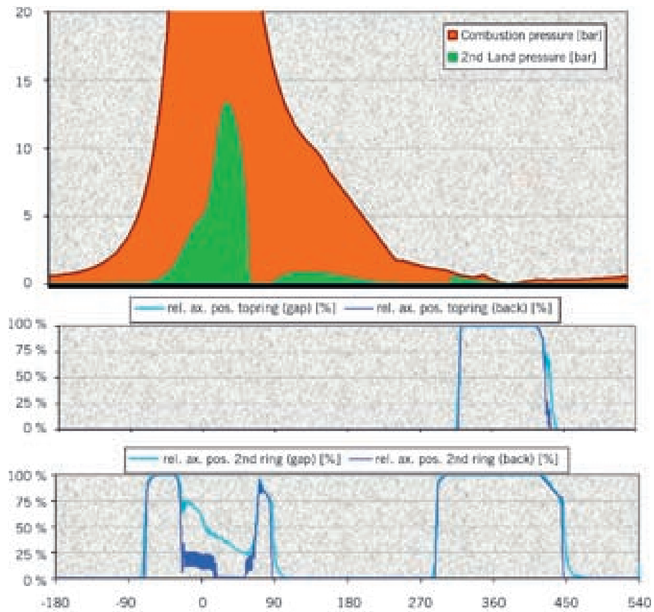

❶ Starting point of pressure relationships and the ring movement percentage in the investigated 2 liter, four cylinder Otto engine

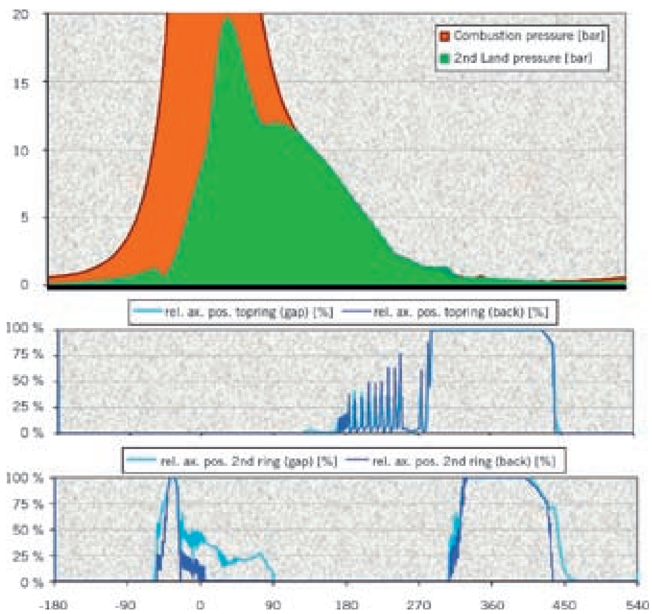

❷ Effects of reduced closed gap on the second ring

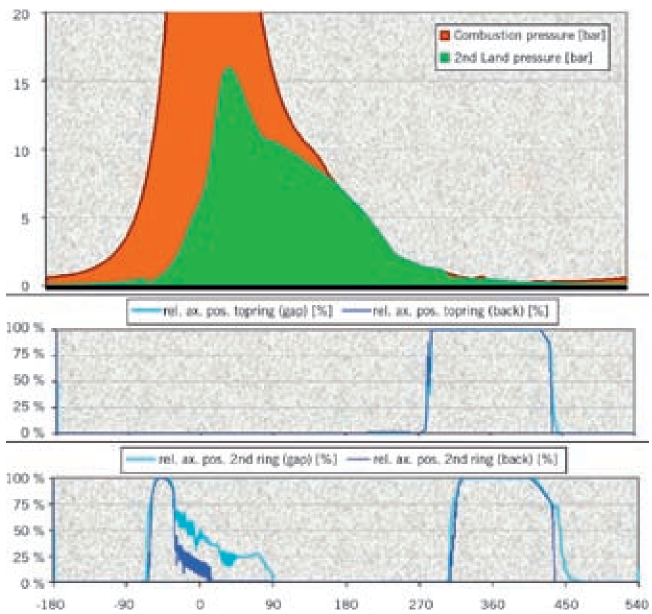

❸ Comprehensively optimized piston-piston ring system with approximately 15 % less blow-by

engine test bed. A ring pack comprising a rectangular ring in the first groove, a taper-face ring in the second groove as well as a two piece oil scrape ring are used to dynamically seal the combustion chamber.

With the help of the new 3D simulation tool, the actual relationship between intermediate ring pressure values and ring movements were demonstrated in the engine, ❶. From a mathematical point of view, the result was an intermediate ring pressure value of 14.4 bar and a blow-by of 44.8 l/min. Simulated values and real values corresponded well, as the measured blow-by was between 42 and 45 l/min. The sudden decrease of the intermediate ring pressure is clearly discernible and results from the movement of the second ring during the combustion phase.

In current designs, the ring gap of the second ring is used to stabilize the entire behavior of the system. The development of the intermediate pressure and its influence on the desired behavior of the first ring therefore depends on the sealing properties of the second ring. In this case, the ring gap is typically opened gradually due to missing detailed information. However, this can result in an increase in blow-by.

If the closed gap of the second ring is reduced in the course of the optimization in order to reduce blow-by, the 3D simulation immediately shows an increase of the intermediate ring pressure to almost 20 bar. By this measure, the behavior of the second ring is stabilized, and blow-by falls to 33 to 35 l/min. This analytically calculated improvement was verified on the test bed. However, oil consumption also rose. Sensitivity analyses and design modifications made the cause of this clear, ❷. The first ring is in an unstable position and flutters in the exhaust phase during which it cannot find a stable position on the piston groove flanks and therefore no longer seals effectively. This results from the higher intermediate ring pressure, which destabilizes the first piston ring. Without being able to recognize these procedures in detail, the smaller closed gap would likely be ruled out as an optimization measure.

However, thanks to the 3D simulation, the actual ring behavior during a position change is known and a targeted optimization was possible. The intermediate ring volume was thus optimized and simultaneously adapted to the smaller closed gap of the second ring. ❸ shows the effect of this optimization on a system level. The intermediate ring pressure now reaches 16 bar and, as a result of this moderate increase in comparison to the initial situa-

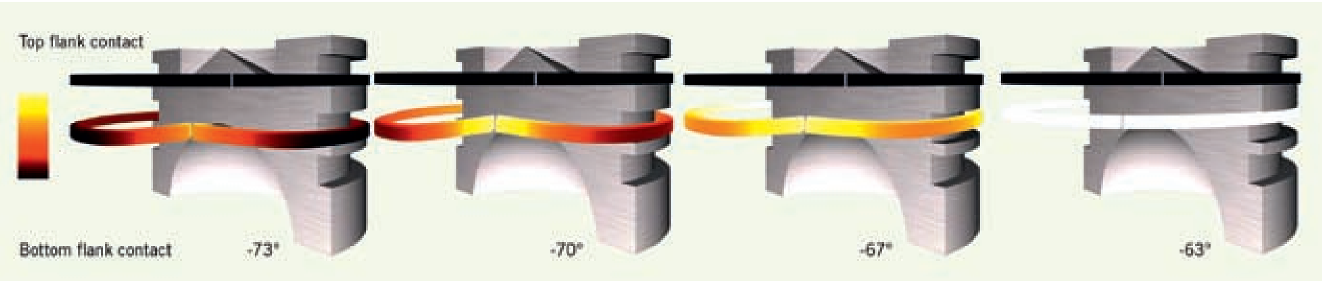

❹ Simulation of the movement of the compression ring and the second ring during the combustion cycle tion (as shown in ①), the second ring is in a more stable position during the combustion phase. As a consequence there is no more fluttering of the first ring. By means of these targeted and harmonizing single measures, the blow-by was reduced to 36 to 38 l/min, without having an effect on the oil consumption. The result is equivalent to an improvement of approximately 15 %.

CAUSES OF PISTON RING DYNAMICS

During every power stroke of the piston, the piston rings pass through highly dynamic movements. Under the influences of forces and moments, they change position in different cyclical areas, from a position on the top edge of the groove to a position on the bottom edge of the groove where the rings are supported against the various influences of forces and directions of movement.

As shown in the simulation, gas and friction forces not only create axial forces but also moments regarding the piston ring's center of gravity. Therefore, the position change already occurs when the total force can no longer overcome these moments. Situations can occur where the position change can extend over several degrees of crank angle (up to 60°), during which the piston ring no longer seals uniformly but is surrounded by combustion gases.

❹ shows the simulation's visualization of the actual movement behavior of the compression ring and the second ring at approximately 70° before TDC. While the top ring achieves a stable position on the bottom groove flank as a result of the already existing high compression pressure, the taper-face ring is forced into motion by the acting forces and moments and shows a twist as well as an axial direction component. During the motion from the bottom to the top groove flank, the ring supports itself on the bottom groove flank (ring back) as well as on the top groove flank (gap end). This is initiated as the piston ring withdraws from the twisting motion at the gap ends, resulting from the higher degree of freedom at the gap ends.

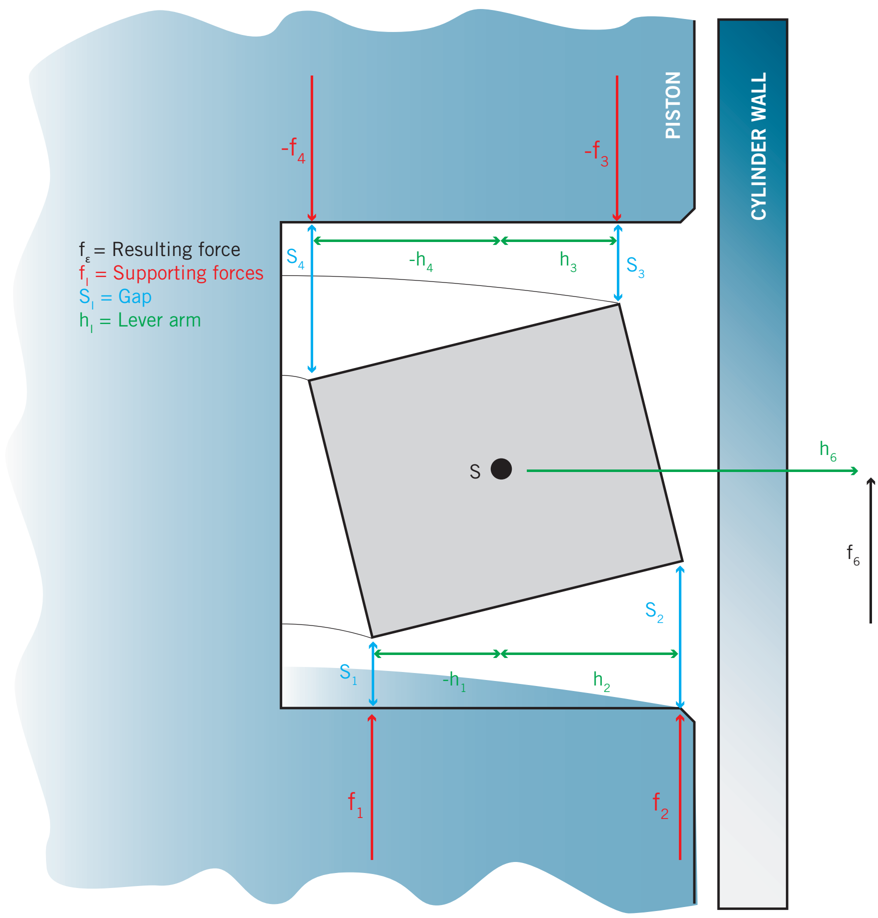

❺ Schematic figure of the supporting forces and acting moments on a piston ring

DEFORMATION OF THE PISTON RING BY FORCES AND MOMENTS

All piston rings experience radial bending when mounted into the groove. The main axes of the moments of inertia of rings with non-rectangular cross sections are not perpendicular to the cylinder axis due to the asymmetrical cross section. Such rings attempt to resist radial bending by twisting and arching in an axial direction. But even a ring with a symetrical cross section twists and arches if it is loaded with moments or axial forces and even when the forces or moments are constant on the circumference. The calculation and derivation of the differential equation for the twist and bending (induced by forces and moments of the gas dynamics in convergent and divergent grooves), while taking the reacting supporting forces as well as the mass and friction forces into consideration, are explained in detail in [1]. The supporting forces and the result-

❻ Kinematic acting mechanism to describe the stability of the piston ring position on the groove flanks ing movement behavior result from a reaction to the twisting and bending in the piston groove, ❺.

❻ describes the kinematic acting mechanism for a criterion that describes the stability of the piston ring position on the groove flanks by means of a very simplified model. Here, the course of pressure in the groove flanks is seen as linear and the low friction force is neglected. The total force comprises the forces of mass and gas. The total moment equals the gas moment, as the force of mass acting at the center of gravity does not exert a moment.

EQ. 1

$$F = F_{mas} - \frac{1}{2}\, a\, \Delta p$$
$$M = M_{gas} = -\frac{1}{12}\, a^2\, \Delta p$$

To achieve equilibrium, the moment is supported by the lever arm h.

EQ. 2

$$(F_{mas} + F_{gas})\, h = M_{Supporting\ force} = M$$

EQ. 3

$$h = \frac{-\frac{1}{12}\, \Delta p\, a^2}{F_{mas} - \frac{1}{2}\, \Delta p\, a}$$

If the lever arm is mathematically outside the piston ring, a support on only one groove flank is not possible. The equilibrium of forces and moments of a ring then requires the supporting forces on the top and bottom groove flank. Therefore, the following criterion is found for the stability of the position on only one groove flank:

EQ. 4

$$-\frac{a}{2} \leq h \leq \frac{a}{2}$$

The insertion of the new criterion in the equation results in:

EQ. 5

$$F_{mas} \leq \frac{1}{3}\, \Delta p\, a \quad \text{or}$$
$$F_{mas} \geq \frac{2}{3}\, \Delta p\, a$$

GAS DYNAMICS

The calculation of gas flows and the resulting pressure is a fundamental component for the calculation of ring movement. It is not sufficient only to calculate the flow volume as the condition p(x), (position-related pressure in the axial clearance) decisively determines the position and twist of the piston ring. The flow rate is constant in the axial clearance but the gas pressure is dependent on the gap geometry. The position and deformation influence the gap geometry.

The gas flow solution is carried out under the following physical properties: The flow is a subsonic flow. The sound velocity cannot be exceeded in the axial clearance. Due to the proportion of axial height to length, a solution is only possible if the friction in the clearance and the resulting heat exchange are taken into consideration. The mathematical solution of the flow can therefore neither be carried out isothermally nor adiabatically.

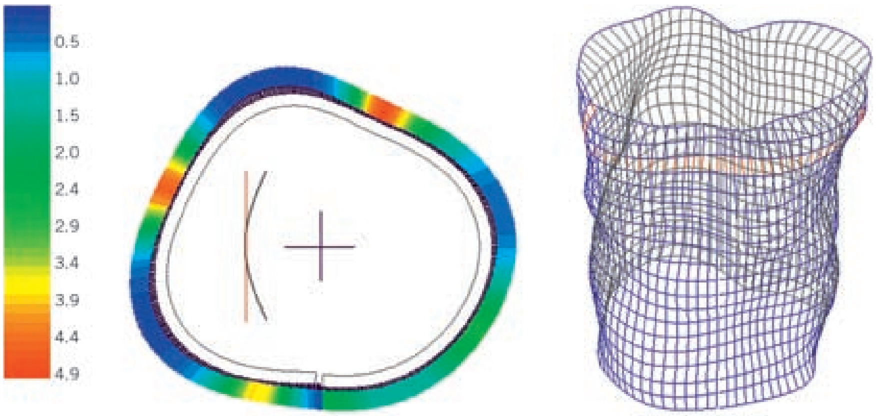

❼ Three dimensional analysis of hydrodynamics under the influence of cylinder distortion and radial pressure

HYDRODYNAMIC FORCES AND FRICTION

In addition to gas and mass forces, and the resulting moments, radial forces from hydrodynamics and friction are exerted on the piston ring. The radial forces, the residual stress of the ring and the pressure of the dead volume behind the ring are in balance with the oil pressure between the cylinder wall and the running surface. Boundary conditions for the oil pressure are the gas pressures above and below the piston ring.

A solution of these processes via the FEA would lead to impracticable calculation times due to the required short time intervals and the amount of load and rotational speed points, which would be counterproductive for short development cycles. Instead, the method integrated in Moris solves the cylinder deformation directly. The known stress and bending behavior serve as a basis for this. To determine the radial forces on the piston ring, its elastic properties are mathematically described and brought into balance with the oil pressure between the cylinder wall and the running surface of the ring. Pressure and oil film thicknesses are solved with the help of Reynold's differential equation under consideration of each of the stiffness matrices as well as the radial displacement (caused by cylinder distortions), temperature components and piston ring radial pressure distribution, ❼.

SUMMARY

The new 3D simulation tool, Moris, enables Federal-Mogul to analyze the real movement of piston ring position changes in detail. The validity and accuracy of the 3D analysis is shown in engine optimization. The better understanding of real processes influences targeted optimization measures on the complete piston, piston ring and running surface system level. Moris works thoroughly analytically and solves the movement behavior in a direct and targeted way. The tool consciously avoids using indirect ways via FEA programs to ensure an acceptable simulation speed on common work stations. Thus, the effects of design variations are speedily determined and short development cycles are supported.

REFERENCE

[1] Mittler, R., Mierbach, A., Richardson, D.: Understanding the fundamentals of piston ring axial motion and twist and the effects on blow-by, ICES2009-76080, May 2009

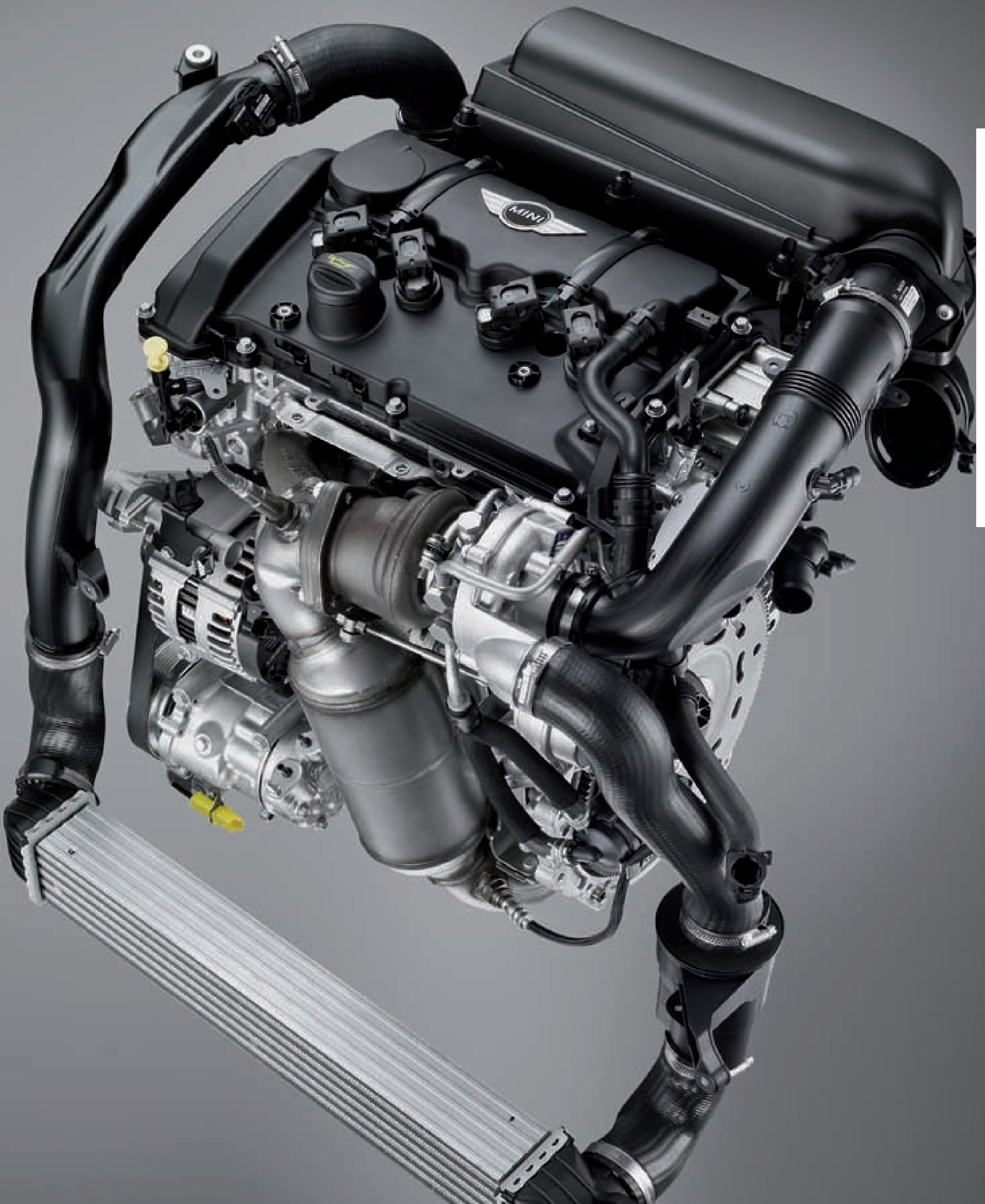
MINI

THE NEW MINI ENGINE WITH TWIN POWER TURBO

AUTHORS

DIPL.-ING. BERNHARD LECHNER
is Team Leader of Drivetrain Performance for Small Inline Engines within the BMW Group in Munich (Germany).

DR.-ING. GERRIT KIESGEN
is Head of Small Inline Engines Projects within the BMW Group in Munich (Germany).

DIPL.-ING. JENS KRIESE
is Manager of Small Inline Engines Project within the BMW Group in Munich (Germany).

DIPL.-ING. JOHANN SCHOPP
is Head of Design for V-engines and Cooperation Engines within the BMW Group in Munich (Germany).

With BMW providing leadership, the BMW Group and PSA Peugeot Citroën have jointly developed a new family of small four-cylinder gasoline engines, which since 2006 is found in all variants of the Mini, Peugeot and Citroën cars. This engine family has been thoroughly revised. The focus here was another reduction of fuel consumption and emissions with simultaneous consideration of dynamic improvements.

DEVELOPMENT TARGETS AND TECHNCAL CHARACTERISTICS

Despite the target conflict between the goal of the necessary advanced engine technique and business conditions, the requirements of the two cooperation partners are fully implemented. Absolute priority in the revision of the engine family was the commonality with the existing components and the use made of the production invests with both partners. Altogether both partners are up to eight engine variants. The range extends from 55 kW to 147 kW, ❶.

To implement the target catalogue requirements for the top version of the turbocharged engine, ❷, the world's new TVDI technique was used the first time for a four-cylinder engine. TVDI stands for a combination of twin-scroll turbo charger with fully variable valve train and direct injection. Through the implementation of the TVDI combustion process, the consumption, compared to the previous engine of the first generation will be further reduced significantly. In the EU test cycle the fuel consumption saving is 9 %.

For the TVDI technique the twin-turbo power technique at the BMW Group six-cylinder engines were the godparents. The newly designed cylinder head is manufactured in the BMW engine plant in Hams Hall, where since 2006 the engines are mounted for the Mini. The cooperation partner PSA is supplied with the completely manufactured cylinder head.

Since the naturally aspirated engines with the fully variable valve train already provide an excellent base for low fuel consumption, only a consistent friction optimization was carried out on all components. Further reductions in fuel consumption could be achieved by technical features such as a map regulated oil pump and an optimized control strategy of the mechanically switchable water pump.

DESIGN

The engine concept provides a solid basis for the naturally aspirated engines as well as for the turbo engines. For manufacturing technical reasons the geometry of the engine family for all derivatives is largely identical. These include among other things the cylinder distance of 84 mm, the bore of 77 mm and the height of the crankcase. The two 1.6 l engines also have the stroke of 85.5 mm and the displacement of 1598 cm³ in common.

CRANKCASE WITH BEDPLATE

The crankcase is made of an AlSi alloy with cast-in iron cast liners that go to the top of the crank housing (Open Liner). With this, the high specific power of the engine can be realized with a simple cylinder head gasket concept.

The bedplate is also made of an AlSi alloy and forms together with the crankcase a stiff basis for good acoustic properties. The previously in the turbo charged engines used sintered inserts for the crankshaft bearings could be eliminated, ❸.

CRANK DRIVE

For the new TVDI engine the forged steel crankshaft of the current turbo engines could be taken over. The main bearings with a diameter of 45 mm have been through the use of bearings in „Micro-Grooving“ technique friction optimized and are classified as five-fold.

The cracked trapezoidal con-rods are taking over parts from the first engine generation. Again, the bearing clearances were pushed to the upper acceptable limit to minimize the losses.

The pistons of the turbo charged direct injection engine are provided with four valve pockets and a central combustion chamber for the charge stratification.The micrograph of the piston and the piston coating was for the TVDI optimized to minimize friction and acoustic. The first ring groove is hard anodized. To reduce the thermal load for the turbo engines the pistons are cooled with oil jets.

CYLINDER HEAD

The cylinder head for the TGDI version is produced in low-pressure casting with a twin cavity from the material AlSi with a special heat treatment.

By switching the turbo top engine to the TVDI combustion process there was

DESCRIPTION		VVT 55 KW	VVT 72 KW	VVT 90 KW	TGDI (PSA) 115KW	TVDI 135 KW
POWER	kW	55	72	90	115	135
@ RPM	rpm	5000	5500	6000	6000	5500
TORQUE	Nm	140	153	160	240	240
@ RPM	rpm	2250	3000	4250	1400	1600
OVERBOOST	Nm	–	–	–	+ 20	+ 20
GOVERNED SPEED	rpm	6500	6500	6500	6500	6500
AIR-FUEL-MIXTURE GENERATION	–	MPI			DI	
SPECIFIC POWER	kW/dm³	34	45	56	72	84
DISPLACEMENT	cm³	1598				
STROKE / BORE	mm	85.8 / 77.0				
CRANKCASE MATERIAL	–	Aluminum with iron cast liner				
CYLINDER DISTANCE	mm	84.0				
CRANKCASE LENGTH	mm	420				
CRANKCASE HEIGHT	mm	210				
COMBUSTION RATIO	1:	11.0			10.5	
CON-ROD	–	cracked trapezoidal con-rods				
CAMSHAFTS	–	2 chain driven assembled camshafts				
CAM VARIABILITY	–	Intake and exhaust phase control			Intake phase control	as VVT
VALVE TIMING	–	roller rocker arm, hydraulic valve lash adjustment				
VALVE LIFT INTAKE / EXHAUST	mm	0.2-9.5 / 9.0			9.0 / 9.0	0.2-9.0 / 9.0
VALVES PER CYLINDER	-	4				
INTAKE VALVE Ø	mm	30.0			28.8	29.7
EXHAUST VALVE Ø	mm	25.1			26.2	
MAIN BEARING Ø	mm	45				
CON-ROD BEARING Ø	mm	45				
ENGINE WEIGHT (BMW STANDARD)	kg	107			115	121
FIRING ORDER	–	1-3-4-2				
ECU	–	MEV17.2.2			MED17.4.2	MEVD17.2.2
FUEL RANGE	ROZ	91-98 max. E25				
FUEL RATING	ROZ	95			98	
EMISSIONS EU	–	EU5				
EMISSIONS US	–	–	–	ULEVII	–	ULEVII
EXHAUST SYSTEM	–	three-way catalyst, close-coupled				
COOLING	–	switchable water pump map regulated cooling temperature				

❶ Technical data

❷ The 1.6 l TVDI engine for Mini Cooper S

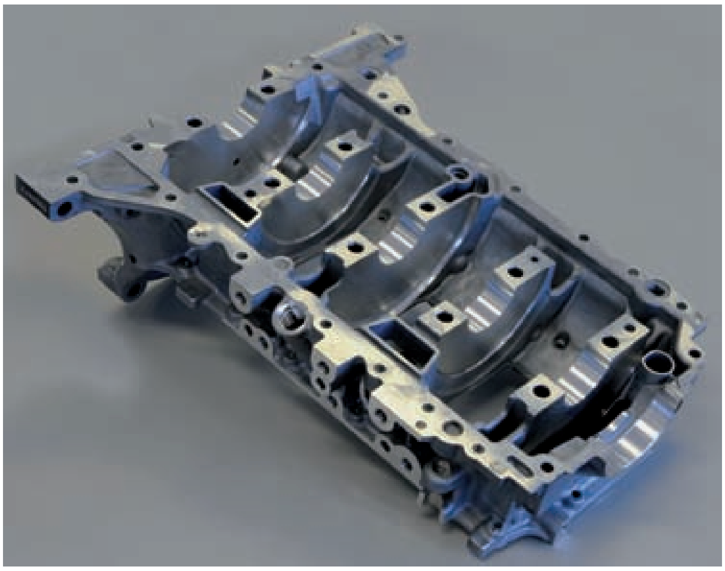

❸ Bedplate without sinter inserts

the need for an additional cylinder head variant. The basis for the new TVDI cylinder head was the cylinder head of the TGDI. It was supplemented with the possibilities of the fully variable valve train. Due to the extreme package conditions in the cylinder head it was decided to use the 3rd generation of the VVT adjustment. Therefore a sensor for the position of the VVT eccentric shaft is no longer necessary. All components of the fully variable valve trains are supported in roller bearings and identical between VVT and TVDI.

Through an intensive optimization of the cylinder head cooling (longitudinal flow) it was possible to use a gravity chill casting with cost-effective secondary alloy as for the TGDI.

From the experiences of the current direct injection engine a new crankcase ventilation system was developed. The micro oil separation has improved significantly and the blow-by discharge goes directly by puncture holes into the inlet channels. At full load the discharge takes place before the turbine of the turbo charger. Due to this new crankcase ventilation system and together with the TVDI combustion process a carbonization of the intake valves will be prevented.

To ensure the cleanliness of the machined cylinder head prior to the assembly, a new purification procedure is used, developed by the BMW plant Hams Hall. Robots lead the cylinder head first to high-pressure washing troughs (10 bar) and then high-pressure lances (300 bar) blown through the critical channels.

OIL PUMP AND OIL CIRCULATION

The chain driven gear pump provides an amount of oil depending on the need. A bypass to reduce the too highly raised oil volume flow is not required. Due to the map regulated oil pump, ❹, and through the elimination of unnecessary work the oil pump consumes less energy than conventional oil pumps. It lowers the fuel consumption of the TVDI engine in the EU test cycle by about 2.5 %. 1.5 % are coming directly through the oil pressure drop, a further 1 % resulting from the shutdown of the oil jets for piston cooling. During the initial filling the amount is 4.2 l fuel-efficient engine oil, the quantity of oil for service is 3.7 l.

AUXILIARY EQUIPMENT

At the back end of the exhaust camshaft the vacuum pump is flanged. It produces the vacuum for the brake booster. For the turbo engine it also produced the vacuum for the waste gate control. The working volume of the vacuum pump was reduced by about 35 % in comparison to the 1st engine generation. This leads to a reduc-

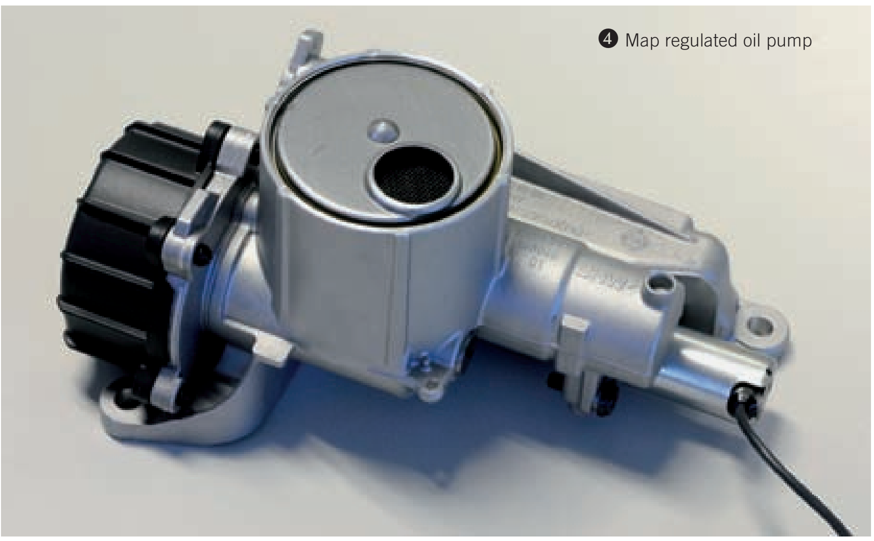

❹ Map regulated oil pump

tion in drive power and therefore to a further reduction in fuel consumption. The air conditioning compressor and the various generator types are mounted on cast-on brackets.

ENGINE PERIPHERALS

The intake manifolds modules of the engines are made of plastic. To make the induct parts suitable in all vehicle platforms without generating variants the complete intake manifolds with attached silencer are arranged fixed to the engine. The well-proven plastic throttle body was taken over.

The axial piston high pressure pump made from aluminium was revised for the TVDI and works with 120 bar system pressure. For resistance to Ethanol the fuel feed pump parts are coated. The integrated Volume Control Valve (VCV) is controlled by the engine control unit.

The 7-hole injectors are arranged at the side of the cylinder head and supplied with fuel from a common stainless steel rail and suppressed from this rail.

As with the TGDI for the TVDI a twin-scroll turbo charger is used, ❺. The high variability of the TVDI system could lead to a further improved response at low speeds (low-end torque). The cast iron manifold remains double-flow (Cyl.1/4 and 2/3). The material is Niresist and allows a maximum exhaust gas temperature before turbine of 950 °C. The exhaust gas separation will be maintained in the turbocharger just before the turbine. The turbocharger housing is made from cast steel to ensure the durability in the high-loaded bifurcation wall area. The maximum approved turbine speed is 216,000 rpm. The maximum boost pressure of the 135 kW version is 1.8 bar absolute. In the over-boost mode the boost pressure is increased to 2.0 bar absolute.

MODULAR ENGINE ANCILLARIES AND THERMAL MANAGEMENT

The reliable belt drive was taken over from the previous engine. Generator and air compressor are driven by a single Poly-V belt. The belt is tightened with a one arm torsion spring tensioner. The surrender of a second belt level was achieved by driving the coolant pump through a friction gear.

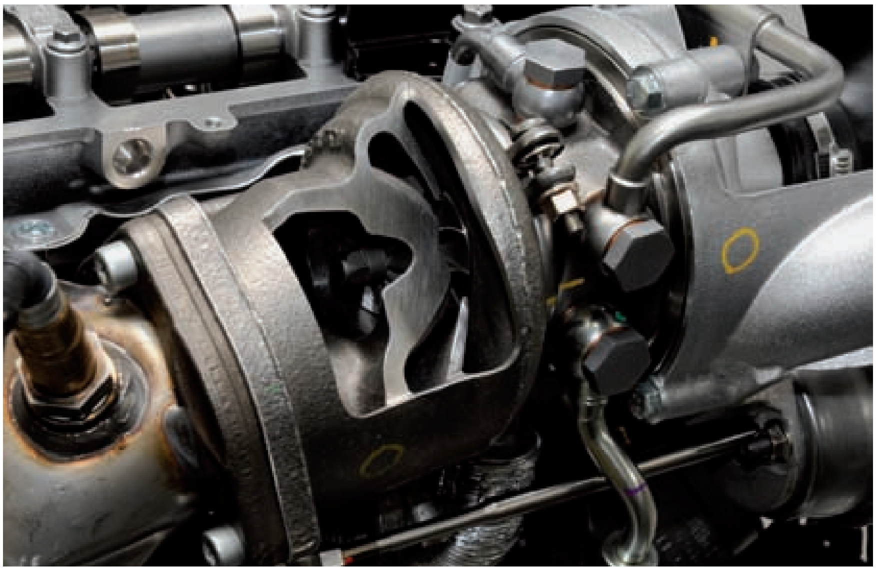

❺ Twin-scroll turbo charger

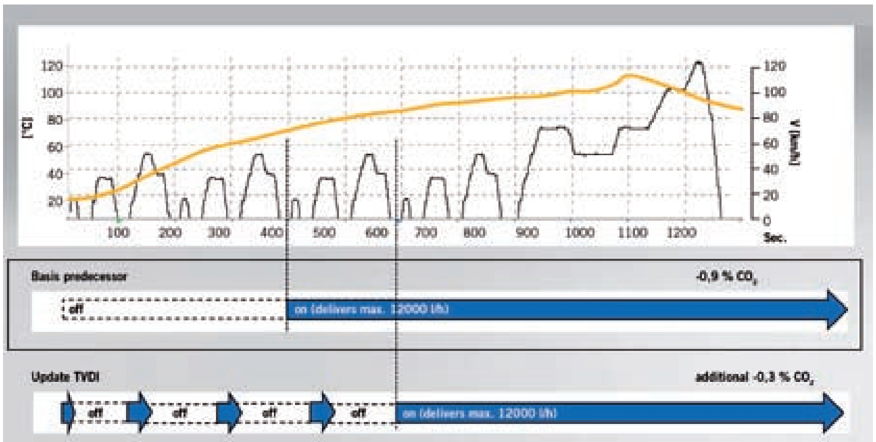

❻ Switching strategy water pump

Between the water pump and the pulley on the crankshaft is a friction wheel located which is attached to a supporting arm. About an electrically actuated eccentric gear the position of the friction wheel can be changed and the water pump can be activated. To save drive power and to accelerate the warm-up of the engine the coolant will be only circulated when the engine is at warm operating temperature.

So far the switchability of the water pump, ❻, was only used with the ECE variants of the normally aspirated engines. This led to a fuel saving in the EU test cycle of 0.9 %.

In the revising of the engine family the switchable water pump is in use now with the entire family. In addition the water pump is cycled several times, resulting to a further saving of about 0.3 % of fuel in the EU test cycle. This situation regulated adapted amount of coolant is one of the many measures to reduce fuel consumption. In countries under the U.S. emission laws (FTP75) a permanent water pump drive is used due to diagnostic reasons.

ENGINE FUNCTIONS TVDI

The combination of twin-scroll turbo charger, direct injection and fully variable valve train (TVDI) makes the engine an innovative engine in the entire competition. By the complex twin-scroll turbo charger technique the usually very annoying turbo lag has been almost completely avoided.

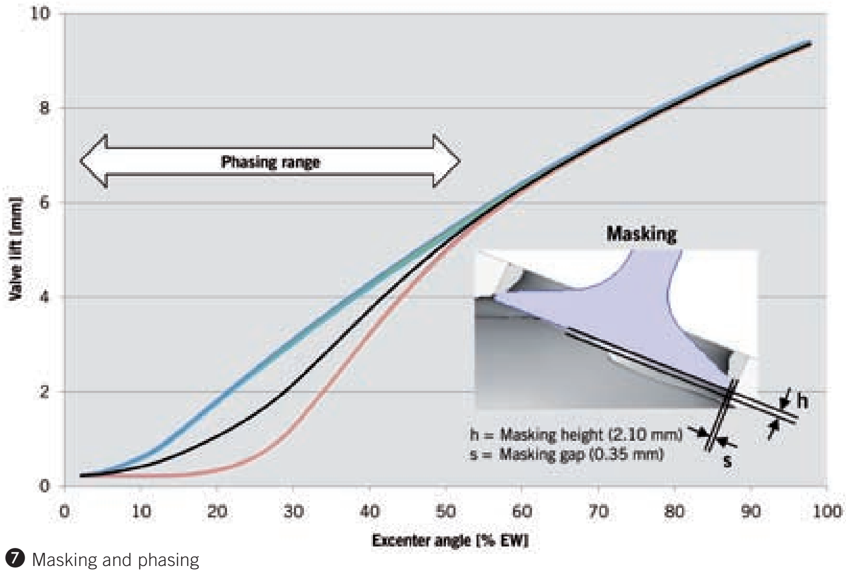

❼ Masking and phasing

The fully variable valve control system operates on the principle of the throttle-free load control and regulates the power of the engine with a continuous adjustment of intake valve lift and intake valve opening times. This technique with a nearly lossless load control which is similar to the Valvetronic of the BMW Group allows low fuel consumption and perfect response of the engine, ❼, ❽, ❾.

In partial load the engine will be operated with a high internal residual gas. This needs extreme valve timing with low intake valve lift together with late closing of the exhaust valves and early closing of the intake valves. The load control in partial load works with a continuously variable valve lift and the opening phase of the intake valves (EIVC = early intake valve closing).

At the full load the load is controlled by the boost pressure. The switch in the transition area between the two kinds of load controlling is torque neutral. The engine still has a throttle, but this takes only emergency operation and diagnostic functions. In normal operation it is constantly as open as the manifold pressure is 50 mbar below the ambient pressure to ensure the tank venting. The turbo charged engine is equipped with a direct injection. The mechanically driven two-piston high pressure pump sits at the far end of the intake camshaft and supplies the fuel injectors over a stainless steel rail with fuel.

The high-pressure injectors are injecting the fuel with a maximum pressure of 120 bars sideways into the combustion

The variable valve train together with many individual measures to reduce friction is an unbeatable relationship between fuel economy and performance. Through adding the fully variable valve train and due to measures for friction reduction the fuel consumption compared to the previous engine could be reduced further significantly. In the EU test cycle the fuel consumption saving is 9 %. The direct injection engine works with all fuel and oil qualities and is not dependent on sulphur-free fuel.

COMBUSTION PROCESS

A twin-scroll turbo charger is used for the TVDI direct injection engine. The channels of respectively two cylinders are separated in the exhaust manifold and in the turbo charger through an appropriate channel design. With reduced fuel consumption the turbine receives an additional boost so that the turbo charger can accelerate earlier.

The effect is clearly felt because the full turbo charge comes already at 1600 rpm. The on turbo charged engines often criticized "turbo lag" is almost completely avoided and the build-up of the torque is as fast as on an engine with mechanical supercharger (compressor).

The exhaust gas stream accelerates the turbine wheel up to a speed of 216,000 rpm. A pressure relief valve (Waste Gate) with integrated check valve guards the boost pressure of absolute 1.8 bar max (with overboost 2.0 bar max). A Dump Valve is regulating the intake manifold pressure during coast down when the throttle is closed. The pre-compressed fresh air is cooled down in an intercooler before it enters the combustion chamber in order to increase the charge level. The intercooler is positioned in the vehicle beneath the water cooler.

The maximum exhaust temperature is monitored by the engine electronics and is limited to 950 °C. To preserve the oil and water cooled turbo charger from damage due to overheating an electric auxiliary water pump runs automatically after the engine shutdown. This dissipates the excess heat energy and prevents coking of the oil pipes.

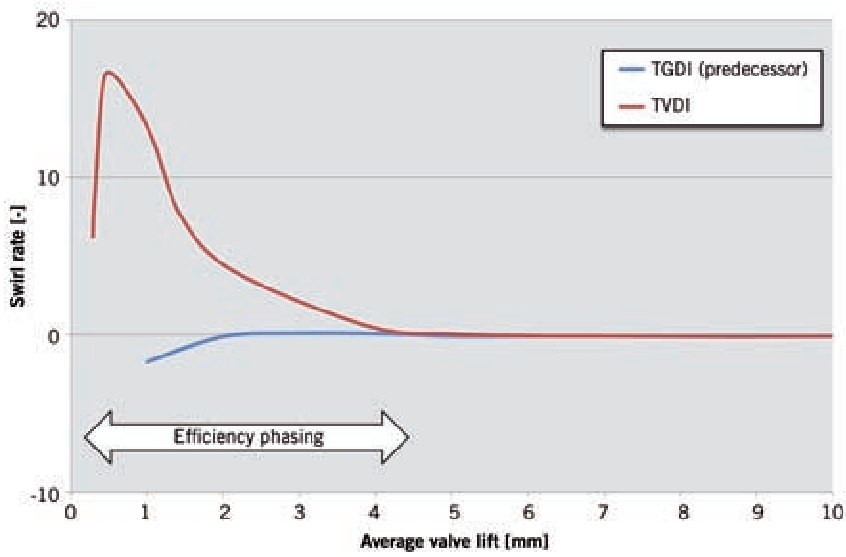

❽ Charge motion through swirl

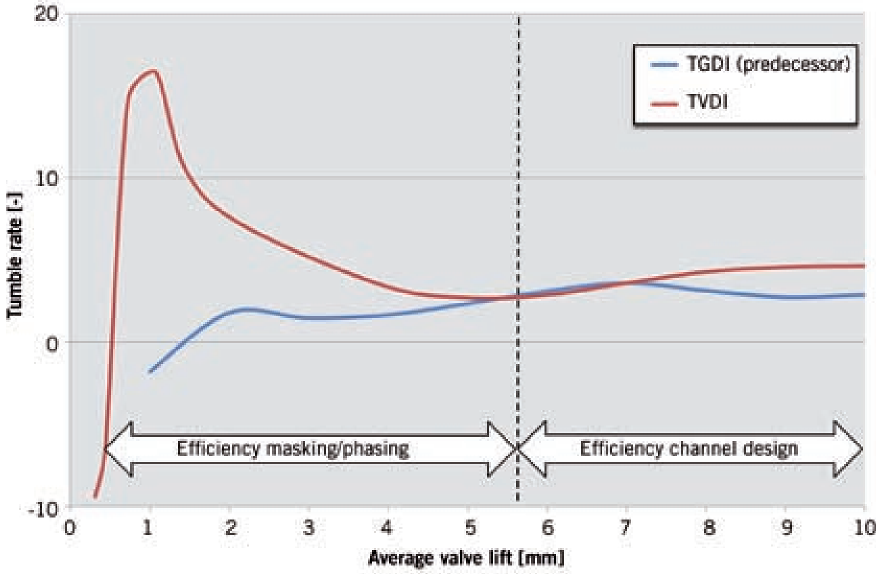

❾ Charge motion through tumble

chamber. The air-fuel-mixture in the combustion chamber is distributed homogeneous (Lambda = 1.0). Single ignition coils for each spark plug providing an optimal ignition voltage. Every coil is individually controlled by the ECU. The turbo engine is highly compressed for a turbo charged gasoline engine with a compression ratio of 10.5:1. Therefore a cylinder selective knock control monitors the combustion process and corrects if necessary the ignition angle and the boost pressure.

EFFICIENCY

The fuel consumption of the 135 kW engine was again reduced compared with the outstanding value of the predecessor, ❿. Through the introduction of the TVDI combustion process and the friction measures a reduction of 9 % was possible. The main technical measures are:

: fully variable valve train
: twin Vanos
: map regulated oil pump
: friction optimized base engine
: friction optimized vacuum pump (for brake booster)
: switchable water pump.

The fuel consumption in the EU test cycle (KV01) is 5.8 l/100 km, equivalent to a CO_2 emission of 136 g/km.

This puts the TVDI engine in the map point 2000 rpm / BMEP = 2.0 bar at the level of stratified charged naturally aspirated engines and represent a new benchmark for homogeneous turbo engines.

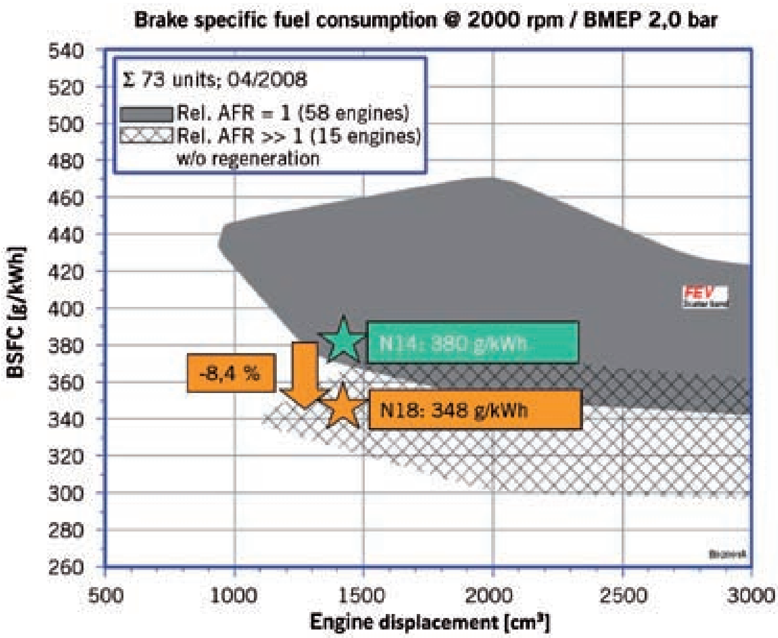

❿ Comparison fuel consumption TGDI vs. TVDI

EMISSIONS

The 135 kW engine in the Mini Cooper S meets the strict EU5 emission standards and ULEV II (Ultra Low Emission Vehicle) as well the „Japan Green Star Label“ and can therefore be worldwide homologated.

For the quick heating of the catalyst to its operating temperature, some special optimized settings are chosen for this mode. This was only possible by the flexibility of the TVDI combustion process.

These functional measures are supported by the design of the engine:

: turbo charging
: fully variable valve train
: masking and Phasing for high combustion stability and residual gas compatibility
: high charge motion through tumble intake channel also at full load
: high pressure direct injection + multi hole injector (seven-hole, Bosch HDEV5)
: double injection with time-offset
: optimized combustion chamber geometry for raw emissions
: close-coupled catalyst with optimized exhaust back pressure
: catalyst coating technique with low thermal aging
: continuous Lambda control with very fast operation readiness
: special functions for catalyst heating.

To meet today's emission regulations it is necessary to bring the catalyst as quickly as possible to the minimum operating temperature. For this, the engine starts with optimized operating strategies. These are for example extreme cam timing (late exhaust and intake open), double injection with time-offset, a late ignition angle and an increased idle speed. Due to the new developed fast Lambda sensor it is possible to use an air-fuel-

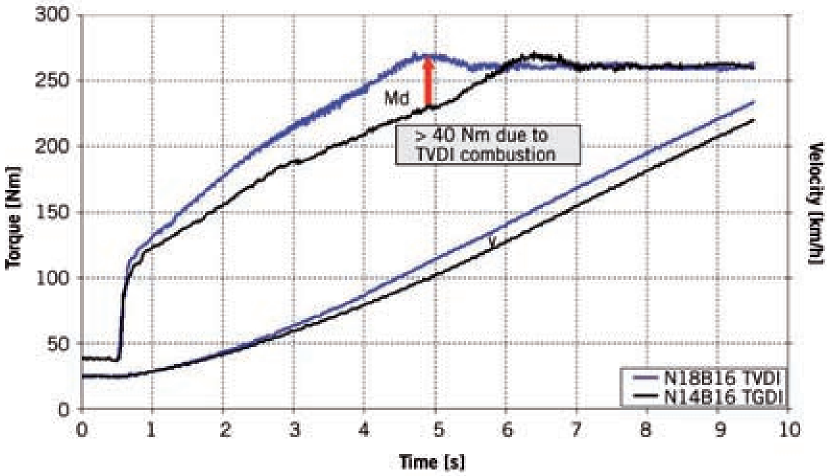

⓫ Comparison torque build-up TGDI vs. TVDI (torque and velocity increase in the 6th gear)

mixture of lambda = 1.05 already 6 s after start which leads to a further reduction in raw emissions. Despite all these measures the engine has a good running smoothness due to the TVDI combustion process.

A globally uniform catalyst system for all country variants could be realized. On a secondary air system is not necessary. For the ULEV II version (U.S.) an additional underbody catalyst has been installed. This is mainly used to meet the high requirements of the American onboard diagnostic (OBDII).

DYNAMIC

The turbo charged direct injection engine combines the torque behaviour of a Diesel with the benefits of a modern gasoline engine. Even at 1600 rpm the maximum torque is there and remains nearly constant up to 5000 rpm. During acceleration the overboost function raised the torque additionally for a short time.

The engine has a brake horsepower of 135 kW at 5500 rpm and a maximum torque of 240 Nm from 1600 rpm upwards, ⓫. The Overboost function raises the torque to 260 Nm.

ELECTRIC AND ELECTRONIC

To meet the increased requirements of the actuators and sensors, the ECU had to be revised. Due to new chips with faster CPU and more memory a development of existing functions was possible.

The control and evaluation of a fast oxygen sensor is one of them, as well as advanced knock detection for super knocking and the control of the map regulated oil pump. Also future requirements of the US-OBD were considered.

Especially for the TVDI there was the need to integrate the control of the variable valve train. The ECU is leaning closely to the control of the BMW six-cylinder inline turbo engine. The VVT3 position detection is working indirectly with around the drive shaft of the servo motor mounted Hall sensors that transmit motion in a direction-signal pattern for the ECU. Special software calculates the needed commutation as well as the current position and plausibility. This will result in lower component costs with constant accuracy and higher adjustment dynamics. With the two-channel Flex-Ray module the ECU's are fit for the future needs of an electrical vehicle network.

SUMMARY

The cooperation between the BMW Group and PSA Peugeot Citroën has been updated successfully with the further development of the four-cylinder engine family. The partly different aims of both manufacturers could be brought together again so that neither the high technique requirements of the Mini brand nor the PSA principle of „design to cost“ are injured. Already today the decision to continue the cooperation and adapt the engine family to future CO_2 guidelines and emission legislations was made.

REFERENCE

[1] Kessler, F.; Kiesgen, G.; Schopp, J.; Bollig, M.: „Die neue Vierzylinder-Motorenbaureihe aus der BMW/PSA-Kooperation“. In: MTZ 68 (2007), Nr. 7-8

PEER REVIEW ATZ | MTZ

PEER REVIEW PROCESS FOR RESEARCH ARTICLES IN ATZ AND MTZ

STEERING COMMITTEE

Prof. Dr.-Ing. Lutz Eckstein	RWTH Aachen	Institut für Kraftfahrzeuge Aachen
Prof. Dipl.-Des. Wolfgang Kraus	HAW Hamburg	Department Fahrzeugtechnik und Flugzeugbau
Prof. Dr.-Ing. Ferit Küçükay	Technische Universität Braunschweig	Institut für Fahrzeugtechnik
Prof. Dr.-Ing. Stefan Pischinger	RWTH Aachen	Lehrstuhl für Verbrennungskraftmaschinen
Prof. Dr.-Ing. Hans-Christian Reuss	Universität Stuttgart	Institut für Verbrennungs-motoren und Kraftfahrwesen
Prof. Dr.-Ing. Ulrich Spicher	Universität Karlsruhe	Institut für Kolbenmaschinen
Prof. Dr.-Ing. Hans Zellbeck	Technische Universität Dresden	Lehrstuhl für Verbrennungsmotoren

ADVISORY BOARD

Prof. Dr.-Ing. Klaus Augsburg
Prof. Dr.-Ing. Bernard Bäker
Prof. Dr.-Ing. Michael Bargende
Prof. Dipl.-Ing. Dr. techn. Christian Beidl
Dr.-Ing. Christoph Bollig
Prof. Dr. sc. techn. Konstantinos Boulouchos
Prof. Dr.-Ing. Ralph Bruder
Dr. Gerhard Bruner
Prof. Dr. rer. nat. Heiner Bubb
Prof. Dr. rer. nat. habil. Olaf Deutschmann
Dr. techn. Arno Eichberger
Prof. Dr. techn. Helmut Eichlseder
Dr.-Ing. Gerald Eifler
Prof. Dr.-Ing. Wolfgang Eifler
Prof. Dr. rer. nat. Frank Gauterin
Prof. Dr. techn. Bernhard Geringer
Prof. Dr.-Ing. Uwe Grebe
Prof. Dr.-Ing. Horst Harndorf
Prof. Dr. techn. Wolfgang Hirschberg
Univ.-Doz. Dr. techn. Peter Hofmann
Prof. Dr.-Ing. Bernd-Robert Höhn
Prof. Dr. rer. nat. Peter Holstein
Prof. Dr.-Ing. habil. Werner Hufenbach
Prof. Dr.- Ing. Roland Kasper
Prof. Dr.-Ing. Tran Quoc Khanh
Dr. Philip Köhn
Prof. Dr.-Ing. Ulrich Konigorski
Dr. Oliver Kröcher
Dr. Christian Krüger
Univ.-Ass. Dr. techn. Thomas Lauer
Prof. Dr. rer. nat. Uli Lemmer
Dr. Malte Lewerenz
Dr.-Ing. Markus Lienkamp
Prof. Dr. rer. nat. habil. Ulrich Maas
Prof. Dr.-Ing. Martin Meywerk
Prof. Dr.-Ing. Klaus D. Müller-Glaser
Dr. techn. Reinhard Mundl
Prof. Dr. rer. nat. Cornelius Neumann
Dr.-Ing. Lothar Patberg
Prof. Dr.-Ing. Peter Pelz
Prof. Dr. techn. Ernst Pucher
Dr. Jochen Rauh
Prof. Dr.-Ing. Konrad Reif
Prof. Dr.-Ing. Stephan Rinderknecht
Dr.-Ing. Swen Schaub
Prof. Dr. sc. nat. Christoph Schierz
Prof. Dr. rer.-nat. Christof Schulz
Prof. Dr. rer. nat. Andy Schürr
Prof. Dr.-Ing. Ulrich Seiffert
Prof. Dr.-Ing. Hermann J. Stadtfeld
Prof. Dr. techn. Hermann Steffan
Dr.-Ing. Wolfgang Steiger
Prof. Dr.-Ing. Peter Steinberg
Prof. Dr.-Ing. Christoph Stiller
Dr.-Ing. Peter Stommel
Prof. Dr.-Ing. Wolfgang Thiemann
Prof. Dr.-Ing. Helmut Tschöke
Dr.-Ing. Pim van der Jagt
Prof. Dr.-Ing. Georg Wachtmeister
Prof. Dr.-Ing. Jochen Wiedemann
Prof. Dr. techn. Andreas Wimmer
Prof Dr. rer. nat. Hermann Winner
Prof. Dr. med. habil. Hartmut Witte

Scientific articles of universities in ATZ Automobiltechnische Zeitschrift and MTZ Motortechnische Zeitschrift are subject to a proofing method, the so-called peer review process. Articles accepted by the editors are reviewed by experts from research and industry before publication. For the reader, the peer review process further enhances the quality of the magazines' content on a national and international level. For authors in the institutes, it provides a scientifically recognised publication platform.

Therefore, since the No. 4 issues of 2008, ATZ and MTZ have the status of refereed publications. The German association "WKM Wissenschaftliche Gesellschaft für Kraftfahrzeug- und Motorentechnik" supports the magazines in the execution of the peer review process. The WKM applies to the German Research Foundation (DFG) for the magazines to be included in the "Impact Factor" (IF) list.

In the ATZ | MTZ Peer Review Process, once the editors has received an article, it is reviewed by two experts from the Advisory Board. If these experts do not reach a unanimous agreement, a member of the Steering Committee acts as an arbitrator. Following the experts' recommended corrections and subsequent editing by the author, the article is accepted.

IMPRINT

MTZ WORLDWIDE

www.MTZonline.com

Founded 1939 by Prof. Dr.-Ing. E. h. Heinrich Buschmann and Dr.-Ing. E. h. Prosper L'Orange

Organ of the Fachverband Motoren und Systeme im VDMA, Verband Deutscher Maschinen- und Anlagenbau e.V., Frankfurt/Main, for the areas combustion engines and gas turbines
Organ of the Forschungsvereinigung Verbrennungskraftmaschinen e.V. (FVV)
Organ of the Wissenschaftliche Gesellschaft für Kraftfahrzeug- und Motorentechnik e.V. (WKM)
Organ of the Österreichischer Verein für Kraftfahrzeugtechnik (ÖVK)
Cooperation with the STG, Schiffbautechnische Gesellschaft e.V., Hamburg, in the area of ship drives by combustion engine

07-08 I 2010 – July-August 2010 – Volume 71
Springer Automotive Media I Springer Fachmedien Wiesbaden GmbH
P. O. Box 15 46 · 65173 Wiesbaden · Germany I Abraham-Lincoln-Straße 46 · 65189 Wiesbaden · Germany
Amtsgericht Wiesbaden, HRB 9754, USt-IdNr. DE811148419

Managing Directors Dr. Ralf Birkelbach (Chairman), Armin Gross, Albrecht Schirmacher I **Senior Advertising** Armin Gross I **Senior Marketing** Rolf-Günther Hobbeling
Senior Production Christian Staral I **Sales Director** Gabriel Göttlinger

EDITORS-IN-CHARGE
Dr.-Ing. E. h. Richard van Basshuysen
Wolfgang Siebenpfeiffer

EDITORIAL STAFF

EDITOR-IN-CHIEF
Johannes Winterhagen (win)
phone +49 611 7878-342 · fax +49 611 7878-78462
johannes.winterhagen@springer.com

VICE-EDITOR-IN-CHIEF
Ruben Danisch (rd)
phone +49 611 7878-393 · fax +49 611 7878-78462
ruben.danisch@springer.com

CHIEF-ON-DUTY
Kirsten Beckmann M. A. (kb)
phone +49 611 7878-343 · fax +49 611 7878-78462
kirsten.beckmann@springer.com

SECTIONS
Electrics, Electronics
Markus Schöttle (scho)
phone +49 611 7878-257 · fax +49 611 7878-78462
markus.schoettle@springer.com
Engine
Ruben Danisch (rd)
phone +49 611 7878-393 · fax +49 611 7878-78462
ruben.danisch@springer.com
Online
Katrin Pudenz M. A. (pu)
phone +49 6172 301-288 · fax +49 6172 301-299
redaktion@kpz-publishing.com
Production, Materials
Stefan Schlott (hlo)
phone +49 8191 70845 · fax +49 8191 66002
Redaktion_Schlott@gmx.net
Research
Dipl.-Ing. (FH) Moritz-York von Hohenthal (mvh)
phone +49 611 7878-278 · fax +49 611 7878-78462
moritz.von.hohenthal@springer.com
Service, Event Calendar
Martina Schraad (mas)
phone +49 611 7878-276 · fax +49 611 7878-78462
martina.schraad@springer.com
Transmission
Dipl.-Ing. Michael Reichenbach (rei)
phone +49 611 7878-341 · fax +49 611 7878-78462
michael.reichenbach@springer.com

PERMANENT CONTRIBUTORS
Richard Backhaus (rb),
Dipl.-Reg.-Wiss. Caroline Behle (beh),
Prof. Dr.-Ing. Stefan Breuer (sb),
Jürgen Grandel (gl), Ulrich Knorra (kno),
Prof. Dr.-Ing. Fred Schäfer (fs),
Roland Schedel (rs)

ENGLISH LANGUAGE CONSULTANT
Paul Willin (pw)

ADDRESS
P. O. Box 15 46, 65173 Wiesbaden, Germany
redaktion@ATZonline.de

MARKETING I OFFPRINTS

PRODUCT MANAGEMENT AUTOMOTIVE MEDIA
Sabrina Brokopp
phone +49 611 7878-192 · fax +49 611 7878-78407
sabrina.brokopp@springer.com

OFFPRINTS
Martin Leopold
phone +49 2642 9075-96 · fax +49 2642 9075-97
leopold@medien-kontor.de

ADVERTISING

AD MANAGER
Britta Dolch
phone +49 611 7878-323 · fax +49 611 7878-78140
britta.dolch@gwv-media.de

KEY ACCOUNT MANAGEMENT
Elisabeth Maßfeller
phone +49 611 7878-399 · fax +49 611 7878-78140
elisabeth.massfeller@gwv-media.de

AD SALES MANAGER
Sabine Röck
phone +49 611 7878-269 · fax +49 611 7878-78140
sabine.roeck@gwv-media.de

AD SALES
Frank Nagel
phone +49 611 7878-395 · fax +49 611 7878-78140
frank.nagel@gwv-media.de

DISPLAY AD MANAGER
Petra Steffen-Munsberg
tel +49 611 7878-164 · fax +49 611 7878-443
petra.steffen-munsberg@gwv-media.de

AD PRICES
Price List No. 53 (10/2009)

PRODUCTION I LAYOUT
Heiko Köllner
phone +49 611 7878-177 · fax +49 611 7878-78464
heiko.koellner@springer.com

SUBSCRIPTIONS
VVA-Zeitschriftenservice, Abt. D6 F6, MTZ
P. O. Box 77 77, 33310 Gütersloh, Germany
Renate Vies
phone +49 5241 80-1692 · fax +49 5241 80-9620
SpringerAutomotive@abo-service.info

YOUR HOTLINE TO MTZ
Editorial Staff
☎ +49 611 7878-393
Reader's Service
☎ +49 611 7878-151
Advertising
☎ +49 611 7878-395

SUBSCRIPTION CONDITIONS
The eMagazine appears 11 times a year at an annual subscription rate of 269 €. Special rate for students on proof of status in the form of current registration certificate 124 €. Special rate for VDI/ÖVK/VKS members on proof of status in the form of current member certificate 208 €. Special rate for studying VDI members on proof of status in the form of current registration and member certificate 89 €. The subscription can be cancelled in written form at any time with effect from the next available issue.

HINTS FOR AUTHORS
All manuscripts should be sent directly to the editors. By submitting photographs and drawings the sender releases the publishers from claims by third parties. Only works not yet published in Germany or abroad can generally be accepted for publication. The manuscripts must not be offered for publication to other journals simultaneously. In accepting the manuscript the publisher acquires the right to produce royalty-free offprints. The journal and all articles and figures are protected by copyright. Any utilisation beyond the strict limits of the copyright law without permission of the publisher is illegal. This applies particularly to duplications, translations, microfilming and storage and processing in electronic systems.

Springer Automotive Media is a brand of Springer Fachmedien. Springer Fachmedien is part of the specialist publishing group Springer Science+Business Media.

GENERATION AND INJECTION OF DIESEL-WATER EMULSIONS

AUTHORS

PROF. DR.-ING. CHRISTOF SIMON
is Head of the Department of Piston Engines and Turbomachinery at the Trier University of Applied Sciences (Germany).

DIPL.-ING. (FH) BJÖRN-CHRISTIAN WILL
is CFD Project Engineer at the Department of Piston Engines and Turbomachinery at the Trier University of Applied Sciences and Research Associate at the Chair of Turbochmachinery at the Duisburg-Essen University (Germany).

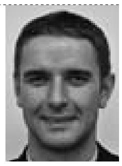

DIPL.-ING. (FH) M. ENG. HEINRICH DÖRKSEN
is Project Engineer at the Department of Piston Engines and Turbomachinery at the Trier University of Applied Sciences (Germany).

DIPL.-ING. (FH) CAND. M. ENG. CHRISTIAN MENGEL
is Student Assistant at the Department of Piston Engines and Turbomachinery at the Trier University of Applied Sciences (Germany).

Diesel-water emulsions have the advantage of significantly reducing both soot and NO_x in the diesel engine exhaust gas. Emulsions can be classified into pre-mixed and on board mixed emulsions. Compared with the pre-mixed emulsions, the on board mixed emulsions have the advantage that the water concentration can be adjusted as required from the engine operation condition. A new injection system was developed at the IFT (Institute of Vehicle Technology) at the Trier University of Applied Sciences to minimize the time lag between emulsion generation and deployment in the injector. The emulsion can now be mixed not only on board but also on injector.

THE SEAL OF APPROVAL FOR SCIENTIFIC ARTICLES IN MTZ.
MTZ PEER REVIEW
RECEIVED 2009-10-09
REVIEWED 2009-10-15
ACCEPTED 2010-01-18
REVIEWED BY EXPERTS FROM RESEARCH AND INDUSTRY.

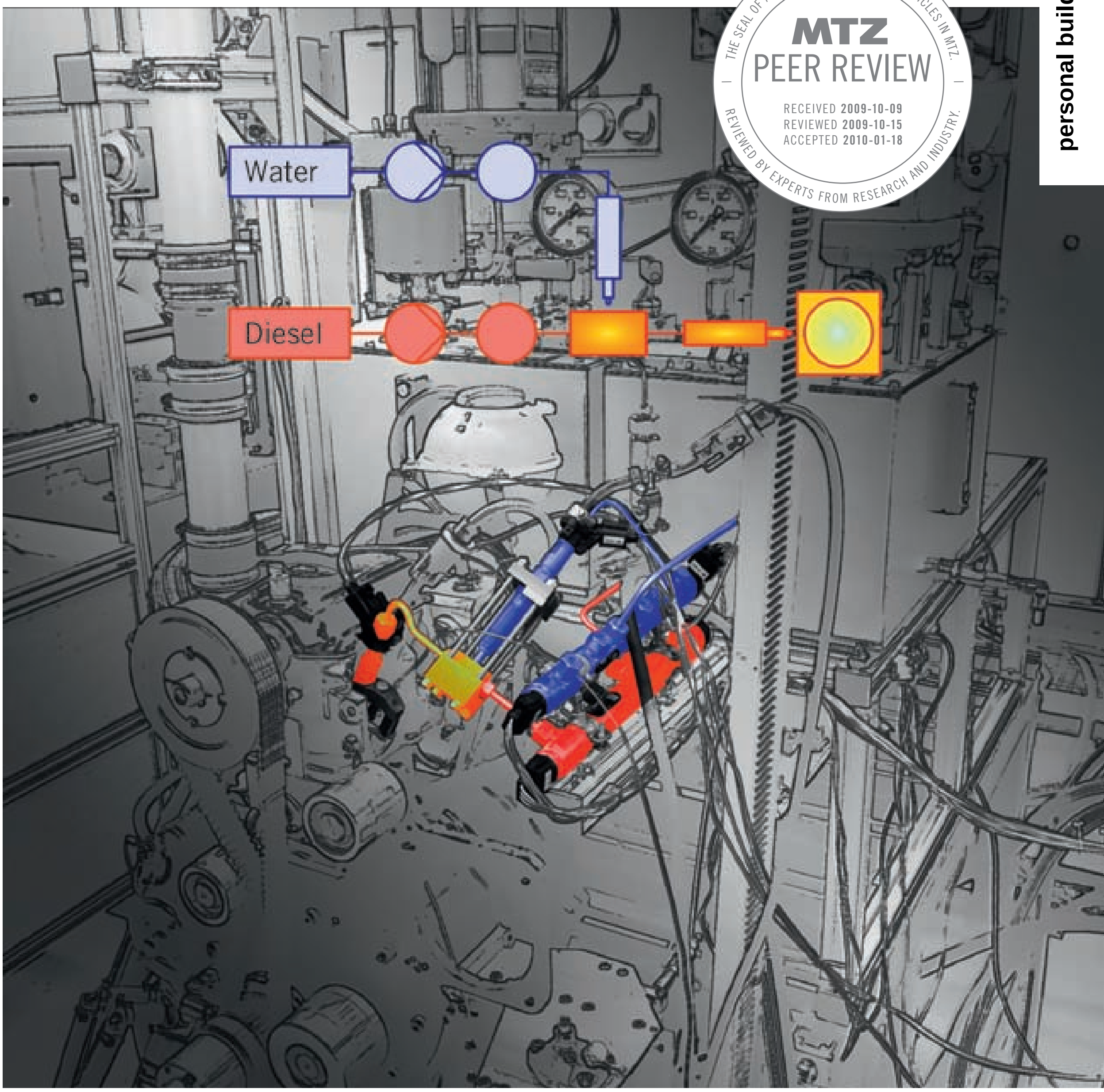

1 INTRODUCTION

The diesel engine is still one of the most economical power machines which are used in many fields of engineering (automotive engineering, power engineering, block heating and power plant). Being rather uncomplicated with regard to carbon monoxide and hydrocarbon formation, the relation between nitrogen oxide and soot formation poses a bigger problem.

The present emission limits prescribed by law have forced the car manufactures to install proper emission reduction systems on their engines in the past and the future limitations will certainly require additional reduction measures. To do so, principally two opportunities remain. On the one hand, engine modifications which influence the combustion process and therefore the pollutant formation are possible. On the other hand, exhaust gas aftertreatment which is used to convert harmful substances to a large extent into ecological ones could be useful. While internal engine measures, such as NO_x reduction, usually result in an increase in soot loading of the exhaust gas and vice versa (soot NO_x trade-off), exhaust gas aftertreatment systems, as for example diesel particulate filters, SCR and NO_x storage catalytic converters, generally do not operate neutrally with respect to fuel consumption.

In contrast to this, the use of diesel-water emulsions, respectively microemulsions, can reduce both soot and NO_x simultaneously to significantly weaken the soot NO_x trade-off [1, 2, 3, 4].

The soot reduction caused by the microemulsion is founded primarily in the increased hydroxyl radical formation and possibly also in the formation of "micro explosions" according to the present state of science [2, 3, 5, 6]. The NO_x reduction results mainly from reduced combustion temperatures.

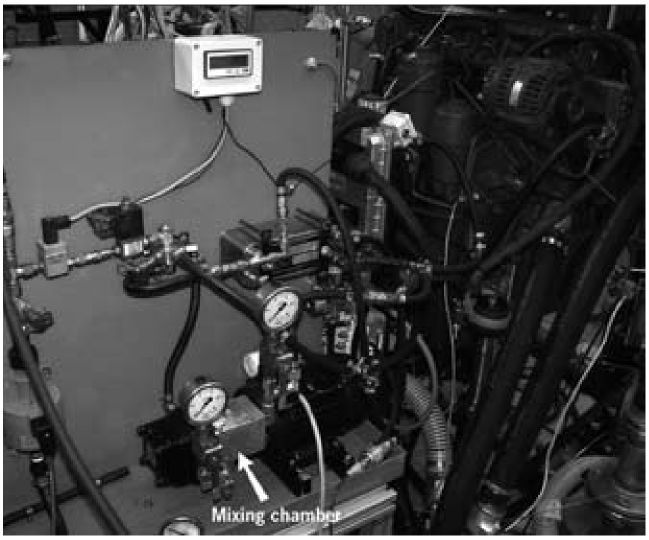

❶ Test engine with emulsion mixing unit

Microemulsions are, in contrast to conventional emulsions, thermodynamically stable mixtures of diesel, water and surfactants and have been developed at the Institute of Physical Chemistry at the Cologne University under direction of Prof. Dr. R. Strey.

An optimal emission reduction by diesel-water emulsions is only ensured if a corresponding diesel-water mixture ratio can be provided at any engine operating point. The engine start and warm up phase have proven to be particularly problematic.

In principle, the diesel fuel should not be mixed with water during the startup process and not until the engine has reached its operating temperature. However this presupposes that the diesel-water (micro) emulsion can be adequately produced and injected during the engine operation.

In the recent years, numerous studies with both premixed and on board mixed diesel-water emulsions were carried out at the IFT. The pre-mixed emulsions (always microemulsions) had a fixed diesel-water mixture ratio [1]. The on board generated emulsions were prepared in a mixer unit of the Scarabaeus company and could be adjusted with the desired diesel-water mixture ratio according to the set operating point of the motor [4]. System related the new adjusted mixture reaches the injection valve with a time delay when the operating point changes. To minimize this dead time a new fuel injection system was developed at the IFT where the mixing process takes place right in front of the injector.

2 ON BOARD MIXING OF DIESEL-WATER EMULSIONS

Unlike the premixed emulsions, on board mixing offers the possibility of supplying the engine with the desired mixture close to the engine itself. During the critical operation phases such as the engine's warm-up phase, the addition of water to diesel can be eliminated entirely.

2.1 TEST FACILITY

❶ shows the engine with the mixing equipment as it is currently assembled in the engine laboratory of the IFT. The engine is an up to date turbocharged four-cylinder industrial motor with common rail fuel injection (injection pressure 1400 bar), intercooler and cooled EGR of the Deutz AG. It is certified to EPA TIER3 and EU COM IIIA. The maximum rated power and maximum torque are at 113 kW/2100 rpm (overpower of 116 kW/1900 rpm) and 668 Nm at 1500 rpm.

The diesel-water emulsion is generated using a mixing device of the Scarabaeus company. Diesel and water are separately supplied to the mixing unit and brought together in the mixing chamber of the system to form a homogeneous diesel-water emulsion. To improve the water mixing behavior an emulsifier (approximately 1 % based on the amount of water) is added. As mentioned above, this system allows to adjust the emulsion to the operating point and a constant water addition related to the fuel amount. In the study presented below, the water/fuel ratio was at a constant rate of about 30 % for all operating points.

2.2 MEASUREMENTS DIESEL FUEL – DIESEL-WATER EMULSION

The performance, consumption and emission behaviour of the engine were investigated with on board mixing of the diesel-water emulsion. The effect of the emulsion on the aforementioned oper-

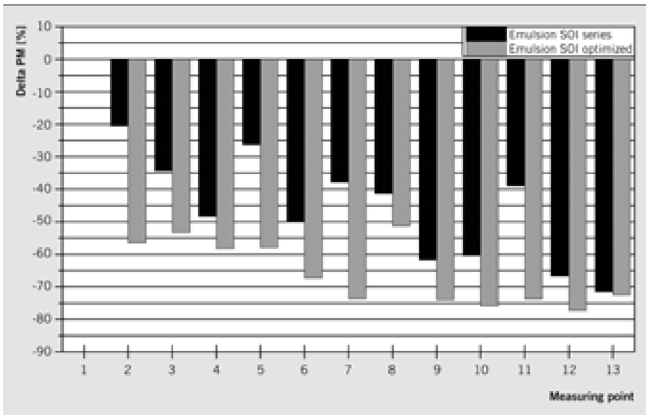

❷ Relative change of particulate mass using emulsion-fuel with and without SOI adjustment to diesel operation

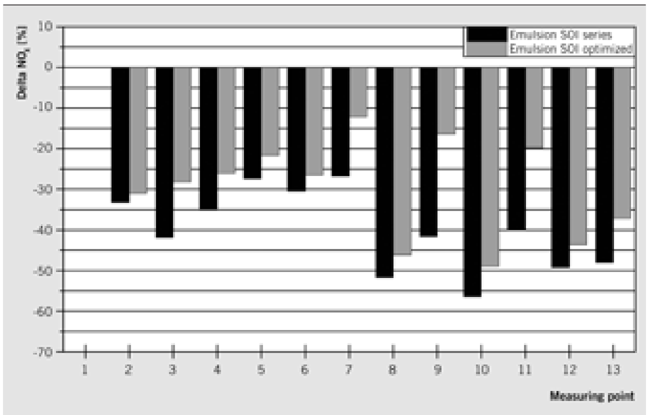

❸ Relative change of NO_x concentration using emulsion-fuel with and without SOI adjustment to diesel operation

ating parameters will be shown here through depiction of particle loading PM, NO_x concentration and the specific fuel consumption for each point of the 13-point test (with exception of the idle point).

The relative change in the soot loading, the NO_x concentration and the specific fuel consumption is shown using emulsion either with series injection timing (SOI) and with optimized, emulsion adapted, prerouted SOI. Afterwards it is compared to pure diesel operation. According to ❷ (black columns), the soot loading decreases noticeably when emulsion and series SOI are used compared to operating with pure diesel. The averaged decrease in the soot loading over the 13-point test is about 52 %, with a NO_x reduction of about 37 %, ❸. Although the specific fuel consumption for the series injection point according to ❹ slightly increases in some areas of the 13-point test, on average a reduction in consumption of about 1 % can be expected. When using emulsion the injection point needs to be adapted. Due to the extended injection time and a slightly higher ignition delay the injection point has to be brought forward. The results for this measure are also shown in ② to ④.

A prior injection point up to 4 degree crank angle leads to a further reduction of the soot loading at about 66 %, while the NO_x reduction is slightly weakened as expected. The specific fuel consumption shows an average reduction of 2 % for a prior SOI.

The necessary power for the water pump to deliver the water into the mixing chamber can be neglected.

Combining the emulsion usage with an after treatment of exhaust gases (particulate traps, NO_x storage or SCR cat) could further reduce the fuel consumption at about 1 to 2 % because of the extended regeneration phases resulting from decreased out of engine emissions. The overall consumption reduction could possibly assumed to be about 3 %.

3 ON INJECTOR MIXING OF DIESEL-WATER EMULSIONS

Shifting the mixing chamber directly to the injection nozzle of the engine minimizes the time between the formation of the emulsion and the deployment in the injector. Therefore the "new" emulsion is immediately available at a new engine operating point after a few ms which was the motivation for developing a new injection system at the IFT, ❺. The project was supported by the AiF (Arbeitsgemeinschaft industrieller Forschungsvereinigungen) respectively the BMBF (Bundesministerium für Bildung und Forschung) [7].

However, this supposes a spontaneous formation of a homogenous diesel-water emulsion. To investigate this and to optimize the geometry of the mixing chamber, a low pressure experimental injection setup with an interchangeable mixing chamber (made of Plexiglas) was assembled. It was used for accomplishing numerous basic fluid flow experiments [8].

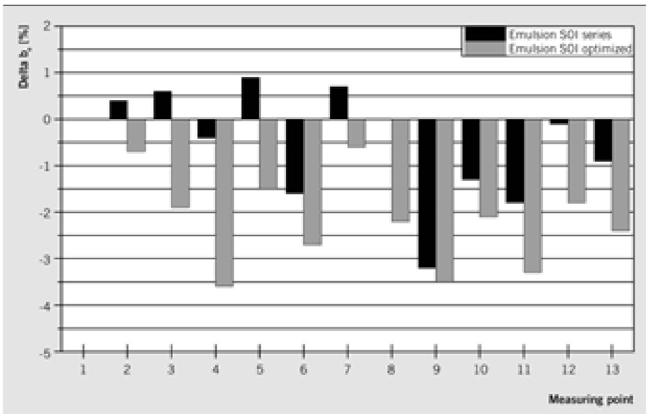

❹ Relative change of specific fuel consumption using emulsion-fuel with and without SOI adjustment to diesel operation

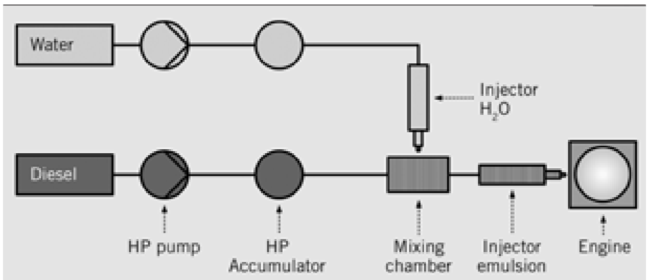

❺ Setup of the injection system

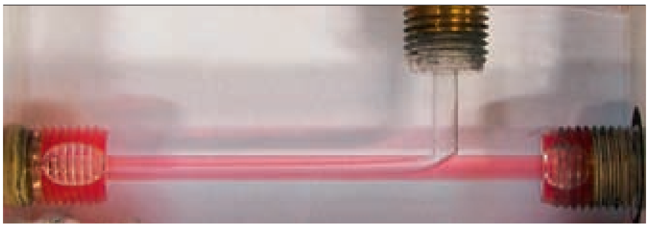

❻ Diesel-water mixing behaviour without surfactant

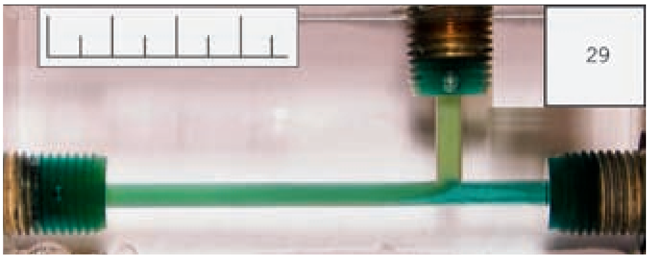

❼ Diesel-water mixing behaviour with surfactant

❻ shows the mixing behavior of diesel and water in the test rig without the addition of an emulsifier. No mixing of diesel and water could be observed in this case. The water flows like a "streamline" through the pipe without interacting with the diesel phase. In case of adding an emulsifier a homogenous mixture is formed after a short flow path, ❼. Numerous experiments [8] verified that even under relatively low pressures of about 4 bar, homogenous mixtures establish within a few ms by applying proper surfactants.

At the same time intensive 3D numerical calculations were performed, using an up to date CFD code, to investigate flow structure and mixing behavior [9]. ❽ shows the comparison between experimental and numerical results for the flow in the mixing chamber. The agreement for the low pressure cases was very good whereas in case of high pressure (up to 2000 bar) the numerical simulation showed deficiencies in modeling the mixing of the two phases but the prescription of the overall unsteady flow process was correct. According to the simulation, only a fractional homogenization is visible at the end of the mixing facility, ❾.

The numerical model consisted of a straight pipe for the diesel which was connected to the water pipe in form of a t-junction. Due to the high pressure, both fluids could not be treated as incompressible anymore. To reflect this, a relationship between the fluid density and the pressure was deduced from the equation of state, neglecting the temperature. The maximum streamline diversion of the flow occurs where the water enters the diesel pipe and consequently this is the place where the lowest pressures are apparent. The local values fall below the vaporization pressures of both liquids leading to the formation of two additional gas phases. Consequently four different phases interact in the mixing chamber, two liquid and two gaseous. It can further be noticed that the flow is highly transient because the outlet, as well as the water inlet into the mixing chamber are stroked in dependence of the desired engine operating point.

The multiphase interaction caused by cavitation combined with fluid compressibility and the highly transient flow process could not be captured sufficiently in the present model.

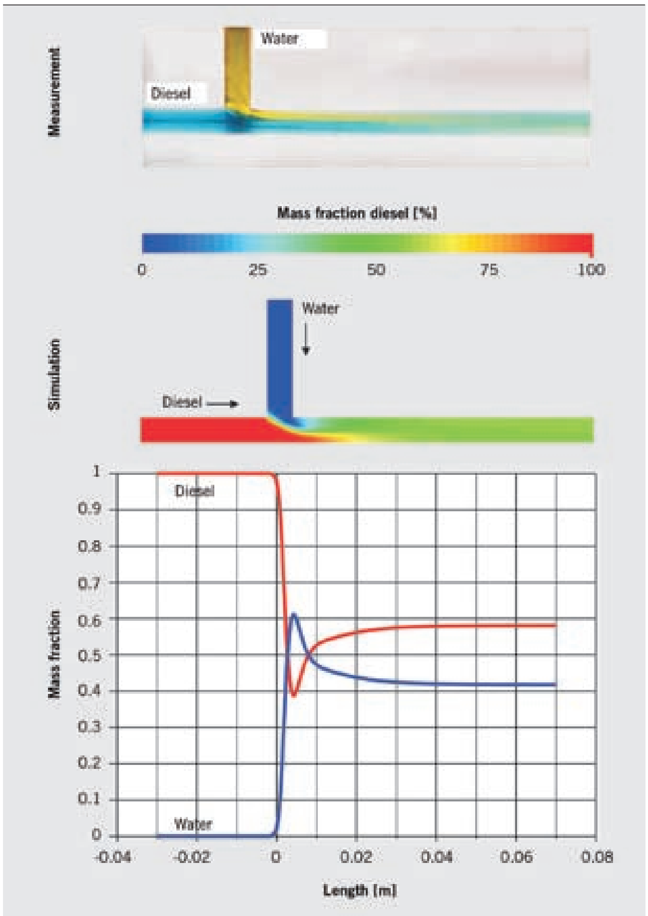

❽ Diesel-water mixing behaviour in the low pressure case, comparison of calculation and measurement

These preliminary experiments in the low pressure test rig and also numerical considerations were followed by extensive investigations on a temporarily constructed high-pressure test facility.

After completion of the basic experiments, the high pressure test rig was installed on the single-cylinder research engine [10]

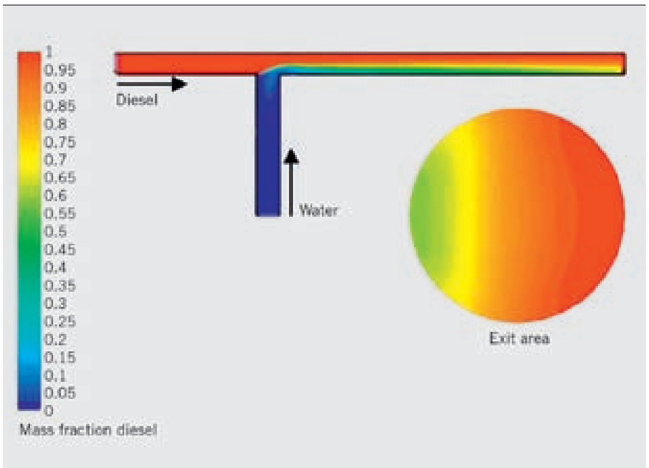

❾ Diesel-water mixing behaviour in the high-pressure case of the IFT, ⑩, where it is currently operated in this state. It consists of two high pressure pumps (maximum pressure 2000 bar) and two rails for diesel and water, a mixing unit located right in front of the injection nozzle and a second injector for water injection into the mixing chamber.

In the newly developed injection system the fuel is transported by the high pressure pump via the diesel rail to the mixing chamber and is then delivered to the injection nozzle. At the same time the water is injected via the water dose injector either stroked (up to three strokes possible) or continuously into the mixing chamber.

The main task of this high pressure injection test rig was to simulate the injection process in case of pure diesel as well as in case of additional injection of water using an appropriate control unit (FI^{2RE}). Together with an injection curve indicator (EVI), the corresponding magnitudes to set up the FI^{2RE} were identified, which in turn could be used to determine the desired injection amount and injection devolution per load cycle in dependence on certain engine parameters.

To identify the response behavior of the engine after changing the diesel-water mixture ratio, the water supply was stopped for consistent amount of injected fluid. Consequently more diesel fuel is injected which caused to an increase of the mean effective pressure. The pressure can thus be seen as an indicator for the responsiveness of the system. ⑪ shows the trend of the mean effective pressure versus several injection cycles. It becomes clear from this that for the present assembly of the mixing chamber and 100 mm fuel feed pipe between mixing chamber and injection nozzle a change in the pressure can be observed after 20 load cycles which finally diminishes after 75 cycles. Assembling the mixing chamber closer to the injection nozzle further reduces the necessary cycles. If the water injector would be mounted directly at the injection nozzle, as originally planned, the mixing chamber would be needless and the necessary amount of cycles could possibly reduced below 10.

3.1 FUEL INJECTION

The fuel is delivered from the high pressure pump via a pressure accumulator to the diesel rail and then through the mixing chamber to the injection nozzle. A commercial 7 hole piezo injector was used. As already mentioned above, the high-performance electronic control system allows multiple injections and a variation of the form of the injection devolution. In fact any injection profile can be applied.

3.2 WATER APPORTIONING

The water apportioning is accomplished using the same injector as for the diesel whereas the original nozzle body was replaced by an insert with a single, centrally mounted hole with a diameter of 3 mm on the nozzle tip. The water is delivered from the high pressure pump directly to the water-rail and from there to the injector. The water injection unit is connected to the mixing chamber via an inhouse clamping system. To prevent the water injection nozzle from lifting during fuel injection, the water pressure must always be slightly higher than the diesel pressure; otherwise the diesel would flow into the water.

The triggering of the injector is also carried out by the FI^{2RE}, which allows either a continuous or a pulsed water-injection into the mixing chamber, while the amount of water is controlled by the injection time.

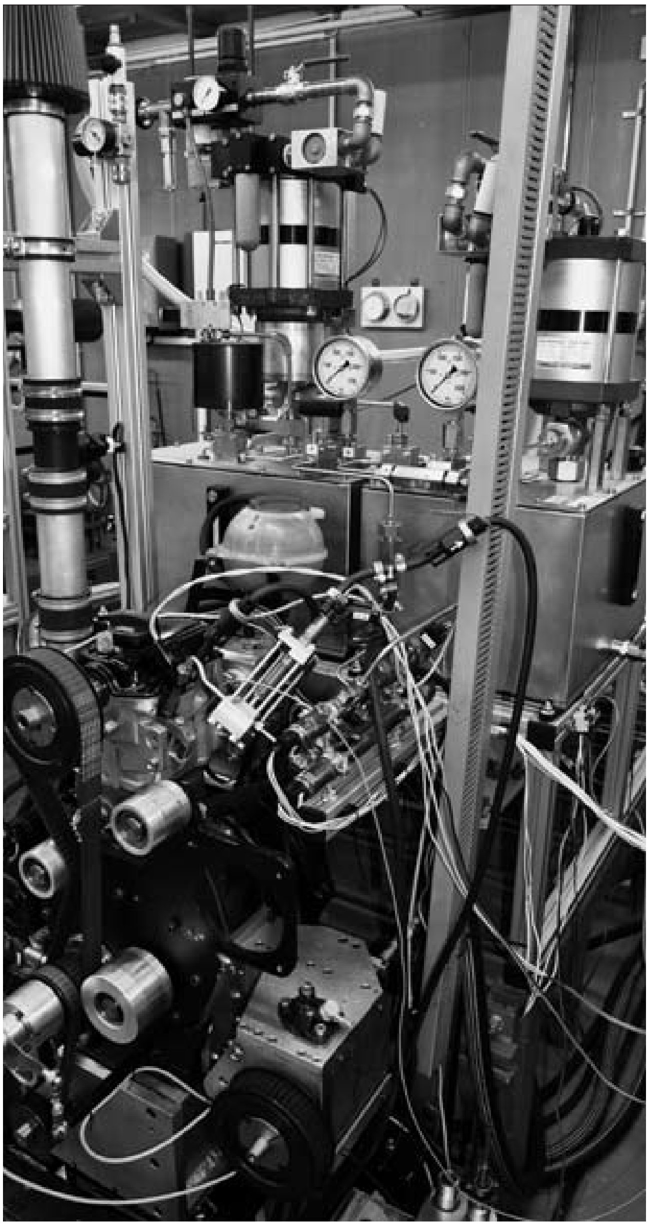

⑩ Single-cylinder research engine with on injector mixing system

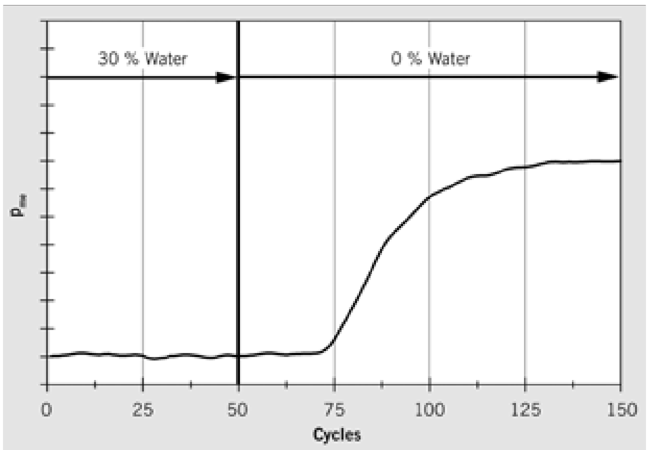

⑪ Response behavior of the injection system by changing the diesel-water mixture ratio

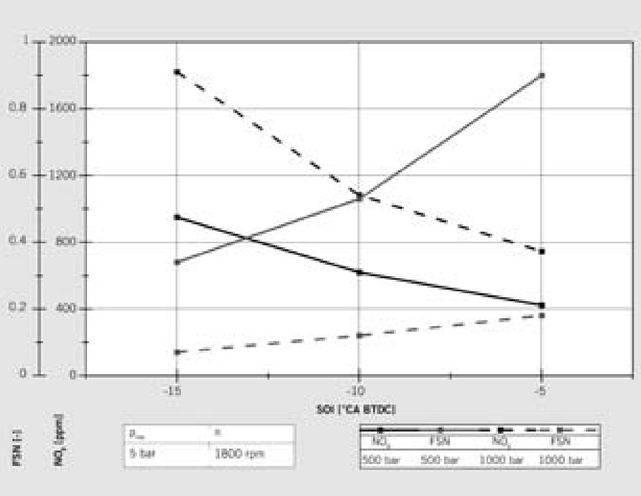

⓬ NO_x and soot loading as a function of the injection point at different injection pressures

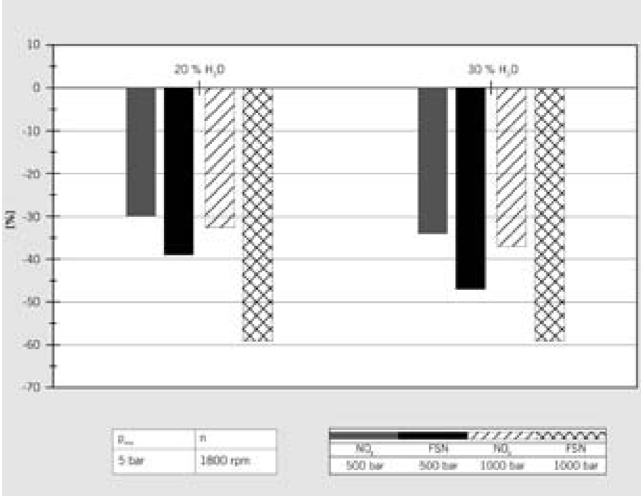

⓭ Relative change of the NO_x and soot concentration in dependence on water fraction and injection pressure to diesel operation

3.3 MIXING CHAMBER

The original idea of directly discharging the water into the fuel channel of the diesel injector (in-injector system) was abandoned because of the narrow space close to the engine. Instead, a mixing chamber was mounted in front of the diesel injector which consisted of stainless steel and has been designed for pressures up to 4000 bar. The water is supplied perpendicularly to the main flow direction in the mixing chamber using the injector described in 3.2, ⑩.

3.4 MEASUREMENTS ON THE ENGINE

Below, some results are discussed that were obtained with the above described injection system on the single-cylinder research engine.

First some tests were carried out with pure diesel, varying the injection pressure between 500 and 1000 bar, the point of injection and the form of the injection process.

⓬ shows the soot and NO_x devolutions in dependence on the point of injection for pressures of 500 and 1000 bar and pure diesel. From the SOI at -10 degree crank angle, FSN decreases from 0.53 about 36 % for an injection pressure of 500 bar and a prior shifted injection point at -15 degree crank angle. Moving the SOI to -5 degree crank angle results in a FSN increase about 70 %. The NO_x concentration behaves exactly the opposite way following the soot NO_x trade-off. Moving the injection point to a prior crank angle leads to an increase from 600 ppm about 60 % while a shifting to a delayed crank angle causes a lowering about 33 %. An increase in the injection pressure to 1000 bar results in a noticeable soot reduction and a visible increase in the NO_x concentration, ⑫.

After performing a functional test of the injection system, water was injected into the mixing chamber. The water fraction was adjusted to 20 % respectively 30 % (related to the fuel amount) for injection pressures of 500 and 1000 bar. The injection point was at -15 degree crank angle. As illustrated in ⓭, for an injection pressure of 500 bar the soot reduction at a water fraction of 20 % amounts about 40 % and 47 % at a water fraction of 30 %. Simultaneously, the nitrogen oxide concentration noticeably decreases about 30 % at 20 % water fraction and about 34 % at 30 % water fraction. At 1000 bar injection pressure the decrease of soot and NO_x for each of the two water fractions is in the same order of magnitude namely 32 % to 37 % for NO_x and about 59 % for soot.

The present system does not allow a conventional recirculation of the fuel into the fuel tank, respectively the high pressure pump (which would lead to a change of the mixing ratio). Therefore the emulsion was collected in a separate reservoir during the test runs at the one cylinder engine. For future series applications the system needs to be adopted accordingly.

4 SUMMARY

In Section 2 of this paper, the reduction of harmful emissions with diesel-water emulsions, even on a modern, ATL charged diesel engine with common rail fuel injection and cooled EGR has been demonstrated. Soot respectively NO_x reductions of up to 66 % respectively 35 % are possible for an adjusted injection point. At the same time, the specific fuel consumption could also be slightly reduced by adaptation of the injection point. With some further adjustments of specific engine operating parameters to the emulsion, such as the EGR rate and the pre and post injection, certainly a further positive influence on both the exhaust gas composition and presumably also on fuel consumption can be expected. The present results prove that the soot NO_x trade-off is significantly weakened by the use of a diesel-water emulsion on an up to date diesel engine.

In section 3 a new injection system was presented which allows the formation of a diesel-water emulsion not only on board but on injector". The major advantage of this system is that during the engine operating point, the dead time between emulsion production and deployment in the injector can be minimized so that the "new" emulsion is practically immediately available. The functionality was demonstrated and the positive effect of the emulsion on the exhaust gas composition was, as already shown in section 2, confirmed by various measurements.

REFERENCES
[1] Strey, R.; Simon Ch.: Ruß- und NO_x-Reduktion dank Dieselkraftstoff-Wasser-Mikroemulsion. In: MTZ 2005 Nr. 6
[2] Hountalas, D. T.; Mavropoulos, G. C.; Zannis, T. C.: Comparative Evaluation of EGR, Intake Water Injektion and Fuel/Water Emulsion as NO_x Reduction Techniques for Heavy Duty Diesel Engines, SAE Technical Paper Series 2007-01-0120
[3] Bemert, L.; Wulff, P.; Engelskirchen, S.; Strey, R.: Mikroemulgierte Kraftstoffe mit Biokomponenten, FAD-Konferenz 2008, Dresden
[4] Berenz, A.; Dörksen, H.; Simon, Ch.: Gegenüberstellung der Leistungs- und Abgasdaten beim Betrieb eines Dieselmotors mit reinem Dieselkraftstoff und einer Diesel/Wasser-Emulsion. Industrieprojekt, Januar 2008
[5] Skoglundh, M.; Gjirja, S.; Denbratt, I.: Reduction of Soot Emissions from a Direct Injection Diesel Engine using Water-in-Diesel Emulsion and Microemulsion Fuels, SAE Technical Paper Series 2007-01-1076
[6] Bemert, L.; Strey, R.: Mikroemulsionen als alternative Kraftstoffe. Dissertation am Institut für Physikalische Chemie der Mathematisch-Naturwissenschaftlichen Fakultät der Universität zu Köln, 2009
[7] Dörksen, H.; Simon, Ch.: Entwicklung einer neuen Betriebsart von Dieselmotoren mit Diesel-Wasser-Mikroemulsion. AiF/BMBF-Forschungsprojekt, Sept. 2006 bis Aug. 2009
[8] Düpre, A.; Dörksen, H.; Simon, Ch.: Untersuchung des Mischungsverhaltens von Diesel-Wasser-Mikro- Emulsionen an einem Modell-Einspritzprüfstand. Diplomarbeit am IFT der FH Trier, Aug. 2007
[9] Berenz, A.; Simon, Ch.; Will, B. Ch.: Simulation des Durchmischungsverhaltens von Diesel-Wasser (Mikro-) Emulsionen. ANSYS Conference & 26th CADFEM Users' Meeting 2008, 22.-24. Okt., Darmstadt
[10] Pauls, R.; Simon, Ch.: Einfluss der geschichteten Wassereinspritzung auf das Abgas- und Verbrauchsverhalten eines Dieselmotors mit Direkteinspritzung. In: MTZ 2004 Nr. 1

THANKS

The second project which is part of this report was funded by the Federal Ministry for Education and Research (AiF / BMBF) under Project Number 1756X06. The responsibility for the content of the publication lies with the authors. The authors thank the AiF and the BMBF for financial support. The Authors also thank the Deutz AG for the provision of a test engine to perform measurements of the first Part of this report.

AUTHORS

DIPL.-ING. MICHAEL FIEBIG
is Research Assistant at the Institute for Combustion Engines (VKA) at the RWTH Aachen University (Germany).

DIPL.-ING. MARKUS SCHÖNEN
was Research Assistant at the Institute for Combustion Engines (VKA) at the RWTH Aachen University (Germany).

DIPL.-ING. ULRICH GRÜTERING
is Executive Director at the Institute for Combustion Engines (VKA) at the RWTH Aachen University (Germany).

PROF. DR.-ING. STEFAN PISCHINGER
is Head of the Institute for Combustion Engines (VKA) at the RWTH Aachen University (Germany).

INFLUENCES OF ENGINE OPERATING PARAMETERS ON REACTIVITY OF DIESEL SOOT

The regeneration characteristics of diesel particulate filters are mainly determined by the properties of the stored soot. It is possible to exert specific influence on the soot burning behavior by modifying the soot characteristics. For this reason, the impact of engine operating parameters on the reactivity of diesel exhaust particulates was examined as part of a FVV research project No. 954 "Reactivity of Soot" at the Institute for Combustion Engines (VKA) of the RWTH Aachen University. The emitted diesel exhaust particulates were characterized with the help of various analysis methods. Further investigations using diesel particulate filter loaded with soot made it possible to show a correlation between soot reactivity of the emitted soot and the regeneration characteristics in the DPF. The insights gained were used in an alternative DPF regeneration strategy.

THE SEAL OF APPROVAL FOR SCIENTIFIC ARTICLES IN MTZ.
MTZ
PEER REVIEW
RECEIVED 2010-02-25
REVIEWED 2010-03-19
ACCEPTED 2010-05-04
REVIEWED BY EXPERTS FROM RESEARCH AND INDUSTRY.

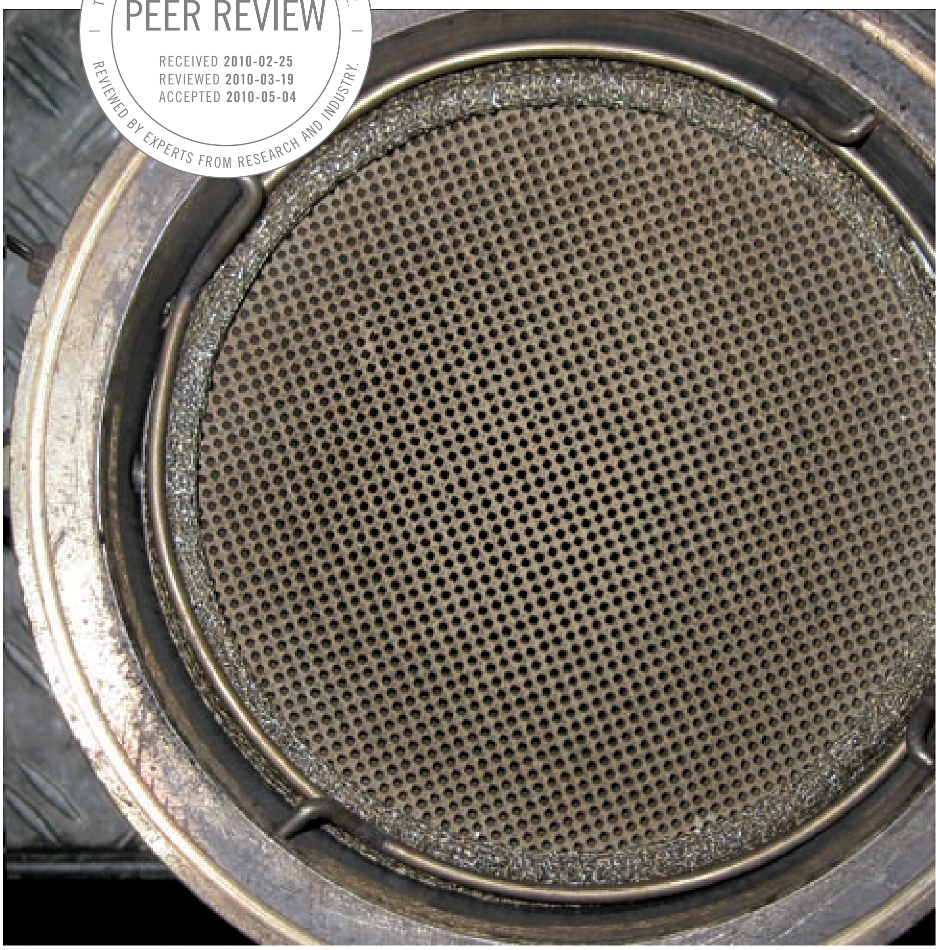

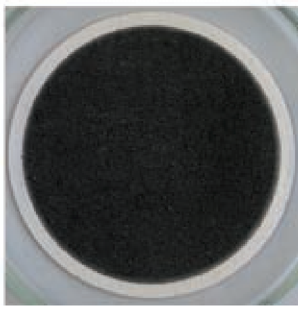

1	INTRODUCTION
2	TEST BOUNDARY CONDITIONS AND EXECUTION
3	PARTICULATE ANALYTICS AND DEFINITION OF REACTIVITY
4	DETERMINING PARTICULATE REACTIVITY IN THE DPF
5	ALTERNATIVE REGENERATION STRATEGY
6	CONCLUSION

1 INTRODUCTION

Complying with increasingly stringent exhaust emission limits for diesel engines typically requires the use of a diesel particulate filter (DPF) in order to reduce particulate emissions. The diesel soot retained in the DPF is oxidized periodically by means of regeneration at high exhaust temperatures of more than 600 °C. It is not very helpful to reduce the resulting increased fuel consumption by using additives that lower the soot ignition temperature because of the higher ash content as well as the need for additional components such as metering units and tanks. Lowering the soot ignition temperature using modified engine operating parameters offers an alternative for optimizing the DPF operating strategy and therefore for reducing the fuel consumption penalty, the dilution of lubrication oil, the thermal stress of the turbocharger and of the catalytic coatings of the exhaust aftertreatment system.

2 TEST BOUNDARY CONDITIONS AND EXECUTION

2.1 TEST BOUNDARY CONDITIONS

We conducted tests using an institute-owned 2.2 l passenger car DI diesel engine in order to characterize the soot properties; the engine specifications are shown in ❶. The investigations were based on the operating points OP1 (n = 1500 rpm and bmep = 2 bar) and OP2 (n = 2000 rpm and bmep = 5 bar), whereas a base calibration in lean-burn as well as in rich-burn engine operation was accomplished for both operation points. The exhaust aftertreatment system consisted of an (optional) diesel oxidation catalyst (DOC / EU4 series / 5.66 × 6") and a diesel particulate filter (DPF / Corning DuraTrap AC / 5.66 × 6" / 200 cpsi / 12 mil). In addition to the uncoated DPF, a platinum-coated filter (CDPF / 20 g Pt/ft^3) was used.

2.2 EXECUTION

By systematically modifying the engine parameters, the engine's variables that are responsible for generating a reactive particulate phase were analyzed. The objective was to create a comprehensive assessment of all significant operating parameters contributing to soot formation and to show their impact on soot reactivity. In the process, the engine's operating conditions were modified from the diesel-typical lean-burn operation in particular in the direction of late, cold combustion down to rich-burn engine operation (λ = 0.97). The reactivity of the raw particulate emissions was quantified using chemical/physical analyses. Next, particulate regeneration in the DPF was analyzed for operating settings indicating a high particulate ignition quality in comparison to the reference operation.

The air and fuel path of the recorded engine operation parameters was modified maintaining a neutral load level, ❷. The air/fuel ratio was adjusted during lean-burn operation by modifying the EGR rate and during rich-burn operation by restricting fresh air supply. The intake manifold pressure was modified at a constant fresh air mass flow – controlled via the throttle valve – by adjusting the EGR actuator or the VTG. This resulted in different ratios between the degree of restriction and EGR. Changes to the fuel path were made by varying the start of injection and the injection pressure as well as introducing early postinjection during rich-burn operation. We did not conduct tests with late postinjections into the exhaust port, since they do not have any impact on soot reactivity and merely lead to an increase in HC emissions, the SOF portion, and the dilution of lubrication oil. The boundary conditions were the maximum turbine inlet temperature of 820 °C as well as the maximum HC concentration of 3000 ppm (C3) in order to meet application limits relevant in practice.

3 PARTICULATE ANALYTICS AND DEFINITION OF REACTIVITY

3.1 PARTICULATE ANALYTICS

To determine the chemical/physical particulate properties, particulate samples were taken upstream as well as downstream of the DOC on quartz filters from the undiluted exhaust at constant volumetric flow using a 190 °C heated line and 175 °C at the sampling filter. This ensured a good approximation to the particulate composition in the DPF. The soot load mass was determined by weighing the filter under controlled conditions. The particulate

ENGINE	2.2-l Four-cylinder in-line engine
AIR PATH	: Four-valve technology : Turbocharger with variable turbine geometry (VTG) and charge-air cooler (CAC) : Cooled high pressure exhaust gas recirculation (HP-EGR) : Throttle valve : Swirl flap
FUEL PATH	: Common rail (Bosch) : CP3 (p_{max}: 1600 bar) : Solenoid valve injectors
RATED POWER	100 kW at 4000 rpm
MAXIMUM TORQUE	330 Nm (1200-2400 rpm)
FUEL	Low-sulfur diesel fuel (B5)
MEASURED EXHAUST COMPONENTS	CO, CO_2, O_2, HC, NO_x Black smoke number

❶ Test object data

ADJUSTMENT PARAMETERS	ADJUSTMENT RANGE
Distance between pilot injection and main injection	10 → 46° KW
Start of main injection	10 → -13° KW
Distance between main and post injection	20 → 70° KW
Injection pressure	300 → 1370 bar
Intake manifold pressure via EGR / VTG (degree of EGR throttling split)*	600 → 1290 mbar
λ (via EGR rate / air mass)	0,9 → 4,9

❷ Adjustment parameters and ranges
(*constant air mass controlled via throttle valve)

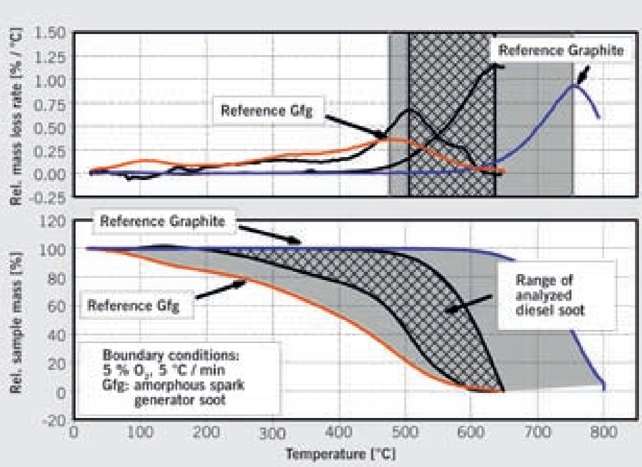

❸ Range of variation of soot reactivity

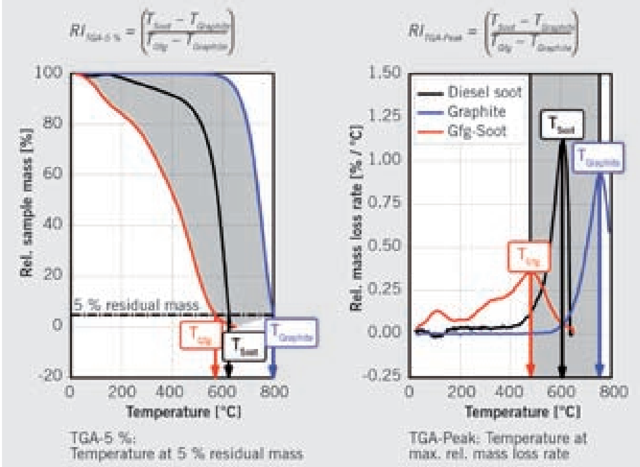

❹ Definition of the reactivity indices (RI) based on the TGA

samples were characterized analytically using thermal gravimetric analysis (TGA) and the BET method. The TGA was carried out with 5 % oxygen and 95 % helium 6.0 at a heating rate of 5 °C/min up to a maximum of 800 °C (analyzer: Thermo Cahn TG 2121). By continuously determining the mass during the heating up phase, the temperature-dependent mass losses caused by evaporation and oxidation were recorded until it was fully burned off. Since we can rule out influences caused by material transport with the TGA method, we used it to determine the purely temperature-dependent oxidation capability of the particulates. With the help of the BET method, the specific surface of particulate samples at select operating settings was determined by ICG-2 of the Forschungszentrum Jülich (analyzer: Micromeritics Gemini 2360).

3.2 DEFINITION OF REACTIVITY

In order to quantify soot reactivity, graphite (C ≥ 99 %, Sigma-Aldrich) and graphite spark generator (Gfg) soot (Gfg 1000, Palas) were analyzed as reference soots in addition to the engine soot samples by means of TGA in the same way as in [1]. Gfg soot with its highly amorphous structure represents the maximum soot reactivity that can be reached, whereas graphite features the lowest reactivity, ❸. The hatched area in the recordings of the relative sample mass and the relative mass loss rate marks the area of diesel soot generated by varying the engine parameters. In particular the point of the maximum mass loss rate shows that soot with near-Gfg properties can be generated by changing the operating parameters.

The absolute temperature of the maximum mass loss rate or a defined relative residual sample mass is not sufficient to quantify soot reactiveness. Therefore, two reactivity indices (RI) were defined by standardizing to certain temperatures for the TGA evaluation, ❹.

The reactivity index $RI_{TGA\text{-}5\%}$ is based on the temperature where the sample has oxidized to 5 % of its initial mass. This provides a good approximation to the point of complete soot burn-off and represents an index for the accumulated change of the sample. Furthermore, we standardized to the temperature at a maximum mass loss rate as a clearly defined peak ($RI_{TGA\text{-}Peak}$). It was possible to find a clear empirical correlation between this and the $RI_{TGA\text{-}5\%}$, ❺.

Due to the extensive particulate analysis only select samples (in particular for the critical variation limits) were subjected to the TGA analysis and an additional RI was identified based on the exhaust composition. We found an empirical correlation between the (logarithmic) mass ratio of the CO to the soot emissions upstream of the DOC ($RI_{CO/soot}$) and the $RI_{TGA\text{-}Peak}$, allowing the soot to be evaluated with the help of the measured test bench variables.

For a later transfer of the TGA results to the regeneration characteristics in the DPF it has to be taken into account that the reactivity determined via TGA does not include influences of mass transfer. In the Arrhenius plot a correlation between the determined reactivity and the activation energy can be expected. In the DPF there are further significant influences on the reaction rate, which are summarized in the frequency factor. These parameters are the specific soot surface and the packing density of the soot cake impacting the reaction in the range of the Knudsen diffusion (pore diameter < mean free path).

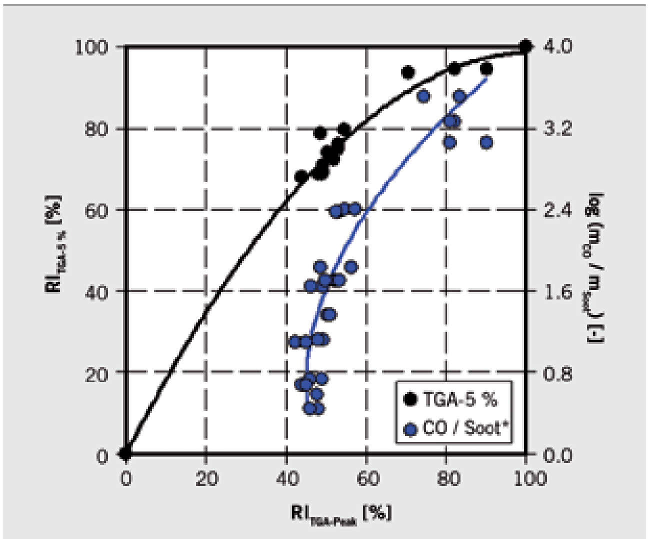

❺ Comparison of the reactivity indices (*soot mass concentration calculated via black smoke number and Mira correlation)

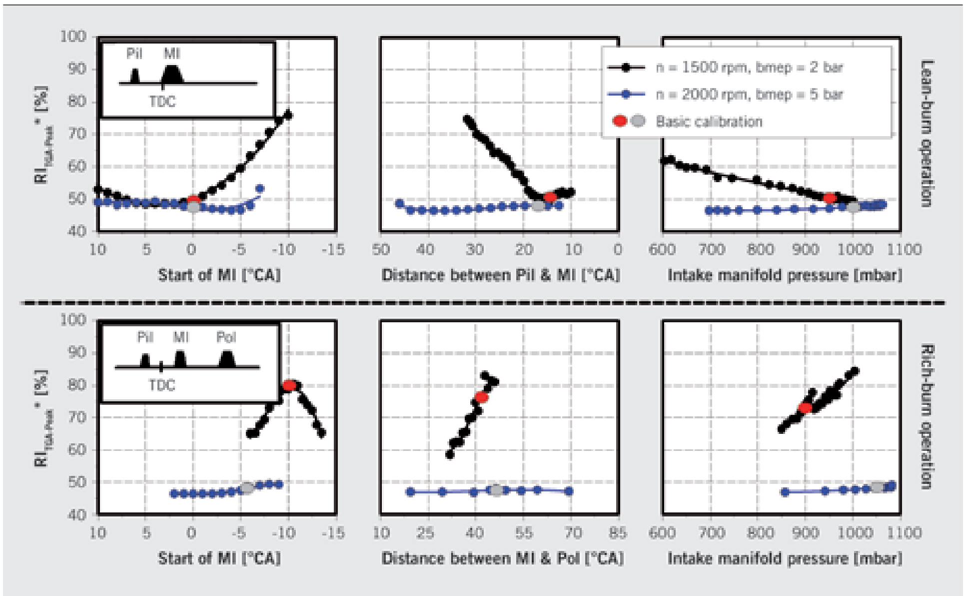

❻ Main influencing factors on the soot reactivity of particulate samples (PiI = pre injection, MI = main injection, PoI = post injection; calculated via correlation to m_{CO}/m_{Soot})

3.3 INFLUENCE OF THE ENGINE PROCESS CYCLE ON REACTIVITY

The objective of varying the parameters in particular was to represent engine operation with delayed or cold combustion, since increased soot reactivity was expected here due a reduced change in soot structure in the direction of graphite [3]. If we enter the RI calculated from the emissions via the correlation in ⑤ RI into ❻ over the modified operating parameters, we can identify three main influencing parameters in each case that affect soot reactivity during lean-burn and rich-burn operation.

During lean-burn operation, we can achieve a higher reactivity in comparison with the basic calibration by retarding the ignition timing of the main injection, by advancing timing of the pilot injection, and by using throttling. During rich-burn operation, retarding the ignition timing of main or postinjection as well as dethrottling are beneficial. Varying the main injection we can see an optimum in OP1. Moving postinjection to very late injection points is limited due to high HC emissions. It was not possible to detect a significant influence of modified injection pressure or air/fuel ratio on soot reactivity in either lean-burn or rich-burn operation. Though, depending on the engine operation mode a higher reactivity in rich-burn engine operation can be seen. In general, OP1 has a clearly higher potential of generating higher soot reactivity than OP2 with the higher load. So the positive individual result of OP1 cannot be transferred to other operation conditions. For further analyses on the DPF, we used operating settings while combining the main influencing parameters with the best possible soot characteristics, but for component protection reasons, we were not able to exploit the maximum range of variation of all parameters.

4 DETERMINING PARTICULATE REACTIVITY IN THE DPF

4.1 DETERMINING REGENERATION EFFICIENCY

To create a correlation between soot analytics and the regeneration conditions in the DPF, partial DPF regenerations were carried out on the engine test bench. The DPF was loaded with soot under the operating settings derived above and regenerated for 360 s at 600 °C. The regeneration efficiency, defined as the quotient between oxygenated and initial soot load mass, was then compared to the RI, ❼. Initially, we were not able to find a direct correlation between regeneration efficiency in the DPF and the analytically determined $RI_{TGA\text{-}Peak}$, which is why we conducted a further analysis of the influencing factors on soot regeneration in the DPF.

4.2 ANALYSIS OF SOOT BURN-OFF IN THE DPF

For a detailed analysis of the influencing factors on the thermal soot burn-off rate, the kinetic reaction approach based on Eq. 1 and Eq. 2 was used for simulation calculations [2]:

EQ. 1
$$\dot{m}_{Soot,\,Oxi} = \psi_{O_2} \cdot m_{Soot} \cdot e^{\frac{-E_a}{R \cdot T}} \cdot k_o \cdot S_R$$

EQ. 2
$$S_R = S_{R,\,BET} \cdot k_{SV,\,Load}$$

Since the exhaust gas oxygen concentration Ψ_{O2} and the soot temperature T are the same for all experiments due to the specified regeneration procedure, the soot oxidation speed $\dot{m}_{Soot,\,Oxi}$ is determined by the soot characteristics in the form of activation energy E_a as well as the specific soot surface S_R. The latter was described via the specific surface $S_{R,BET}$ that can be directly determined by means of the BET analysis as well as a correction factor $k_{SV,Load}$ depending on the space velocity during DPF loading, which shows the influence of the pore diffusion. Because of this correction the base frequency factor k_0 was assumed as constant.

By the use of SMPS measurements Pischinger et al. [3] proved a shift of the particle size distribution in rich-burn engine operation to larger particle diameter at a constant particle number. The specific surface of the BET as well showed a clear dependence on the air/

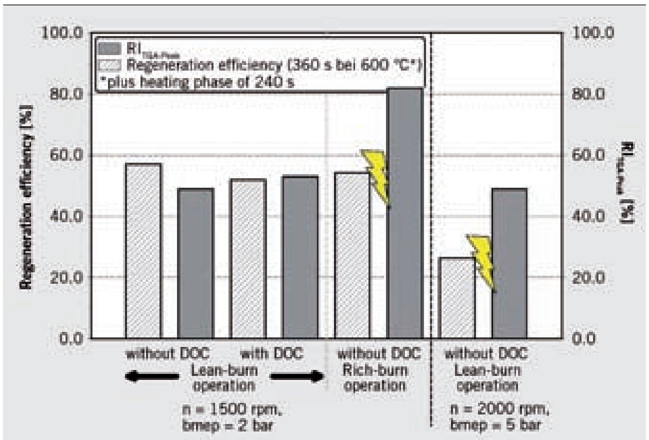

❼ Comparison between soot analytics and regeneration efficiency

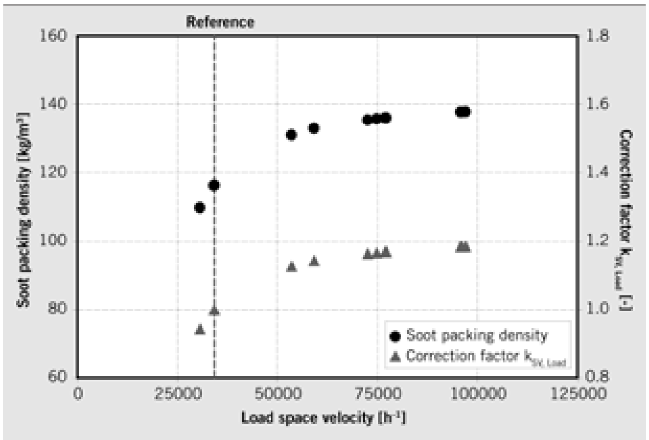

❽ Influence of load space velocity on soot density

fuel ratio. For rich-burn operation of the OP1, it is approximately one third (34 m^2/g) in comparison to lean-burn operation (96 m^2/g). The specific surfaces of soot samples for which no BET analysis was made were interpolated or extrapolated via the air/fuel ratio [3, 4].

The reason why space velocity has an influence on the reaction rate is the varying soot packing density caused by different flow conditions in the DPF during soot loading and was determined via the Peclet number following [5] (assumptions: effective DPF surface 2.5 m^2, primary particle diameter 35 nm, diffusion coefficient $D_m = 6 \cdot \times 10^{-10}$ m^2/s), ❽. This influence was eliminated while taking the soot samples for purposes of chemical/physical characterization under constant volumetric flow.

An increase in soot packing density respectively a reduction of the soot porosity decreases the amount of oxygen within the soot cake and consequently leads to a slower oxidation reaction. A comparable influence on the regeneration efficiency was earlier illustrated in [6]. The specific surface was corrected by normalizing to the reference packing density ρ_{Ref} in OP1 (lean-burn operation), Eq. 3:

EQ. 3	$k_{SV,\,Load} = \dfrac{\rho_{Soot}}{\rho_{Ref}}$

The quantification of the influencing variables from Eq. 1 was done by projecting the parameters on a required regeneration temperature for identical regeneration efficiency, for which the regeneration of lean-burn operation soot from OP1 at 600 °C soot temperature was selected as a reference, ❾.

For this purpose at first the activation energy was determined based on test bench experiments at almost isothermal DPF conditions, by which the necessary temperature offsets required to achieve the same regeneration efficiency compared to the reference regeneration could be calculated. Using the calculated influence of the activation energy the influences of mass transfer could be determined, too. The example of the base calibration in lean-burn and rich-burn engine operation of OP1 shows that the reduction of the regeneration temperature by 40 °C due to the low activation energy is overcompensated by the lower soot surface.

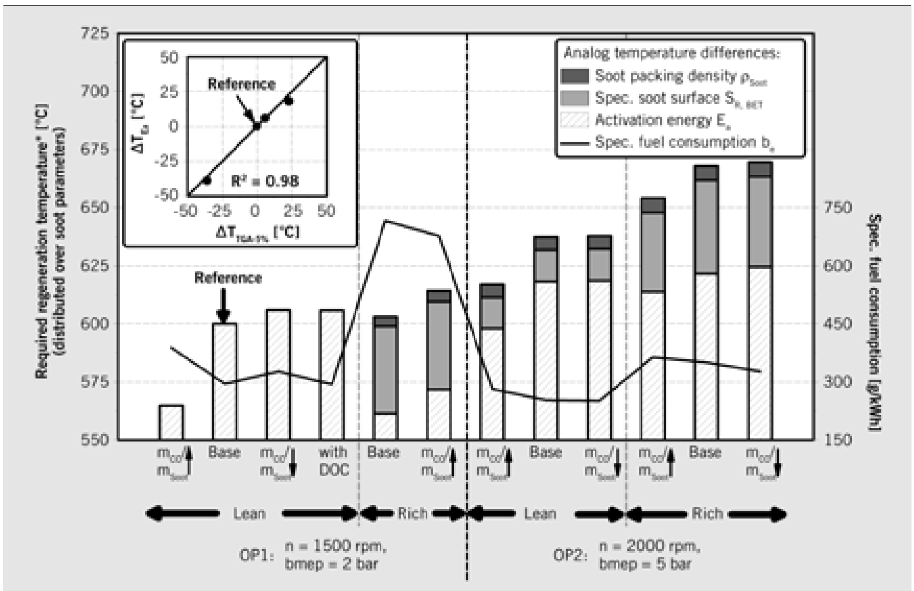

❾ Projection to the required regeneration temperature (*for identical regeneration efficiency with t_{Rgn} = 600 s at T_{Rgn} = 600 °C)

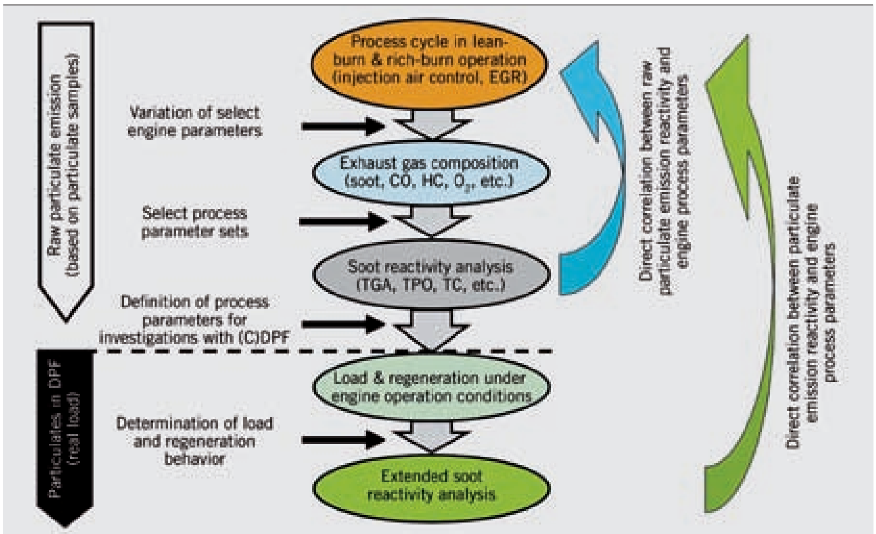

⑩ Soot reactivity analysis procedure

Generating a more reactive particulate species in the OP1 by increasing the CO/soot mass ratio (m_{CO}/m_{Soot} ↑) while taking the high increase in fuel consumption into account does not lead to the desired result. The reduced particulate reactivity at higher engine loads matches findings from earlier investigations [7, 8]. In addition to this, the comparison of the temperature differences from TGA $\Delta T_{TGA\text{-}5\%}$ to those of activation energy ΔT_{Ea}, ⑨ top left, confirms that TGA can be merely be used to evaluate the activation energy and that the soot surface and the soot packing density must also be considered during the analysis of soot reactivity in the DPF on the basis of engine parameters, ⑩.

5 ALTERNATIVE REGENERATION STRATEGY

The gained insights showed, that the reduced activation energy of reactive soot cannot be used in the DPF primarily due to its low surface. This fact however is not valid for last deposited soot particles. Due to the low mass and consecutively only for short-term available reaction enthalpy of this upper soot layer the ignition of lower soot layers is only possible by very fast temperature increase. Because the temperature influence is predominant during short-term heat-up of CDPF by near stoichiometric operation as indicated already by [9], hereupon an alternative regeneration strategy was calibrated, ⑪. From base operation in heat mode (λ = 1.7) the engine is being switched to near stoichiometric operation (λ = 1.1). Via timing of 20 s at λ = 1.1 and 5 s at heat mode within three mode changes the filter temperature is increased by means of HC and CO conversion at the DOC and/or the DPF coating to more than 700 °C, thus causing the soot to ignite, which can be seen from the increased filter outlet temperature. We can therefore trigger regeneration within a few short phases. Operating points with a lower basic temperature (city driving) can therefore efficiently used for regeneration purposes.

The CDPF was loaded with comparably unreactive soot (lean-burn operation without DOC, OP2) and then regenerated. Several

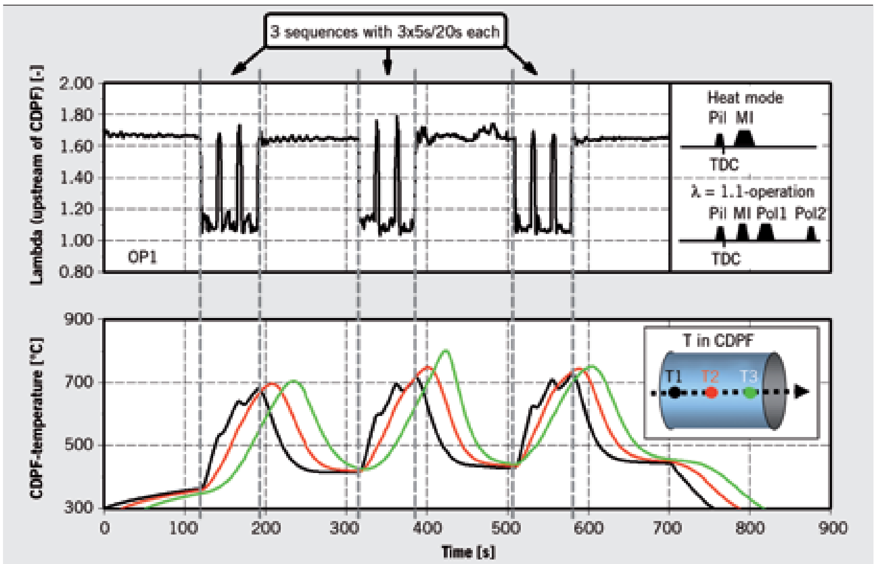

⑪ Intermittent regeneration strategy

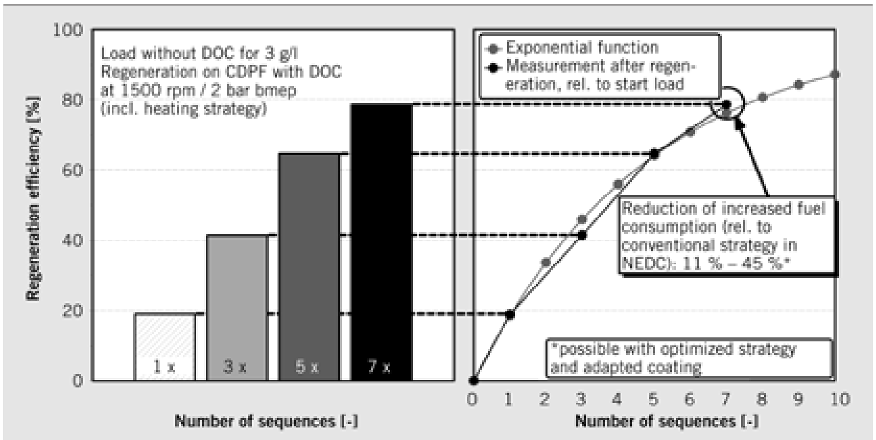

⑫ Performance of the intermittent regeneration strategy

sequences connected in series increase the regeneration efficiency, in which we can see a dependence on the load mass, ⑫. This can be approximated via an exponential function that can be used to forecast the number of sequences required. Furthermore, the alternative procedure must be designed as a function of load and speed. It involves benefits in the regeneration-based fuel penalty and the required regeneration time and thus operational safety compared with a conventional procedure ($T_{entry,DPF}$ = 650 °C) under NEDC conditions (boundary conditions: identical initial soot loading and regeneration efficiency; engine operation point at regeneration: BP1; equal performed work during loading and regeneration). Hererby a decrease of the regeneration-based fuel-penalty consumption of 11 % with comparable oil dilution level is possible. By optimization of strategy and hardware the regeneration-based fuel penalty could be approximately halved. By this means the thermal stress to turbocharger as well as the catalytic coatings at comparable level to conventional regeneration is expected.

6 CONCLUSION

Because we strive to lower a regeneration-based increase in fuel consumption, knowing about the properties of the soot in the DPF is becoming increasingly important. Against this backdrop, soot reactivity was analyzed in detail as part of a FVV project No. 954 on a passenger car diesel engine at the Institute for Combustion Engines (VKA) of the RWTH Aachen University.

We found that the reactivity of the raw particulate emissions can be classified by analyzing the particulate samples by means of reactivity indices and represented directly via the CO/soot mass ratio as a function of the engine process parameters. By modifying the engine parameters, we were able to adjust raw particulate emissions with wide reactivity differences.

DPF regeneration tests for loads with different reactivity indices showed that, in contrast to the positive impact of the lowered activation energy of highly-reactive particulate phases, the reduced specific soot surface has a negative effect on the regeneration efficiency. As a result, generating a highly-reactive particulate phase with a special focus on fuel consumption alone does not lead to the desired result. An intermittent regeneration strategy was developed based on these findings; it can be used to represent advantages with regard to the regeneration-based increase in fuel consumption as well as operational safety in particular during low loads by quickly heating up the DPF. The research results and the analysis process we have developed allow us to create a direct correlation to the engine process parameters that can be used for future soot reactivity investigations.

REFERENCES

[1] Knauer, M.; et al.: Soot Structure and Reactivity Analysis by Raman Mcrospectroscopy, Temperature-Programmed Oxidation, and High-Resolution Transmission Electron Microscopy. In: J. Phys. Chem. A 113, USA, 2009
[2] Höhne, G., Untersuchungen zur oxidativen Regeneration von Diesel-Partikelfiltern. Dissertation, Universität Hannover, 2005
[3] Pischinger, S.; et al.: Untersuchung zu innermotorischer Bildung und Abbrand von Ruß im unterstöchiometrischen Betrieb an einem modernen CR-Dieselmotor. Vortrag, Haus der Technik, 2003
[4] Bönig, M.; Feldermann, C.; Jander, H., Lüers, B.; Rudolph, G.; Wagner, H. G.: Soot Formation in Premixed C2H4 Flat Flames at Elevated Pressure. Proceedings, 23rd Symposium on Combustion, University of Orléans, Orléans, France, 22nd to 27th July 1990
[5] Konstandopoulos, A. G.; et al.: Microstructural Properties of Soot Deposits in Diesel Particulate Traps. SAE 2002-01-1015, USA, 2002
[6] Zikoridse, G.; Sandig, R.: DPF-Beladungsprozedur. FVV-Abschlussbericht, Heft 891, Frankfurt/Main, 2009
[7] Setiabudi, A.; et al.: Appl. Catal. B 50 (3), 2004
[8] Muller, J. O.; et al.: Catal. Today 102, 2005
[9] Pischinger, S.; Sliwinski, B.: Partikelkatalysator mit NO_x-Speicher; Abschlussbericht zum FVV-Vorhaben; FVV Heft 850, 2008

THANKS

The work originated as part of the research project No. 954 “Reactivity of Soot” of the Forschungsvereinigung Verbrennungskraftmaschinen e. V. and was supported by a working group (consisting of representatives from the industry). We want to thank them as well as their Head, Dr. Dieter Rothe, MAN Nutzfahrzeuge AG, as well as the Institute of Hydrochemistry (Prof. Reinhard Nießner, TU Munich), and the DLR Institute of Combustion Technology (Prof. Manfred Aigner, Stuttgart) for their support with the joint research project. The authors want to thank Corning Incorporated for the generous appropriation of resources.

AUTHORS

DIPL.-ING. VOLKER GROSS
was Scientific Assistant at the Institut für Kolbenmaschinen of Karlsruhe Institute of Technology (Germany).

DR.-ING. HEIKO KUBACH
is Group Leader of Research SI Engines at the Institut für Kolbenmaschinen of Karlsruhe Institute of Technology (Germany).

PROF. DR.-ING. ULRICH SPICHER
is Leader of the Institut für Kolbenmaschinen of Karlsruhe Institute of Technology (Germany).

DR.-ING. ROBERT SCHIESSL
is Head of the Laser Diagnostics Group at the Institut für Technische Thermodynamik of Karlsruhe Institute of Technology (Germany).

PROF. DR. RER. NAT. ULRICH MAAS
is Head of the Institut für Technische Thermodynamik of Karlsruhe Institute of Technology (Germany).

LASER-INDUCED IGNITION AND COMBUSTION IN A SI ENGINE WITH DIRECT INJECTION

Laser-induced ignition has shown huge advantages for the combustion of lean air-fuel mixtures in SI engines. A research project founded by the FVV under “DI Laserzündung” and No. 928 was set up at the Institute for Reciprocating Engines (IFKM) and the Institute for Technical Thermodynamics (ITT) at the Karlsruhe Institute of Technology (KIT) to investigate the potential of the laser-induced ignition. The emphasis was on improving combustion initiation and heat release during a direct injection with a spray-guided combustion.

THE SEAL OF APPROVAL FOR SCIENTIFIC ARTICLES IN MTZ.
MTZ PEER REVIEW
RECEIVED 2010-02-17
REVIEWED 2010-03-01
ACCEPTED 2010-04-10
REVIEWED BY EXPERTS FROM RESEARCH AND INDUSTRY.

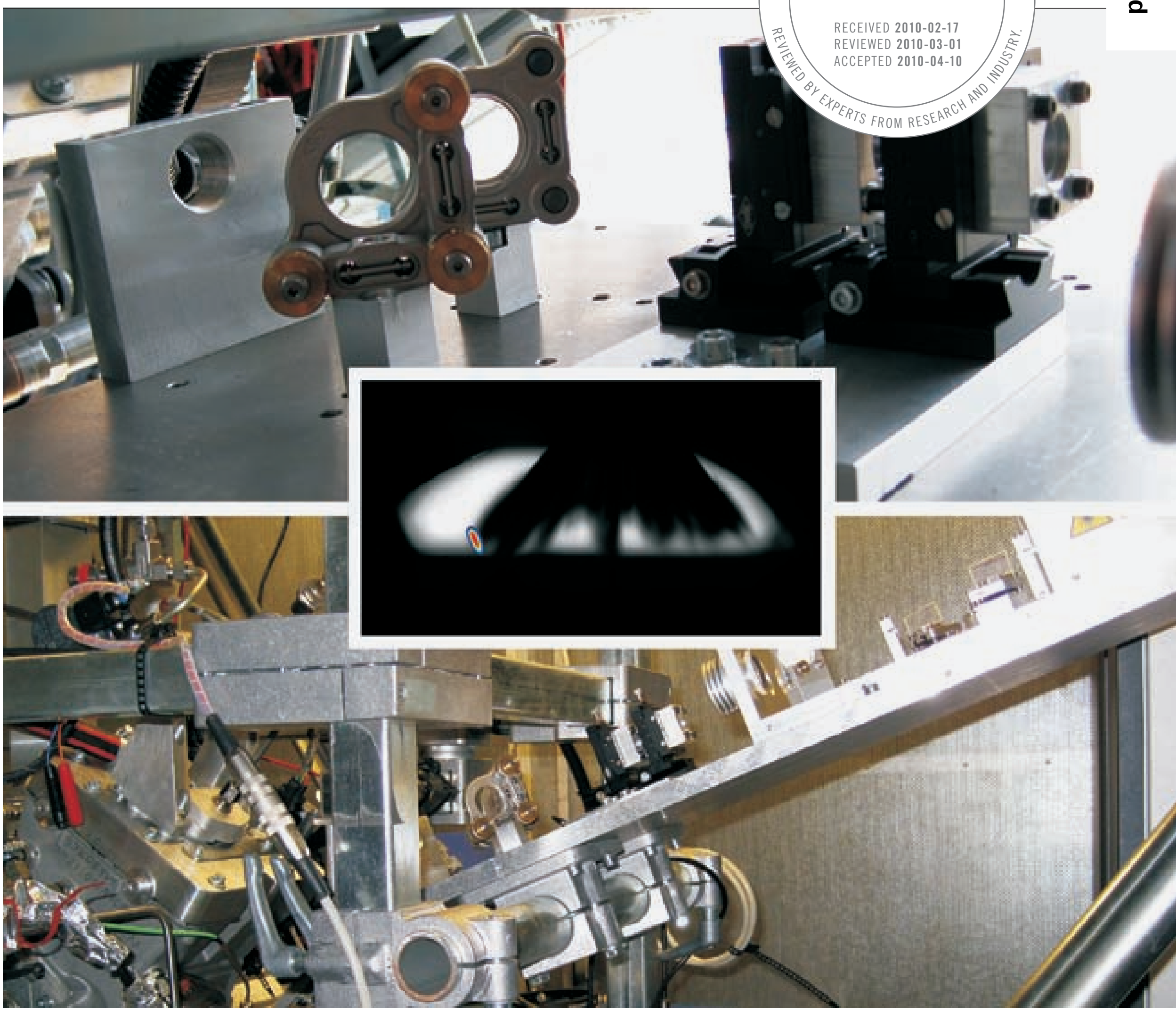

1 INTRODUCTION

Due to the highly stratified mixture SI engines with direct injection and spray-guided combustion pose a challenge to the ignition system. Laser-induced ignition combines the advantages of high efficiency, variable spark location, and wear-free ignition.

Laser-induced ignition of air-fuel mixtures is based on an optical gas breakdown. To generate an optical breakdown, very high intensities are required, which can be accomplished by focusing high energy nanosecond laser pulses. This plasma forms an ignition kernel which is the source for a self-preserving reaction front under adequate conditions. By adjusting the focusing lens the plasma can be shifted into the spray along the optical axis. This offers the possibility to influence the heat release by the location of the ignition kernel [1].

Based on experimental investigations on a single cylinder engine with optical access the Karlsruhe Institute of Technology (KIT) carried out thermodynamical and optical analysis of the combustion with laser-induced ignition. The interpretation of experimental results is supported by the numerical simulation of the ignition process.

2 TEST SETUP AND LASER IGNITION SYSTEM

The basis engine used for the experiments was a M272DE35 single cylinder engine of Daimler AG. In 2006 spray-guided combustion, in combination with exhaust after-treatment for lean mixture, was introduced to the market with this engine [2]. The technical data of the test engine are listed in ❶. For fuel injection and mixture formation, a piezo-actuated outward opening nozzle is used with an injection pressure of up to 200 bar. The standard ignition system is a coil ignition system with an ignition energy of 110 mJ. For optical investigations the engine is equipped with four optical accesses.

The laser ignition system is based on a Nd:YAG double pulse laser with variable repetition frequency. Two independent laser resonators allow different ignition strategies. The pulses can either be divided with a temporal offset or be superimposed. For focussing the laser beam into the combustion chamber a fused silica aspherical lens (f_L = 22.6 mm) is used.

A fine thread allows adjustment of the lens and thus laser spark location. The laser spark plasma can be shifted towards the piston up to a distance of 4.5 mm from the spark gap of the conventional spark plug. The lens is protected from the hot combustion gases by a sapphire window. Both lens and window are adapted to the cylinder head by an optical spark plug. The optical spark is shown in ❷. ❸ presents the arrangement of conventional spark plug, optical path of laser ignition and injection spray. The technical data of the laser ignition system are listed in ❹.

FEATURE	VALUE
Basis engine	Mercedes-Benz M272DE35
Design	Single cylinder, water-cooled, four valves combustion chamber
Compression ratio ε [-]	11.68:1
Displacement V_H [cm³]	583
Bore × stroke [mm × mm]	92.9 × 86
Injector type	Outward-opening
Injection pressure [bar]	200

❶ Technical data of test setup

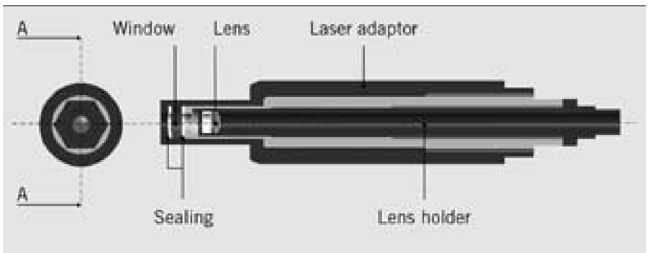

❷ Optical spark plug

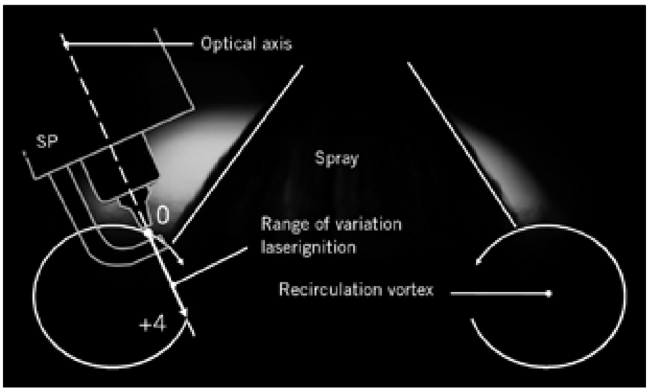

❸ Position of conventional spark plug (SP), optical path of laser ignition and injection spray

FEATURE	VALUE
Type	Nd:YAG
Wave length λ [nm]	1064
Repetition rate f [Hz]	0-50
Pulse length t_P [ns]	4
Pulse energy E_L [mJ]	2 × 25
Beam diameter $Ø_{beam}$ [mm]	≈ 2
M^2 [-]	≈ 1.5

❹ Technical data of the laser system

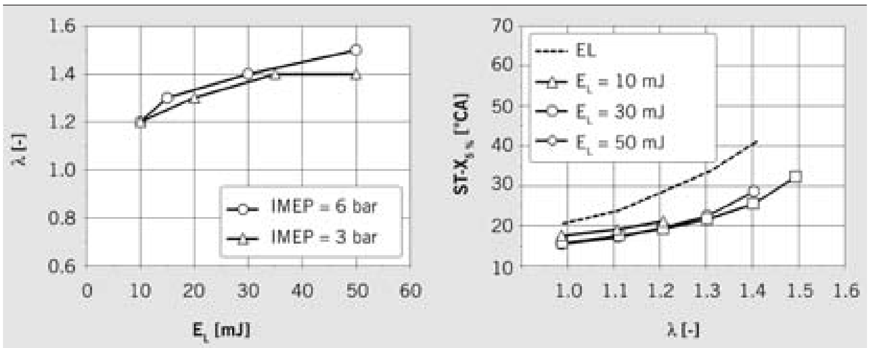

❺ Lean limits (left) and combustion delay (right) at stratified operation

3 SIMULATION MODEL

Two different models were used for the simulation of laser induced ignition. The modelling of the ignition limits is based on a homogeneous chemical reactor which is fed with an air-fuel mixture [3]. Furthermore, the temporal evolution of the cylinder charge in the immediate vicinity of the hot laser spark was modelled with a simple mixing reactor model.

Thus, chemical reactions as well as dissipative processes can be modelled. The model allows a quantitative determination of the conditions (air-fuel ratio, dissipation rate, gas temperature, pressure) under which a successful ignition occurs. With this, the theoretical ignition limits of the laser-induced ignition can be calculated and embedded into CFD models.

4 COMBUSTION INITIATION BY LASER-INDUCED IGNITION

In the following, lean limits and flame development, but also the influence of ignition strategy on combustion in stratified operation mode are discussed.

4.1 LEAN LIMITS AND FLAME DEVELOPMENT

Laser ignition with homogeneous air-fuel mixtures was investigated prior to stratified operation in order to better understand laser-induced ignition. Combustion phasing was adjusted to 8° CA ATDC for these investigations. In ❺, left, lean limits of engine operation are shown for IMEP = 3 bar and IMEP = 6 bar respectively. The minimum ignition energy to operate the engine without misfires is 10 mJ. The lean limits for this energy are λ = 1.2 for both loads. Increasing the laser energy makes it possible to shift the lean limits to λ = 1.4 for IMEP = 3 bar and to λ = 1.5 for IMEP = 6 bar respectively. As can be seen, the ignition limits are shifted towards leaner mixtures for higher loads, which arises from the higher pressure at ignition time compared to the lower load. In addition to a decreased breakdown threshold, energy absorption by the plasma increases for higher pressures. Due to the higher gas density, a larger number of molecules is located in the focal region. Thus a higher fraction of laser energy is absorbed by the plasma and the ignition limit is shifted [4].

Combustion delay for an IMEP = 3 bar for laser-induced and traditional electrical ignition (EI) is shown in the right part of ⑤. It can be seen that compared to electrical ignition, the combustion delay is considerably reduced. Reduced heat losses and the extremely short spark duration of a few microseconds are the reasons for the reduced combustion delay of laser induced ignition. Furthermore, the development of an early flame kernel is not affected by electrodes extending into the combustion chamber.

A comparison of flame propagation with traditional EI and laser-induced ignition (LI) is shown in ❻. The lower part of the

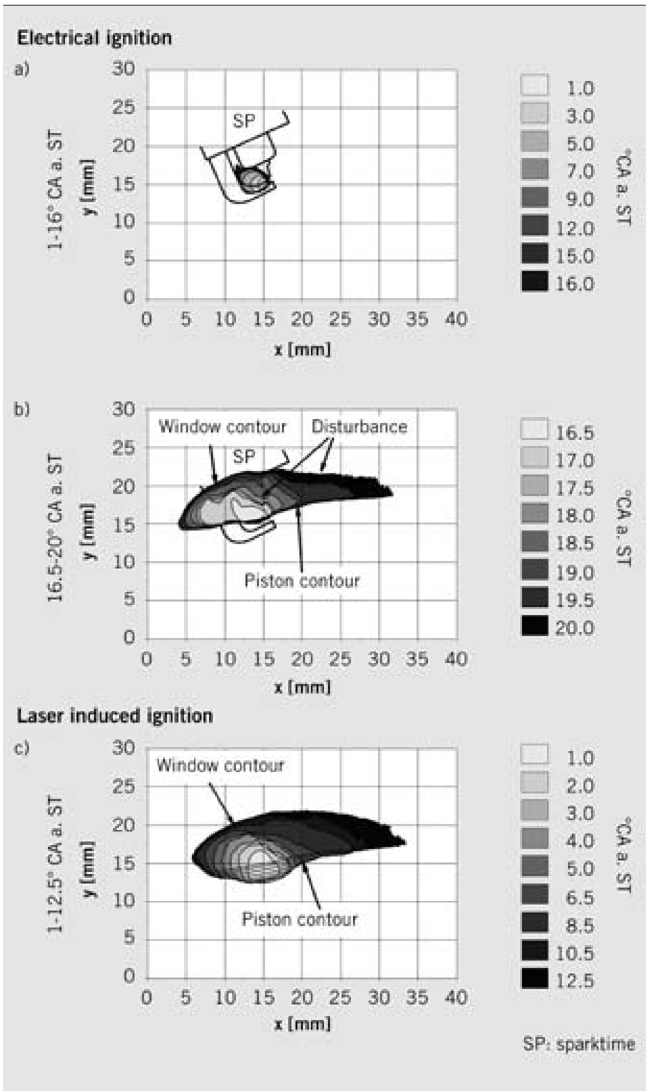

❻ Flame propagation with traditional electrical ignition (a and b) and laser-induced ignition (c) flame is covered by the piston bowl. Flame propagation with laser-induced ignition is almost spherical, see part c of ⑥. With EI the initial disturbance of the flame kernel development, part a of ⑥, due to the heat losses to the spark plug electrodes can clearly be seen in the flame front many crank angles after ignition, part b of ⑥.

4.2 INFLUENCE OF IGNITION STRATEGY ON COMBUSTION IN STRATIFIED OPERATION MODE

The heavy stratification of air-fuel mixture in stratified operation mode leads to a small combustion window in which a reliable ignition is possible. The possibility of varying the laser spark location offers the possibility to shift the spark into the spray in stratified operation mode. Depending on spark location and offset between end of injection and spark timing an combustion window results in which a reliable ignition is possible.

Mixture formation is realized with triple injection for the underlying combustion process. With this injection strategy, the region with stoichiometric mixture around the spark location is considerably increased, as is the time window for reliable ignition. As the combustion of the mixture is carried out after the second injection, spark timing is specified in relation to the end of this injection. To gain knowledge about the temporal evolution of the air-fuel ratio in the vicinity of the spark location, investigations with laser-induced breakdown spectroscopy were carried out at different spark locations [5]. The course of air-fuel ratio at the spark location as well as the control signal of the injector are shown in ❼.

Misfires in percentages depending on spark location and spark timing with single spark and a laser energy of E_L = 50 mJ are shown in the top of ❽ for a mean pressure IMEP of 3 bar and an IMEP of 6 bar respectively. For both loads on the left side the window is limited by the rich air-fuel ratio due to the second injection. On the right side the misfire rate increases as a result of the fast leaning of the mixture. Mixture gradients are smaller on the right side, which can also be seen in the course of misfires.

In fact the mean air-fuel ratio lies between ignition limits for the spark location x = 3 and a spark timing of 14° CA after EOI I2 (End of second injection). However in several cycles it lies beyond ignition limits, causing misfires. Between 4 and 6° CA after EOI I2 the mixture is leaning heavily until the fuel of the third injection causes a further enrichment of the mixture. The smallest combustion window with a width of 4° CA results for the spark locations x = 0 and x = 1. By shifting the spark location towards the piston the combustion window can be expanded to 8° CA. This can be attributed to the smaller gradients of the air-fuel mixture in the centre of the recirculation vortex. Inside the window there are two regions with a slightly increased misfire rate, caused by the lean mixture in this region and cyclic fluctuations of mixture formation. Due to the smaller mixture gradients combustion is more stable for IMEP = 6 bar. For this load the combustion window can be broadened considerably by shifting the spark location towards the piston.

The bottom of ⑧ shows the misfire rate with double spark. Experiments were carried out with a laser energy of E_L = 2 x 25 mJ and the spark location was shifted to the position x = 3. Misfire rate is plotted against spark timing and the distance between the two laser pulses. With the same total energy the robustness of the combustion process can clearly be improved with double spark. For IMEP = 3 bar the region without misfires is twice as wide as with single spark. Best results are obtained for a pulse spacing of 20 µs. For shorter pulse spacings the second pulse leads to a negative impact on the flame kernel developing out of the first pulse. For IMEP = 6 bar the spark timing could be shifted up to 24 °C relative to the second injection without increasing the misfire rate.

5 NUMERICAL SIMULATION OF IGNITION

On the basis of numerical simulation studies were performed to investigate the dependence of the ignition limits on air-fuel ratio and dissipation rate. Furthermore the influence of heat losses and double spark on the ignition limits was examined.

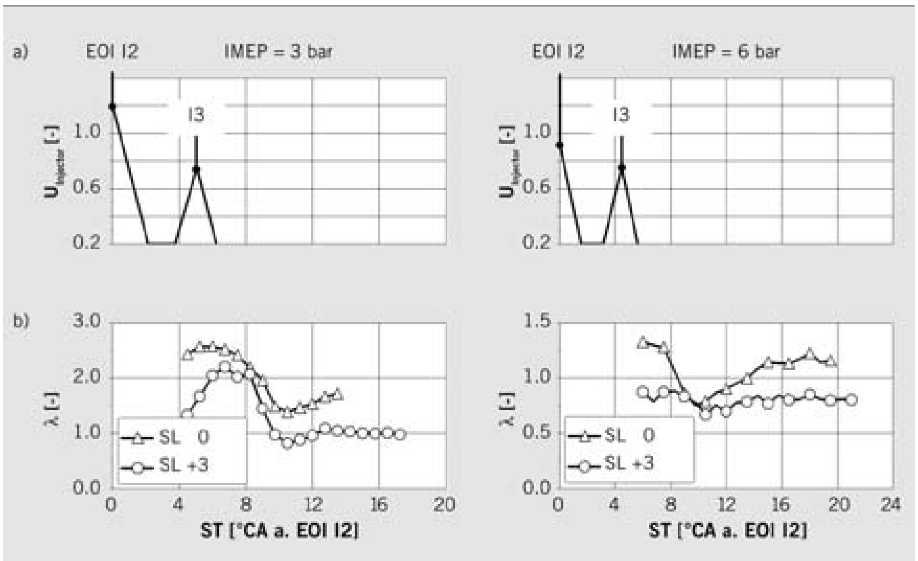

❼ Control signal of injector (a) and air-fuel ratio at the spark location (b) with laser-induced ignition

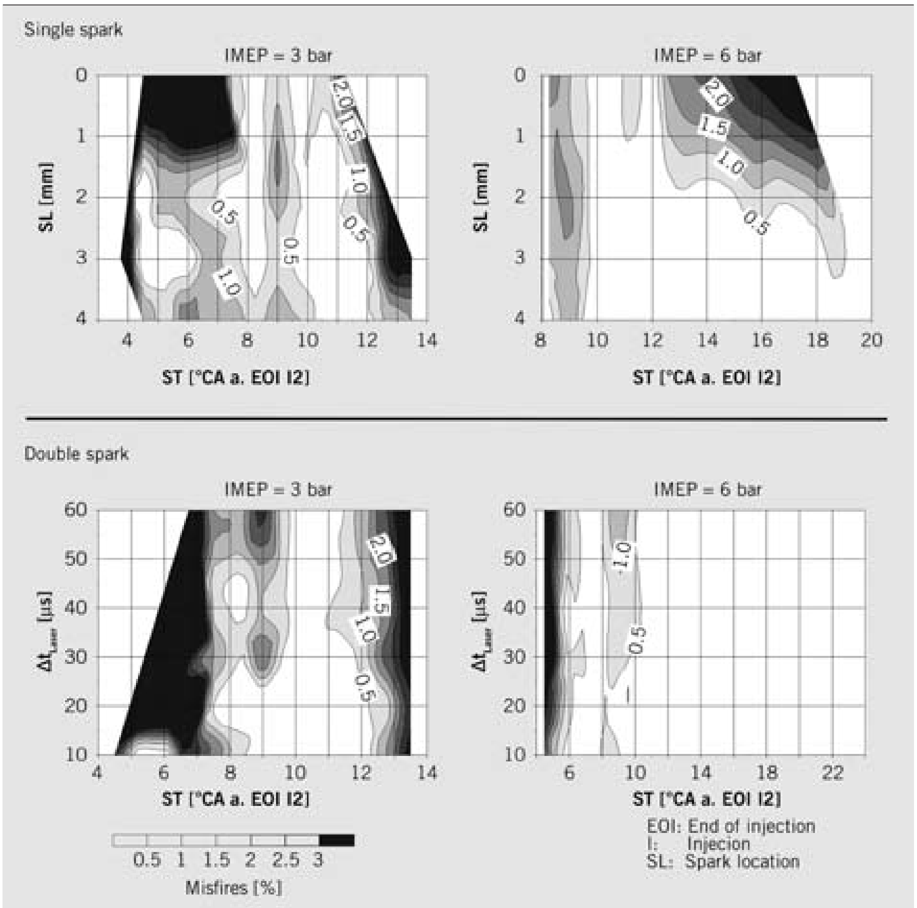

❽ Window for combustion with single (top) and double spark (bottom) at laser spark location x = 3

❾ shows an exemplary simulation result by means of the temporal evolution of the temperature of the hot kernel. Heat losses were neglected.

For successful ignition (part a of ⑨) the temperature of the kernel directly after the laser pulse is 5000 K. After this, temperature initially decreases, which can be attributed to the dissociation of molecules at high temperatures, an endothermic process. This also causes a rapid decrease of fuel mole fraction; however, no combustion (CO_2-formation) occurs yet. The temperature reaches a local minimum and afterwards increases again due to the onset of exothermic reactions. Previously formed products react further and a noticeable quantity of CO_2 is formed. During this phase ($t < 10^{-7}$ s) only a small quantity of unburned gas was mixed into the kernel. Following this, cold unburned gas is mixed slowly into the kernel causing a decreasing kernel temperature. Simultaneously CO_2 is formed by the reaction of the unburned gas. At 10^{-4} s a stationary state results, in which all unburned gas is completely consumed.

An extinction is shown in part b of ⑨. Here, the unburned gas is fed to the hot kernel at a considerably higher rate. Initially the temporal evolution is similar to part a of ⑨, because the supply of unburned gas has no relevance at very short time scales. Starting from approximately 10^{-6} s a difference can be noticed, as the temperature decreases faster and the chemical reaction of the supplied fresh gas cannot compensate for the steep decrease of temperature. At the resulting steady state, there is only unburned fresh gas. This model can be used to calculate the physical boundaries at which successful ignition passes to extinction.

Part a of ❿ shows the ignition limits for different heat conduction rates based on air-fuel ratio and the mixture velocity. Inside the area bounded by the curves ignition takes place, outside the flame kernel is extinguished. Without heat conduction, the ignition limit is mainly affected by mixture velocity. If heat losses are considered, an ignition limit at slow mixture velocities can be observed, and the width of the ignitable region decreases with increasing heat losses. The location of the right ignition limit is not influenced by the heat losses. Furthermore, ignition limits are dependent on air-fuel ratio. Near an equivalence ratio of $\lambda = 1$, the influence is relatively weak. The greatest expansion of the ignitable region can be observed for slightly rich mixtures.

The ignition mechanisms of several temporally or spatially divided laser pulses can also be studied by use of a simulation model. The temporal evolution of the temperature profile for two spatial divided laser pulses is shown in Part b of ⑩ as false colour plot. At t = 0 two laser pulses are created in an air-fuel mixture (near 0.6 and 0.78 mm). One of the pulses has less energy causing only a weak temperature increase and, eventually, extinction. The other pulse causes a locally successful ignition and flame propagation which finally also converts the extinguished mixture of the other pulse.

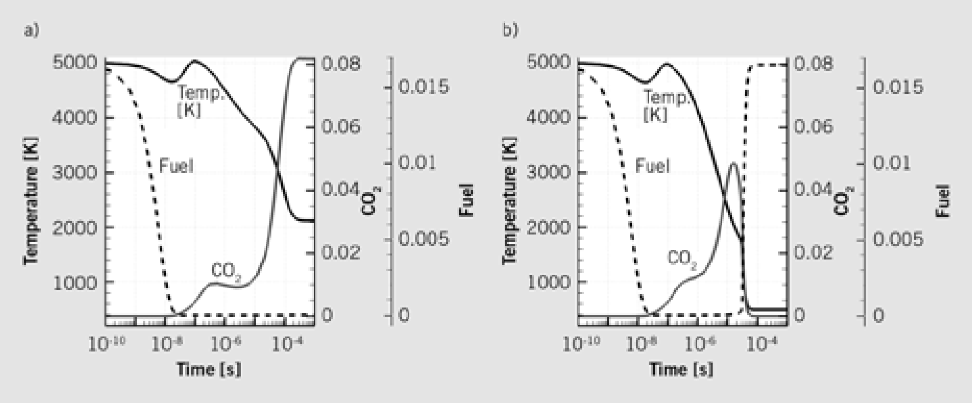

❾ Temporal evolution of temperature and mole fraction of fuel and CO_2 for successful ignition (a) and extinction (b)

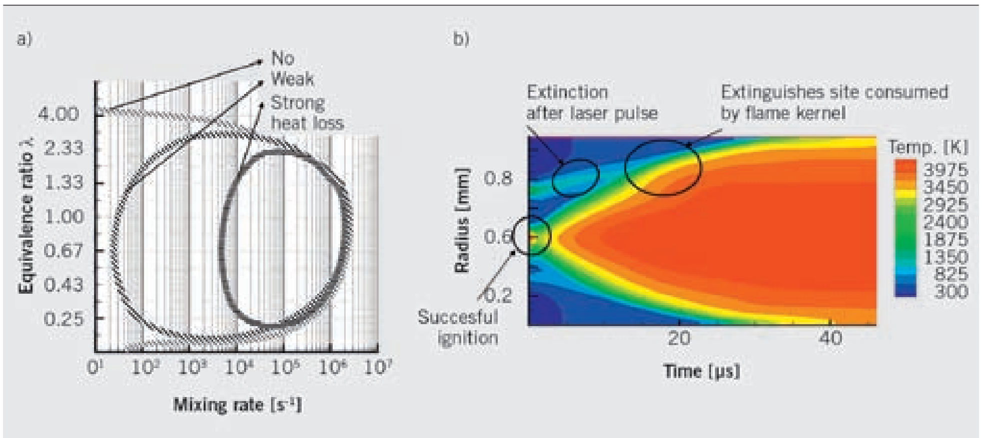

❿ Ignition limits with laser-induced ignition (a); note the non-equidistant scale at the equivalence ratio axis for better representation. Spatio-temporal evolution of temperature (b) for spatially distributed laser pulses; represented by a false color contour plot

The result confirms the use of multiple ignition strategies in engines with heavy stratification of the mixture. As the turbulent flow field in the combustion chamber causes temporal and spatial fluctuations a distribution of the laser energy on several ignition kernels increases the probability for a globally successful ignition.

6 INFLUENCE OF SPARK LOCATION ON THE COMBUSTION PROCESS IN STRATIFIED OPERATION

By moving the spark location into deeper regions of the combustion chamber the mixture formation at the spark location can be influenced indirectly, resulting in differences in heat release. In ⓫ the duration of mixture conversion for the different combustion phases is shown. A deep spark location results in fast combustion and conversion during the first part of the combustion, see part a of ⑪. During the second part of combustion conversion is faster for the upper spark location, see part b of ⑪. This is in contrast to the first part of the combustion and leads in both cases to a similar total combustion duration, see part c of ⑪.

The reason lies within the characteristically heat release of spray-guided combustion. The stratification of the mixture inside the combustion chamber leads to a partially premixed combustion. During the first part the rich mixture in the centre of the combustion chamber is converted, during the second part the lean mixture in the boundary areas of the combustion chamber – with the characteristically slow combustion is converted. After the combustion, mixture formation is proceeding in the parts of the combustion chamber which are not covered by the propagating flame front. The richest mixture is located in the region of the recirculation vortex of the spray where flame propagation begins. Originating from the centre of the vortex air-fuel ratio increases in the direction of the boundary areas. After combustion the flame propagates faster into the rich regions than into the lean boundary areas of the mixture cloud. Due to the faster conversion at the deep spark location there is less time for the transportation of the fuel into the boundary areas of the mixture cloud. There the mixture is leaner causing a slower combustion by the conversion of the lean part of the mixture.

7 SUMMARY

Experimental and numerical investigations of laser-induced ignition were carried out in this FVV No. 928 research project by Karlsruhe Institute of Technology (KIT). Although laser-induced ignition shows good results for the combustion of homogeneous lean mixtures the combustion of stratified air-fuel mixtures is rather difficult. By the use of double laser, ignition in stratified combustion mode could clearly be improved which was confirmed by the numerical simulation. Shifting the laser spark into deeper regions of the combustion chamber has rather a negative impact on the heat release.

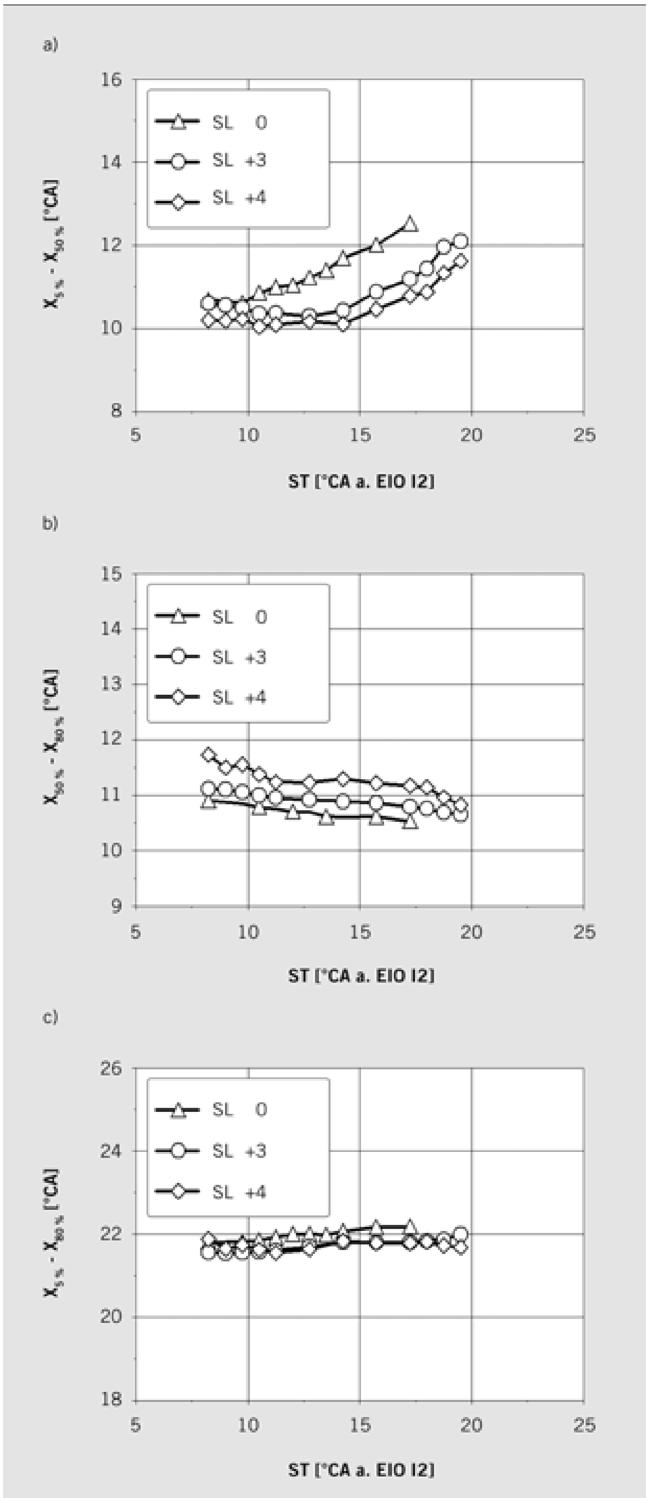

⓫ Combustion duration depending on spark location (SL)

The numerical results show how the propagation of the laser-induced flame kernel is influenced by the interaction of chemical reactions and transport processes. On the basis of simulations, ignition limits can be calculated as a function of physical parameters (for example, air-fuel ratio, gas temperature, pressure and mixing rate), which can be used for the CFD simulation of ignition processes in combustion engines. Laser-induced ignition is in an early stage of development. In this work some potentials of this innovative ignition system were shown. For an application in production engines further investigations are necessary, especially with regard to optical components.

REFERENCES

[1] Geringer, B.; Graf, J.; Klawatsch, D.; Lenz, H. P.; Liedl, G.; Schuöcker, D.; Piock, W. F.; Jetzinger, M.; Kapus, P.: Laserinduzierte Zündung an einem Otto-DI-Brennverfahren der zweiten Generation. 24. Internationales Wiener Motorensymposium, 2003

[2] Schaupp, U.; Altenschmidt, F.; Bertsch, D.; Laudenbach, N.; Voigtländer, D.; Waltner, A.: Das strahlgeführte Mercedes-Benz-Brennverfahren: Robustheitsanforderungen unter Serienaspekten. 6. Tagung Direkteinspritzung im Ottomotor, 2005

[3] Esser, C.; Maas, U.; Warnatz, J.: Chemie der Selbstzündung in Kohlenwasserstoff-Luft-Mischungen bis hinauf zum Oktan und der Bezug zum Motorklopfen. VDI Berichte 574, 269. VDI-Verlag, Düsseldorf, 1985

[4] Bindhu, C. V.; Harilal, S. S.; Tillack, M. S.; Najmabadi, F.; Gaeris, A. C.: Energy Absorption and Propagation in Laser-Created Sparks. Applied Spectroscopy, Volume 58, Number 6, 2004

[5] Groß, V.: Untersuchung der laserinduzierten Zündung an einem Ottomotor mit Direkteinspritzung und strahlgeführtem Brennverfahren. Dissertation, Universität Karlsruhe, 2010

THANKS

This report ist the scientific result of a research project which was initiated by the “Forschungsvereinigung für Verbrennungskraftmaschinen e. V.” (FVV, Frankfurt/Main) and carried out at the Institut für Kolbenmaschinen at the Karlsruhe Institute of Technology (KIT) leaded by Professor Ulrich Spicher and the Institut für Technische Thermodynamik at the Karlsruhe Institute of Technology (KIT) leaded by Professor Ulrich Maas. The work was founded by the Bundesministerium für Wirtschaft und Technologie (BMWi) via the Arbeitsgemeinschaft industrieller Forschungsvereinigungen e. V. (AiF) (AiF-Nr. 14989 N). The project was accompanied by a working group of FVV leaded by Dipl.-Ing. Uwe Schaupp, Daimler AG. The helpful support of the working group is gratefully acknowledged.

DIMETHYLETHER – DIESEL ALTERNATIVE FOR THE FUTURE?

Due to dwindling resources, heavy price volatility and the unilateral dependency on crude oil, the demand for alternatives to diesel and gas fuels is increasing. Dimethylether (DME) seems to present a promising option. Early 2009, within the framework of a six month FVV project (keyword "DME – Alternative Fuels", purpose No. 1005), a potential analysis of DME as a fuel was carried out at the Chair of Combustion Engines (LVK) at the Technische Universität München (TUM). This paper concludes important information about DME from the point of view of heavy duty engine development.

AUTHORS

DIPL.-ING. MARTIN WERNER
is Scientific Employee at the Chair for Internal Combustion Engines at the Technische Universität München (Germany).

PROF. DR.-ING. GEORG WACHTMEISTER
is Director of the Chair for Internal Combustion Engines at the Technische Universität München (Germany).

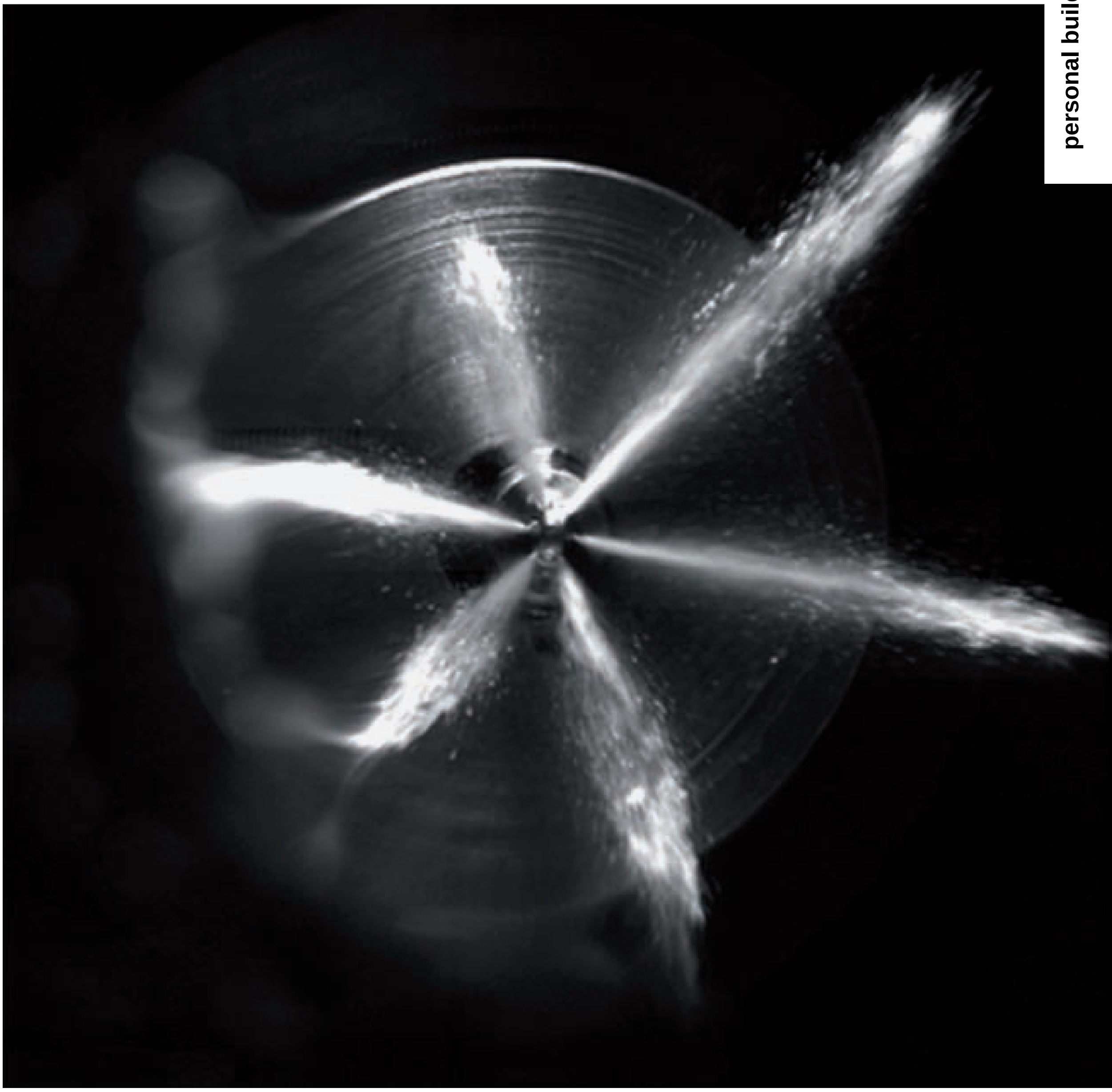

1 AWARENESS IS RISING

The awareness level of Dimethylether (DME) as an alternative fuel was raised predominantly by numerous international research projects within the last couple of years. Compared to diesel fuel, the use of DME in combustion engines at comparable power and efficiency levels leads to significantly reduced pollutant emissions.

A market analysis was carried out in this FVV project in order to assess the production, usage, availability and opportunities, as well as challenges of a – preferably comprehensive – market launch. The combustion engine suitability as well as the state of knowledge about DME was studied with the use of technical literature covering the areas of combustion processes, fuel systems and numerical calculations.

2 MARKET ANALYSIS

The production of DME is based either on fossil energy sources or biomass. It is possible to use fossil energy carriers as natural gas, crude oil, coal or even each kind of bio mass. There are direct or indirect ways of producing DME, ❶. The choice of the raw material as well as the choice of the production process significantly influences the resulting well-to-wheel values (for example emissions, efficiency, costs) [1].

The amounts of DME that are currently available are mainly produced from natural gas via the indirect method. In the next couple of years a strong increase of DME production from coal can be expected. If DME is produced from biomass (Bio DME), it is advisable to use black liquor as raw material, as the well-to-wheel efficiency is favorable in comparison to diesel fuel.

Compared to other renewable fuels of the second generation, Bio DME achieves a higher land utilization ratio and is thus potentially able to replace large quantities of conventional fossil fuels. The production process via the direct method achieves higher overall efficiency degrees, yet is not in large-scale implementation so far [1, 2]. DME is used as an energy carrier in combustion processes or as feed material for the reformation into other substances.

Currently, its use as a fuel plays a diminutive role compared to its utilization in the chemical industry or domestic area. Yet a strong increase in its use as a fuel can be expected. China is pioneering in DME production and utilization. The country wants to produce more than 20 million tons of DME annually by 2018. 50 % of the predicted amount shall then be used as fuel. Other countries such as Egypt, Australia, Indonesia, Japan, Sweden and South Korea are producing or targeting lower quantities [3].

Its market launch could be threatened by the required infrastructural upgrades, the complexity of the necessary engine components' development or the breakthrough of other alternative fuels. There are nevertheless significant advantages, such as its suitability for combustion engines and its characteristics as a multi-source fuel and multi-purpose fuel. The use of DME in the automotive sector will be initially restricted to centrally fuelled vehicles, as in those cases it is not necessary to establish an area-wide infrastructure. For example this could be done in vehicle fleets of public transport and airports. Due to its low emission levels, DME is favorable for vehicles in metropolitan areas.

3 COMBUSTION PROCESSES, FUEL SYSTEM AND COMPUTING

As it features a high evaporation propensity and ignitability, DME seems to be predisposed for the use in diesel engines. Compared to diesel fuel, the combustion of DME runs faster and more quietly, fewer pollutants are emitted and the formation of soot is close to zero. The soot-free combustion is a result of the high proportion of oxygen and the absence of carbon double-bonds. Incurring nitrogen oxides can be reduced via the exhaust-gas return without further soot formation.

With optimized DME combustion processes, the potential inner-engine reduction of emissions could reach a level that renders extensive exhaust aftertreatment systems obsolete. In surrounding conditions DME is gaseous and it needs to be compressed to over 5 bar in order to be found in liquid state, ❷. Otherwise the fuel system may be damaged by vapor bubbles.

Furthermore, compared to diesel fuel, DME is characterized by its lower kinematic viscosity and the according lack of lubricity. Also DME is chemically more aggressive and features a distinct temperature-dependent compressibility. Those characteristics necessitate the separate layout of DME fuel system components and/or the adjustment of conventional diesel fuel systems. Yet the lack of soot problems and its easy fuel mixture generation permits significantly reduced injection pressures (< 500 bar) compared to modern diesel engines. The application of DME-diesel-blends appears to be very promising, as they only require marginal adapta-

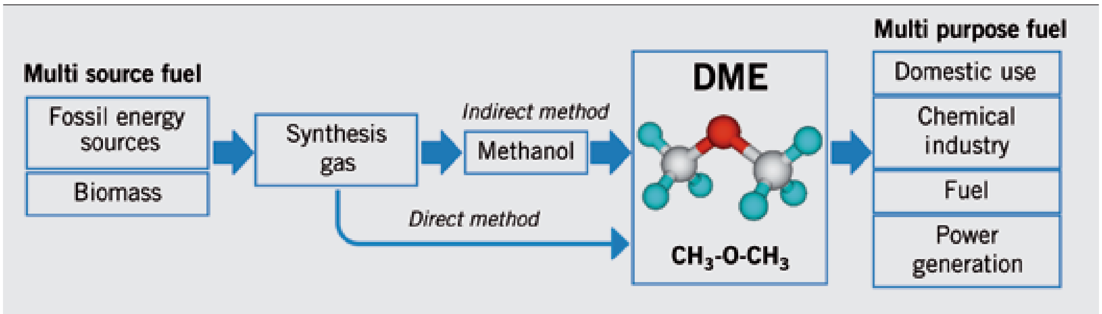

❶ DME production and utilization

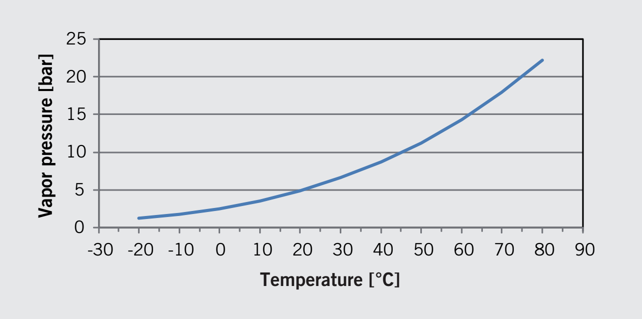

❷ DME vapor pressure curve [1] – at ambient temperature DME is gaseous and needs to be compressed to 5 bar in order to be stocked in liquid state

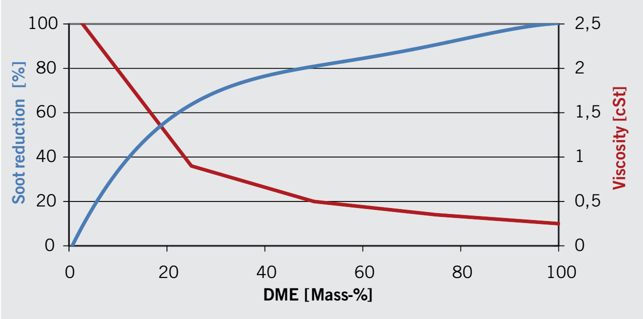

❸ DME-diesel blend: soot reduction and viscosity depending on percentage mixture [1, 4]

tions of the fuel system, small percentages of DME provided. At the same time the soot emission is significantly reduced, ❸. Due to the decreasing viscosity, larger percentages of DME require fundamental adjustments of the fuel system [1, 4].

Several publications describe the use of numerical calculations with DME in engines. Models of reaction kinetics, inner nozzle flow, spray dispersion and combustion are applied and scientifically validated. The required physical data and the applied models are available and were already implemented in various CFD-programs.

REFERENCES

[1] Fujimoto, K.; Ohno, Y.: DME Handbook. Japan DME Forum, Ohmsha, Tokyo, 2007

[2] Eucar European Council for Automotive R&D; Concawe; JRC European Commission Joint Research Centre (Ed.): Well-to-Wheels Analysis of Future Automotive Fuels and Powertrains in the European Context. Version 2c, March 2007, http://ies.jrc.ec.europa.eu/wtw

[3] Taupy, J.: Emergence of DME. In: 2nd International Conference & Exhibition on Gaseous Fuels, Goa, India, 2009

[4] Eirich, J.; Chapman, E.; Glunt, H.; Klinikowski, D.; Boehman, A.; Hansel, J.; Heydorn, E.: Development of a Dimethyl Ether (DME) Fueled Shuttle Bus. In: SAE Paper 2003-01-0756, USA, 2003

THANKS

This paper was written within the framework of the project “DME – Alternative Fuels”, sponsored by theResearch Association for Combustion Engines (FVV) under No. 1005 in the FVA/FVV CO_2 Emissions Research Program. The authors appreciate their strong support to the FVV in Frankfurt/Main (Germany) and to the working group.